2007-08-02

Compartmentalization of HIV-1 in the Secondary Lymphoid Tissues

James Peter Gregson
Brigham Young University - Provo

COMPARTMENTALIZATION OF HUMAN IMMUNODEFICIENCY VIRUS TYPE 1 IN THE SECONDARY LYMPHOID TISSUES

by

James P. Gregson

A dissertation submitted to the faculty of

Brigham Young University

in partial fulfillment of the requirements for the degree of

Doctor of Philosophy

Department of Chemistry and Biochemistry

Brigham Young University

August 2007

BRIGHAM YOUNG UNIVERSITY

GRADUATE COMMITTEE APPROVAL

of a dissertation submitted by

James P. Gregson

This dissertation has been read by each member of the following graduate committee and by majority vote has been found to be satisfactory.

Date	Gregory F. Burton, Chair
Date	David M. Belnap
Date	Keith A. Crandall
Date	Daniel L. Simmons
Date	Barry M. Willardson

BRIGHAM YOUNG UNIVERSITY

As chair of the candidate's graduate committee, I have read the dissertation of James P. Gregson in its final form and have found that (1) its format, citations, and bibliographical style are consistent and acceptable and fulfill university and department style requirements; (2) its illustrative materials including figures, tables, and charts are in place; and (3) the final manuscript is satisfactory to the graduate committee and is ready for submission to the university library.

Date	Gregory F. Burton Chair, Graduate Committee

Accepted for the Department

Date	David V. Dearden, Graduate Coordinator

Accepted for the College

Date	Thomas W. Sederberg, Associate Dean

ABSTRACT

COMPARTMENTALIZATION OF HUMAN IMMUNODEFICIENCY VIRUS TYPE 1 IN THE SECONDARY LYMPHOID TISSUES

James P. Gregson

Department of Chemistry & Biochemistry

Doctor of Philosophy

Follicular dendritic cells (FDCs) reside in the lymphoid follicles of the secondary lymphoid tissues (sLTs). Following the infection of an individual with human immunodeficiency virus type 1 (HIV-1), viral particles are trapped in massive quantities on the surfaces of FDCs. HIV-1 viral compartments are cell types or tissues between which there is a restriction of virus flow. Compartmentalization of HIV-1 creates numerous sites within the body in which the virus can undergo independent evolution, giving rise to a more diverse total viral population. Given the sessile nature of the FDC, I hypothesized that contrary to common assumptions, FDC-trapped HIV-1 is compartmentalized between different sLTs. Furthermore, given that FDC-trapped HIV-1 represents the major source of virus in the host, I postulated that this compartmentalization would likely impact the diversity of HIV-1 associated with the sLTs. I isolated FDCs, macrophages, and T cells from various sLTs, and sequenced

cloned HIV-1 associated with these three cell populations. I subjected the resulting DNA and cDNA sequence data to phylogenetic and other statistical analyses. In support of my hypothesis, I demonstrate that both HIV-1 gp120 and *pol* sequences cloned from FDCs are compartmentalized between different sLTs. This compartmentalization is even apparent between lymph nodes taken from the same lymph node chain. One of the apparent effects of this compartmentalization is to significantly increase the viral genetic diversity in multiple sLTs when compared with diversity in a single sLT. It also appears that the selective pressures on HIV-1 differ among the sLTs. In addition, when proviruses isolated from macrophages from different sLTs were compared, it was also evident that there is compartmentalization of HIV-1 associated with this cell type as well. Finally, I demonstrate that HIV-1 isolated from an unfractionated population of cells from a single sLT, may be an inadequate representation of the total viral population in that sLT. Taken together, my data suggest that the nature of HIV-1 in the sLTs may be more complex than currently appreciated.

ACKNOWLEDGEMENTS

I thank Dr. Gregory F. Burton for his excellent mentoring and friendship during my time in his laboratory. I also thank the other members of my graduate committee, Drs. David M. Belnap, Keith A. Crandall, Daniel L. Simmons, and Barry M. Willardson, for their time, patience, and critical analysis of my work. I would especially like to thank Dr. Loubna Tazi for her invaluable assistance with the statistical analyses in this work. I am also grateful to colleagues in the Burton laboratory, past and present; they have assisted and guided my research and it has been a pleasure to work with them.

I thank my family. Especially I thank my wife Karen for her devotion, and her constant support and encouragement. I thank my children for their unconditional love. I thank my parents and parents-in-law for their confidence in me; this work represents a significant sacrifice on their behalf as well. Finally, I thank God for His love and countless, unending blessings in my life.

TABLE OF CONTENTS

LIST OF FIGURES AND TABLES

INTRODUCTION

The Joint United Nations Program on HIV and AIDS estimate that acquired immunodeficiency syndrome (AIDS) has killed 25 million people worldwide in the last 25 years (1). In 2005 alone, AIDS claimed approximately 3 million lives; tragically, at least 570,000 of these were children. In addition, they estimate that in excess of 40 million people currently live with human immunodeficiency virus (HIV), the causative agent of AIDS, with no prospect of a cure (1). Taken together, these alarming statistics suggest that the AIDS pandemic will be one of the most destructive in human history.

HIV is a lentivirus of the *Retroviridae* viral family. There are two known species of HIV, namely HIV-1 and HIV-2. Of these two viruses, HIV-1 is the more virulent and more readily transmitted. As such, HIV-1 is the cause of the majority of HIV infections globally; HIV-2 infections appear largely confined to West Africa. HIV-1 primarily infects $CD4^+$ cells of the immune system, including macrophages, dendritic cells, and most notably helper T cells. The steady destruction of an infected individual's $CD4^+$ helper T cell population causes the decline and eventual loss of cell-mediated immunity. As a result, the immunodeficient individual becomes increasingly susceptible to opportunistic infections. Without treatment, most infected individuals will develop AIDS and die.

HIV-1 replication cycle

Viral entry: The HIV-1 core is encapsulated by a lipid bilayer derived from the host cell from which the provirus was originally expressed. During the synthesis of new virions,

multiple copies of the viral glycoprotein Env, also referred to as gp160, are packaged in the virion membrane. Env is a trimeric complex that consists of three copies of gp41 non-covalently attached to three copies of gp120. Gp41 anchors Env to the viral membrane via a hydrophobic fusion domain at the N-terminus that also functions in virus-cell fusion (2). Gp120 is the subunit of Env exposed to the external environment; it is heavily glycosylated by the host, which protects the protein (and hence the virus) from recognition by host antibodies.

The principal receptor for HIV-1 is CD4. However, CD4 expression alone is not enough to render a cell susceptible to infection; HIV-1 also requires another cell-surface protein, or coreceptor. Two principal coreceptors have been identified; these are the chemokine receptors CCR5 and CXCR4 (3-4). Initially, gp120 binds CD4 with relatively low affinity. This binding induces a conformational change in gp120 that exposes its coreceptor-binding domains, thereby allowing the high affinity binding of gp120 to the coreceptor (3-4). This high affinity binding triggers a rearrangement of gp41 that allows the N-terminal fusion peptide to penetrate the target cell membrane (3-4). A further rearrangement of gp41 brings the virus and target cell membranes together, allowing fusion of the membranes and subsequent entry of the viral capsid (3-4).

Tropism: As discussed above briefly, HIV-1 primarily infects $CD4^+$ cells that also express either of the chemokine receptors CCR5 or CXCR4 at the cell surface. Strains of HIV-1 that use CCR5 as a coreceptor are termed “R5”, while those that use CXCR4 are termed “X4” (5). There also appear to be some strains of the virus that are dual-tropic and can use either coreceptor; these are typically referred to as “X4R5” isolates.

The Env protein is divided into variable (V) and constant (C) regions. Random mutations, primarily in the variable regions of Env, result in a diverse population of HIV-1 that collectively is able to escape the host immune response. However, variation in the V3 region (or V3 loop) also affects the cellular tropism of the virus. While the exact parameters that dictate tropism are still unclear, some common sequence elements that impact tropism have been reported. In particular, the amino acid at position 25 in the V3 loop appears to be an important residue, where a basic amino acid is indicative of X4 tropic HIV-1 (6-12). An increased net charge in the V3 loop has also been postulated to affect tropism, where greater net charges are associated with X4 tropic HIV-1 (6, 8-12).

For reasons that at present are not fully understood, R5 strains of HIV-1 are selected for during the intial stages of infection, and therefore predominate during the early course of disease (13-15). This is evidenced by those individuals who carry a defective CCR5 allele that contains an internal 32-base pair deletion (CCR5 Δ32). The truncated protein encoded by this gene is not expressed at the cell surface. As a result, CCR5 Δ32 homozygous individuals exhibit a high degree of resistance to HIV-1 infection (16). While R5 strains predominate in the early stages of disease, in approximately 50% of cases the tropism of the virus changes so that during the latter stages of disease an X4 strain predominates (17). X4 strains are typically more virulent than R5 strains and so this tropism switch is usually associated with a more rapid depletion of $CD4^+$ T cells (18). Therefore, while the conditions that precipitate a tropism switch are unclear, the event appears to mark a key step in the progression to AIDS.

Reverse transcription and recombination: The HIV-1 genome inside a viral particle exists in the form of two copies of positive-sense RNA, approximately 10 kb in length. After the viral core enters the host cell, the viral genome is reverse transcribed into double stranded (ds) DNA by the viral reverse transcriptase (RT) enzyme.

In particular, there are two features of the reverse transcription process that significantly impact the evolutionary biology of HIV-1. First, RT has no proofreading activity and its error rate is such that it is estimated that viral genomes with every possible point mutation arise daily (19). Second, RT possesses the ability to jump from one template to another (i.e. strand jumping). If a cell is infected with more than one variant (or quasi-species) of HIV-1, the two copies of the RNA genome in progeny virus may be different. In this scenario, following subsequent infection, reverse transcription can also lead to recombination of the virus as the RT enzyme jumps between templates, carrying the nascent cDNA molecule with it (20). These two mechanisms, error-prone reverse transcription and recombination, coupled with the rapid rate at which HIV-1 replicates, results in a viral population with a high degree of genetic variability. It is this genetic variability that allows the virus to escape effectively from selective pressures, whether in the form of host immune responses or therapy.

Integration, transcription, assembly, and release: After reverse transcription, the ds DNA form of the viral genome is transported to the nucleus and incorporated into the host genome using another viral enzyme, integrase (21-22). The provirus is subsequently transcribed and translated using a combination of host and viral factors (23-24). New HIV-1 virions are assembled at the plasma membrane of the infected host, where they are

eventually released coated in a lipid bilayer derived from the host (24). After the viral particles are released, maturation is completed when the viral enzyme protease cleaves the viral polyproteins into functional structural proteins and enzymes (24).

Viral reservoirs

In 1997, several groups reported that the use of a protease inhibitor in combination with two RT inhibitors had the dramatic effect of reducing HIV-1 in the plasma to undetectable levels in many infected patients (25-27). This approach to the treatment of HIV-1 became known as Highly Active Anti-Retroviral Therapy (HAART). Based on the decay kinetics of the virus in individuals receiving HAART, these initial results raised hopes that complete eradication of the virus may be possible after just three years of therapy (27). However, this early optimism has gradually disappeared in light of the discovery that HIV-1 is able to persist in viral reservoirs (28). A viral reservoir is a tissue or cellular site in which virus accumulates and persists with greater stability than the main pool of replicating virus (28).

Early studies demonstrate that the cells that produce the vast majority of virus in the plasma probably have a half-life of less than a day (29-31). *In situ* hybridization studies suggest that this cell type is mainly an activated $CD4^+$ T cell (32). In an untreated patient, large numbers of $CD4^+$ T cells are infected every day, thus replenishing the rapidly depleting pool of HIV-1 expressing cells. However, in patients receiving HAART, because HIV-1 replication and infection is heavily curtailed, the short-lived pool of virus-expressing cells is quickly diminished without being restored. It is the high turnover of the primary target cell that accounts for the dramatic reduction in plasma HIV-1 levels

after the initiation of HAART, and therefore raised hopes that eradication was possible.

However, a careful analysis of the viral decay kinetics shows that the decay is at least biphasic (27). The much slower rate of the second-phase decay is attributed to "reservoirs" that prevent complete eradication of the virus using HAART (28). The rapid rate of the first phase is contributed by the activated $CD4^+$ T cell, but the nature of the cellular or anatomical reservoir(s) that contributes to the second phase of decay is not clear. Three principal viral reservoirs have been postulated to play a role in second-phase decay. The best studied of these is the latently infected $CD4^+$ T cell. This cell is thought to be a resting memory $CD4^+$ T cell, one which was infected with HIV-1 during a state of activation and just prior to the cell cycling to a resting memory state (28, 33-34). As such, the cell is a long-lived reservoir of stable HIV-1 provirus. Macrophages (MØs) have also been shown to be a major viral reservoir in a primate model (35). Furthermore, the half-life of tissue MØs is estimated to be approximately two weeks (36), which correlates with second-phase decay. A third viral reservoir is the follicular dendritic cell (FDC). *In situ* hybridization studies suggest that FDC-trapped HIV-1 may decay with a half-life of approximately two weeks (37). In fact, mathematical studies suggest that FDC-trapped HIV-1 may actually have a much longer half-life, and also be the primary reservoir responsible for second-phase decay (38). Yet the nature of this potentially dangerous, long-term reservoir remains poorly understood.

FDCs in health

Three cardinal features characterize FDCs: 1) dendritic morphology; 2) localization to lymphoid follicles (germinal centers) of the secondary lymphoid tissues (sLTs); and 3)

the ability to trap and retain antigen in the form of immune complexes (ICs) for years (40, 42-43). When a host is challenged with foreign antigen, the antigen is rapidly opsonized with specific antibody and/or complement proteins to form ICs. These ICs are rapidly transported to the draining lymph nodes (39). Here, phagocytes eliminate the vast majority of these ICs. However, a small portion are trapped and retained on the surface of FDCs (40-41). Work in this area has demonstrated that the principle receptors that trap ICs are CD21 (or CR2), which binds inactive complement 3b fragments, and CD32 (or FcγRII), which binds the Fc portion of IgG molecules (44-45). These trapped ICs have been shown to play several key roles in a healthy immune response. There is evidence that suggests that FDC-trapped ICs are required for B cell affinity maturation, the process by which B cells produce antibodies with increased affinity for their specific antigen during an immune response (46-47). In addition, these ICs may be required for local activation of complement (48). Finally, it should be noted that FDC-trapped ICs are quite stable having a half-life of ~8 weeks (49). As these trapped ICs are slowly released, they are endocytosed by antigen-specific, germinal center (GC) B cells. These GC B cells process and present the endocytosed antigen to GC T cells (42, 50). Thus, via their trapped ICs, FDCs have been implicated in B cell affinity maturation, complement activation, and memory maintenance.

FDCs in HIV/AIDS

Early in acute infection, HIV-1 particles become coated with specific antibody and/or complement (51-54). Just as in a normal healthy state, FDCs are able to trap these HIV-1 ICs on their cell surface via CD21 and CD32 (55-56). This trapping is apparent just three

weeks post infection (57), but likely occurs even earlier. However, in contrast to the minute amount (picogram) of conventional antigen trapped by FDCs (40-41), in an HIV-1-infected individual the virus is trapped in enormous quantities, estimated at ~$1.5x10^8$ copies of viral RNA per gram of lymphoid tissue (37, 58). This massive viral trapping makes the FDC network the largest reservoir of HIV-1 in the body, even though the FDC itself is not productively infected (59).

FDC-trapped HIV-1 remains infectious for months *in vivo* and for weeks *in vitro* with no requirement for ongoing infection and/or replication (45, 60). Throughout the course of the disease, active viral infection and replication persist in GCs, where FDCs reside. The long-term retention of HIV-1 on the surface of FDCs has several negative effects. ICs trapped prior to infection of the host with HIV-1 are lost, as viral ICs overwhelm the FDC network. As a result, there is a decline in antigen-specific B cells and antibodies (61). In addition, as IC receptors on FDCs become overwhelmed with HIV-1 ICs, FDCs are unable to trap new protein antigens. Given that the trapping of ICs by FDCs is required for B cell affinity maturation (46-47), the FDCs inability to trap new antigens likely leads to impairment of this important immune process. Finally, the ongoing viral infection and replication in GCs eventually lead to the destruction of FDC networks through mechanisms that have not yet been defined (62-63). Thus, FDC-trapped HIV-1 represents a large and dangerous reservoir of virus that likely impacts disease pathogenesis and the immediate health of infected individuals.

Viral compartmentalization in sLTs

Viral compartments are cell types or tissues between which there is a restriction of virus flow (64). Compartmentalization of HIV-1 creates numerous sites within the body in which the virus can undergo independent evolution, giving rise to a more diverse total viral population. Thus, the degree to which HIV-1 is compartmentalized directly impacts the genetic diversity of the viral population in an infected individual; and the greater the viral diversity, the more able the virus is to respond to selective pressures from the immune system of drug therapy. Therefore, defining viral compartments, and accurately estimating HIV-1 genetic diversity becomes an important work, and an increasing amount of research has gone into this field.

The sLTs are the sites in which the adaptive immune responses are initiated; they include ~500 lymph nodes (LNs), the spleen, and mucosal-associated lymphoid tissues such as tonsils and Peyer's patches. All but a small fraction of $CD4^+$ T cells, the primary target of HIV-1, reside in sLTs, as do FDCs, the major cellular reservoir of HIV-1. As a result, throughout much of the course of disease, sLTs are the principal site of HIV-1 production and also form the major tissue viral reservoir (52, 65-66). In fact, during the latent stage of disease, the majority of ongoing replication is confined to the GCs of sLTs (55, 67-68).

Compartmentalization of HIV-1 in a variety of different tissues has been well documented (15, 69-80). However, the fact that T cells circulate freely and frequently through the lymphatic system, combined with the ability of HIV-1 to replicate so quickly, led to the assumption that HIV-1 within all sLTs is, to a large degree, homogenous. This assumption is evident in many HIV-1 compartmentalization studies, in which all sLTs are

implicitly considered as a single viral compartment (71, 80-88). In these studies, where HIV-1 in the sLTs is compared to virus in other compartments (e.g. blood, brain), viral sequences are typically isolated from a single LN and are then considered indicative of virus in all sLTs. However, compartmentalization studies to date have, in general, neglected to consider what contributions the FDC may be making to the compartmentalization of HIV-1 within the lymphatic system. Importantly, the FDC is a non-migratory cell type, suggesting there may be a restriction to the flow of virus trapped on FDCs between sLTs.

As described above, following infection of an individual with HIV-1, the virus disseminates throughout the lymphatic system and is trapped on the surface of FDCs in enormous quantities (58). If the nature of FDC trapping of HIV-1 were transitory, it would likely have little impact on the compartmentalization and diversity of the virus in sLTs. However, a number of studies suggest that the FDC is a long-term reservoir of infectious HIV-1 particles (54, 60). In particular, our laboratory has recently demonstrated that much of the virus on the FDC network is archived virus that is several months old (unpublished data). Moreover, that same study suggests that FDC-trapped HIV-1 in different sLTs may be both genetically and functionally different. Given the sessile nature of FDCs, I postulated that HIV-1 trapped on FDC networks may be compartmentalized between different sLTs, and that this compartmentalization may significantly impact the viral diversity in sLTs.

In the compartmentalization studies described above, RNA and/or genomic DNA are isolated from a homogenate of a single sLT (71, 80-88). This experimental approach makes the assumption that sequences taken from a tissue homogenate accurately reflect

HIV-1 quasi-species in a single sLT. Moreover, for practical reasons, parameters such as levels of viral RNA, $CD4^+$ T cell counts, and viral tropism, are often measured from blood samples and used to estimate disease progression in the sLTs (89-91).

While these assumptions and experimental approaches may be useful in providing a generalized picture of what is occurring in sLTs, they cannot elucidate differences that exist between HIV-1 in different cellular and tissue compartments. In addition to my hypothesis regarding the compartmentalized nature of FDC-trapped HIV-1, I postulated that differences may also exist between MØs and T cells in different sLTs. Furthermore, I was also interested in the genetic relationship of HIV-1 associated with FDCs, MØs, and T cells within a single sLT. I postulated that the approach of sequencing HIV-1 from a tissue homogenate may miss significant differences that exist between the viruses associated with different cell types.

I sought to test the following broad hypotheses: 1) HIV-1 is compartmentalized between sLTs; 2) sequencing HIV-1 from a tissue homogenate is an inaccurate representation of all quasi-species in a single sLT. I obtained an array of post motem sLTs, including the spleen, from two patients. I isolated FDCs, MØs, and T cells from the various sLTs, and sequenced the HIV-1 envelope and/or polymerase genes from the various cell fractions. By means of phylogenetic and other statistical analyses, I sought to determine the complexity and relationship of HIV-1 trapped on FDCs, and in MØs and T cells, in different sLTs. I report here that FDC-trapped HIV-1 was indeed compartmentalized between different sLTs, and that this compartmentalization occurred even between closely adjacent LNs from the same infected subject. Furthermore, I provide evidence that indicated that sampling a single sLT may significantly under-

represent overall viral diversity in all sLTs. I also report that HIV-1 isolated from the various cell types in sLTs was markedly different. I found that the extent of viral compartmentalization between cell types varied among different sLTs. In addition, I found that sequencing HIV-1 from a heterogeneous cell population may be an inadequate representation of the diversity of quasi-species in a given sLT.

Taken together, my data suggested that each separate sLT provides an environment with unique selective pressures, so that the relationships and evolution of HIV-1 may be different in any single sLT. This conclusion suggested that HIV-1 diversity in sLTs was far more complex than was currently appreciated.

MATERIALS AND METHODS

Patient tissue samples and patient history

All the research described below complied with all relevant federal guidelines and institutional policies.

In collaboration with the National Disease Research Interchange, multiple tissues from two subjects with AIDS were harvested at autopsy (within 12 h of death) and shipped on wet ice overnight to Brigham Young University.

Patient N1_205 was a 27 year old male with no reported exposure to anti-retroviral medication. The cause of death was CNS mass lesions. I received splenic fragments and several LNs, including three LNs from the right axillary site, and a pancreatic LN.

Patient N2_520 was a 34 year old male with exposure to multiple anti-retroviral medications, the timing and duration of which were unknown. The cause of death was CNS mass lesions. I received three LNs from this subject but they were not characterized as to their location within the body.

Cell isolation

FDCs: LNs were trimmed of excess non-sLT. FDCs were isolated from sLTs following previously published procedures (60). Briefly, tissues were cut into small 1-2 mm cubes and gently enzyme digested for 1 h at 37°C in RPMI 1640 (Hyclone, Logan, UT, USA) containing collegenase (10 mg/ml, Roche Applied Science, Indianapolis, IN, USA), DNase I (1% v/v; Sigma, St. Louis, MO, USA), and gentamicin (Invitrogen, Carlsbad, CA, USA), to release single cells. The released cells were collected and the tissue was

subjected to a further enzymatic digestion. The cells released from both digestions were pooled. An aliquot from the pooled cells was removed prior to cellular fractionation, and used in subsequent analysis described below. FDCs were isolated from the pooled cells by labeling cells with HJ2 (a mouse IgM monoclonal antibody (Ab) that binds human FDCs; kindly provided by Dr. M. Nahm, University of Alabama, Birmingham, AL, USA). This was followed by incubation with ChromePure mouse IgG (Jackson ImmunoResearch Laboratories Inc., PA, USA) to block non-specific IgG interactions, and then incubation with mouse anti-human CD21L (7D6 hybridoma; kindly provided by Dr. Y. J. Liu, DNAX, Palo Alto, CA, USA). CD21L is the long isoform of CR2 and is abundantly expressed on FDCs (44). The cells were washed to remove unbound Ab and incubated with magnetic beads conjugated with rat, anti-mouse-IgM, and rat, anti-mouse IgG (Dynal Biotec, Oslo, Norway). FDCs were positively selected using magnets.

MØs: MØs were isolated by incubating the residual pool of cells with mouse, anti-human-CD16 (Beckman Coulter Inc., Fullerton, CA, USA). After washing, the cells were incubated with rat, anti-mouse IgG dynabeads and mouse, anti-human CD14 dynabeads (Dynal Biotec). CD14 (lipopolysaccharide receptor) and CD16 (Fc gamma receptor III) were selected for isolation because HIV-1 infection can lead to the downregulation of CD14 on MØs, thus requiring more than one marker for isolation. MØs were positively selected using magnets.

T cells: T cells were isolated after the MØs by incubating the residual cell fraction with mouse, anti-human-CD3 dynabeads (Dynal Biotec). CD3 is the signaling complex associated with the T cell receptor. T cells were positively selected using magnets.

Flow Cytometry

A 100 µl aliquot of cells released from each sLT by enzyme digestion was used to analyze cell populations in the different tissues received. Cells were first incubated with mouse ChromePure IgG (Jackson ImmunoResearch Laboratories Inc.) for 20 min and then labeled with mouse, anti-human CD3-PE, mouse, anti-human CD4-FITC, and mouse, anti-human CD14-Cy5 (Beckman Coulter Inc.) for 30 min. Cells were washed with PBS and analyzed for immunofluorescence using an EPICS XL flow cytometer with EXPO32 ADC software (Beckman Coulter Inc.).

RNA extraction and RT-PCR

As FDCs are not productively infected with HIV-1 (59), RNA was isolated and reverse transcribed from the FDC fraction of cells and from HIV-1 virions trapped on the surface of these FDCs. In addition, RNA was also isolated from an aliquot of the heterogeneous post-enzymatic digest population of cells. RNA was isolated using RNA-STAT 60 (Tel-Test, Friendswood, TX, USA). 800 µl of RNA STAT 60 was added to the FDC fraction and incubated at room temperature for 5 min, after which the samples were stored at –80°C until testing. At the time of testing, to each of the samples 160 µl of chloroform (Fisher Scientific, Waltham, MA, USA) was added per 800 µl of RNA-STAT 60; the solution was mixed on a vortexer and then centrifuged at 12,000 x g for 15 min at 4°C.

An equal volume of the aqueous phase (400 µl) from each sample was transferred to a fresh tube containing the same volume of isopropanol (Sigma), and the contents were mixed as above, incubated at –20°C for 30 min, and centrifuged at 16,000 x g for 60 min at 4°C. After discarding the supernatant fluid, the RNA pellet was washed once in 75% ethanol (1.0 ml, Fisher) and the samples were resuspended to a volume of 20 µl in RNase/DNase-free water (ISC Bioexpress, Kaysville, UT, USA). To ensure that there was no contaminating genomic DNA, RNA was DNase I treated according to the manufacturer's protocol (Ambion Inc., Austin, TX, USA). cDNA was generated with oligo-dT primers and murine leukemia virus RT according to the manufacturer's protocol (Roche Diagnostics, Basel, Switzerland). Reverse transcription was carried out at 37°C for 60 min, followed by an inactivation step of 99°C for 5 min.

DNA isolation

DNA was isolated from a second aliquot of post-enzymatic digest cells, and from the MØ and T cell fractions of cells. Cells were resuspended in 50 µl of DNA lysis buffer (0.01% SDS, 0.001% Triton-X 100, 0.42 µg/ml Proteinase K in TE: 10mM THAM and 1mM EDTA) and incubated at 50°C for 12 hours.

Nested PCR

cDNA/DNA amplification was performed by a nested PCR procedure for each sLT source. For patient N1_205 these included a splenic fragment, right axillary LNs 1, 2, and 3, left axillary LN, mesenteric LNs 1 and 2, mediastinal LN, renal/aortic LN, and pancreatic LN. For patient N2_521 these included LNs 1, 2, and 3. For amplification of

gp120 the outer primers were V1outer5', 5'-ATCAAAGCCTAAAGCCATGTGT AAAATTAACCCCAC-3', and V4outer3', 5'-TCACTTCTCCAATTGTCCCTCATATC TCCTCCTCCA-3'; the inner primers were V1inner5', 5'-CATGTGTAAAATTAACCC CACTCTGTGTT-3', and V4inner3', 5'-GGACCCAGAAATTGTAACGCACAGTT TTA-3'. The size of the amplicon generated using the V1inner5' and V4inner3' primers is ~1100 bp. For amplification of the *pol* gene the outer primers were ProRT out5', 5'-CAGAGCCAACAGCCCCACCAGAAGAGAG-3', and ProRT out3', 5'-ACTTGCCC AATTCAATTTTCCCACTAA-3'; the inner primers were ProRT inner5', 5'-CCTTTAG CTTCCCTCAGATCACTCTTTG-3', and ProRT inner3', 5'-GCACTATAGGCTGTAC TGTCCA-3'. The size of the amplicon generated using the ProRT inner5' and ProRT inner3' primers is ~1100 bp. All primers were synthesized by Invitrogen and were chosen so that they would anneal in regions of low variability. For outer PCR, 1 µl of cDNA or 1 µl of cell lysate containing genomic DNA was amplified in a total volume of 50 µl containing 2.5 mM $MgCl_2$ (1.8 mM for *pol* amplification), 100 µM (each) dNTPs, and 200 pM of each primer. I utilized the FastStart High Fidelity PCR System (Roche Diagnostics), which contains Taq DNA polymerase, a proofreading protein that lacks polymerase activity, and buffer. For the inner PCR, 1 µl of outer PCR product was used as template in the same reaction conditions. For both outer and inner PCR, the program of amplification started with a step of 2 min at 95°C. This was followed by 35 cycles of 95°C for 30 s, 60°C for 30 s, and 72°C for 1 min 10 s. An extension step (10 min at 72°C) ended this program. All PCR procedures were conducted in an Eppendorf Mastercycler (Eppendorf North America, Westbury, NY, USA). All PCR amplifications were run with negative controls, and were performed by employing procedures to

minimize likelihood of cross-contamination, including dedicated pipetting apparatus, aerosol-resistant pipette tips, and the use of a laminar flow hood.

Cloning

PCR products were T/A cloned into pCR 3.1 (Invitrogen) by ligating vector with fresh PCR product (less than 30 min after the PCR ended) overnight at 15°C. Products of the ligation reaction (1 μl) were used to transform STBL2 competent cells (Invitrogen). Cells were transformed by heat shock (25 s at 42°C) according to the manufacturer's protocol. The transformed cells were plated on LB plates containing ampicillin (50 μg/ml, Sigma) and individual colonies were screened for the presence of a PCR product insert in pCR 3.1. Briefly, individual colonies were isolated and incubated in LB medium in a 96 well plate at 30ºC overnight. Bacterial cells were centrifuged to create a cell pellet, lysed, and genomic DNA and cellular proteins precipitated and removed by centrifugation. The supernatant containing plasmid DNA was then electrophoresed in an agarose gel. Plasmids containing PCR inserts were identified by relative size. Positive clones were grown in LB medium containing ampicillin (50 μg/ml) and plasmid DNA was isolated from the bacterial clone using the Qiaprep Spin Miniprep kit (Qiagen Inc., Valencia, CA, USA) according to the manufacturer's protocol.

Sequencing

The Qiaprep Spin Miniprep kit yields plasmid DNA ready for direct sequencing. Each clone was sequenced with at least four different primers to generate overlapping sequence. The following primers were used to sequence the Env gene: Npcr, 5'-

CTGGCAACTAGAAGGCACAGT-3'; T7p, 5'-TAATACGACTCACTATAGGG-3' (both Npcr and T7p anneal to the pCR 3.1 vector sequence and thus include the beginning and ending sequence of the cloned HIV-1 genes); V1inn5, 5'-CATGTGTAAA ATTAACCCCACTCTGTGTT-3'; NV4inn3, 5'-AATAGCAGCCCTGTAATATTTGAT GAACA-3'; and envT2, 5'-CCAATTCCCATACATTATTGTG-3'. The following additional primers were used to sequence the *pol* gene: pol2, 5'-GGGCCTGAAAATCCA TACAA-3'; pol4, 5'-GTATGGATTTTCAGGCCCAA-3'; and pol5, 5'-TGCTGCCCTA TTTCTAAG-3'. All primers were synthesized by Invitrogen. A detailed sequencing protocol is available at the Brigham Young University DNA Sequencing Center website (http://dnasc.byu.edu/). Briefly, 2 µl of plasmid DNA was amplified in a 7 µl total volume containing 2 µl RNase/DNase-free water, 1 µM of primer, 1 µL BigDye Terminator v3.1 Cycle Sequencing Kit (Applied Biosystems, Foster City, CA, USA) and 1 µl of buffer supplied with the BigDye kit. The program of amplification consisted of 60 cycles of 96°C for 30 s, 50°C for 15 s, and 60°C for 4 mins. All amplification procedures were conducted in an Eppendorf Mastercycler (Eppendorf North America). Unincorporated labeled nucleotides were removed from the reaction using genCLEAN Dye Terminator Removal Plates (Genetix Ltd., New Milton, UK) according to the manufacturer's protocol. Sequenced DNA was run on an AB 3730XL DNA Analyzer (Applied Biosystems). Sequences were edited using Sequencher 4.2 and 4.5 software programs (Gene Codes Corporation, Ann Arbor, MI), and were aligned using ClustalX (92). The resulting alignments were then checked according to the universal reading frame using MacClade (93).

Phylogenetic analyses

Phylogenies were estimated using Maximum Likelihood (94) with nodal support assessed via bootstrapping (1,000 pseudoreplicates) (95) as implemented in PHYML (96), and Bayesian methods (97) coupled with Markov Chain Monte Carlo (BMCMC) inference as implemented in MrBayes v3.04b (98). Model selection for these analyses followed the procedure outlined by Posada and Buckley (99) as implemented in ModelTest v3.6 (100). For the BMCMC techniques, two independent analyses were run each consisting of four chains. Each Markov chain started from a random tree and ran for 2.0×10^7 cycles, sampling every 1000th generation. In order to confirm that the Bayesian analyses converged and mixed well, the fluctuating value of likelihood was monitored, and the means and variances of all likelihood parameters and likelihood scores from the independent runs were compared using the program Tracer v1.2.1 (101). These phylogenetic analyses were performed on the supercomputing cluster of the College of Biology and Agriculture at Brigham Young University.

Haplotype network reconstruction

Haplotype networks were constructed using the program TCS 1.21 (102). This analysis was implemented in order to determine the genetic relationships between HIV-1 gp120 sequences within a 95% parsimony limit. The networks are displayed so that the colored squares (putative out groups) and circles represent actual cloned sequences, the sizes of which are proportional to the number of clones with the same sequence. Each open circle represents a putative quasi-species in the evolutionary pathway. The solid lines connecting a network suggest two quasi-species can be connected with at least a 95%

degree of confidence. The dashed lines in a network represent a more tenuous connection.

Genetic diversity estimates

Genetic diversity estimates (θ_w) were assessed for HIV-1 gp120 and *pol* sequences using the program LDhat (http: www.stats.ox.ac.uk/~mcvean/LDhat.html). θ_w estimates the likelihood of finding a point mutation at a single site in a sequence, where a value of θ_w = 1 estimates a 100% likelihood.

Testing for positive selection

The dN/dS ratio (ω) is a ratio that compares non-synonymous nucleotide changes (dN) with synonymous nucleotide changes (dS). Non-synonymous changes are nucleotide mutations that also alter the protein sequence. Synonymous changes (or silent mutations) do not alter the protein sequence. ω measures the selective pressure at the protein level. If a non-synonymous change does not alter the fitness of the protein it becomes fixed in the population at the same rate as a synonymous change. Therefore, $\omega = 1$ suggests neutral evolution. If a non-synonymous change results in a more or less fit protein it becomes fixed in the population at a greater or lesser frequency than a synonymous change, respectively. Therefore, $\omega < 1$ suggests negative or purifying selection, and $\omega > 1$ suggests diversifying positive selection. Values for ω were calculated on the codon alignments from the program CODEML in the PAML package 3.14b3 (103). The extent of selection is inferred in each sLT by estimating ω per gene and per site and the proportion of sites (p) with $\omega > 1$ using the codon-based nested models M0 (one ratio),

M1 (neutral), M2 (selection), M3 (discrete), M7 (beta), and M8 (beta and ω) (104-105). Model likelihood scores were compared using a Likelihood Ratio Test (LRT) to determine the best-fit model. When two models are nested, twice the log-likelihood difference was compared with a χ^2 distribution where the degrees of freedom equal the difference in the number of free parameters between the two models. When ω is greater than 1 in M2, M3, or M8, positively selected sites are inferred from the data. The empirical Bayesian approach was also applied to identify the potential sites under diversifying selection as indicated by a posterior probability ($pP > 0.95$) (106).

RESULTS

Genetic relatedness of FDC-trapped HIV-1 gp120 from different sLTs

Previously published work demonstrates that FDCs function as a long-term reservoir of HIV-1 (54-56, 58, 60). These data, coupled with the sessile nature of the cell, suggested that FDC-trapped HIV-1 may be compartmentalized between different sLTs. I sought to determine the genetic relatedness of gp120 sequences from HIV-1 trapped on FDCs, isolated from right axillary and pancreatic LNs, and a splenic fragment obtained from a single infected subject. Due to the rapid rate at which gp120 evolves, I chose to analyze a relatively conserved region of the gene, i.e. C2-C3. I reasoned that analyzing C2-C3 would give a clearer picture of how the gene evolved over a longer period of time, whereas analysis of more variable regions, i.e. V1-V4, would yield a more recent picture of evolution.

To begin to test the hypothesis that FDC-trapped virus represented a unique viral compartment within sLTs, C2-C3 sequences cloned from FDCs from different sLTs obtained post mortem from a single infected individual were subjected to phylogenetic analysis (Figure 1). The data demonstrated that there was in fact compartmentalization of FDC-trapped gp120 between different sLTs. In particular, all sequences cloned from splenic FDCs clustered together into two monophyletic groups. Sequences from the FDCs in the two LNs also showed some grouping according to the LN from which they were cloned. For example, in one branch of the phylogenetic tree, 11 of the 13 sequences in the group were cloned from pancreatic FDCs; in a second branch, 5 of the 6 sequences were cloned from right axillary FDCs. Because PCR resampling is a potential problem

that can complicate HIV-1 compartmentalization studies, I examined the number of unique sequences in my samples and found that that 52 of the 58 sequences analyzed represented distinct quasi-species. This was good evidence that in my PCR I was not resampling a limited number of templates.

Due to the rapid rate at which HIV-1 gp120 evolves, it is difficult to get robust statistical support using conventional phylogenetic methods. TCS haplotype network analysis is designed to measure changes *within* a population of a single species as opposed to phylogenetic methods, which traditionally are used to reflect relationships *between* different species (102). Therefore, I reasoned that applying a TCS network analysis to the sequence data may provide greater statistical support for my initial observations made using phylogentic analyses. Figure 2 is a TCS network showing the genetic relatedness of the same sequences subjected to phylogenetic analyses in Figure 1. The materials and methods chapter provides a description of how this network was constructed and displayed. This TCS network predicted that the majority of sequences analyzed evolved from sequences within the same sLT. For example, sequences isolated from splenic FDCs (haplotypes 4-11 and 45-51) clustered together and showed mutational changes ranging from 1 nucleotide (haplotypes 5-8 from haplotype 4) to 9 changes (haplotype 9 from haplotype 4).

Finally, I analyzed V1-V4 sequences from the same clones (Figure 3). In this TCS network, a similar pattern of compartmentalization was observed, but as expected, analysis of V1-V4 revealed much greater viral diversity. In particular, several of the sequences tested were found at the ends of long branches (e.g. haplotypes 13, 22, 23, 39,

53, 54, and 55), indicating that the virus had evolved through many quasi-species that connect the network.

Genetic relatedness of FDC-trapped HIV-1 *pol* from different sLTs

Because HIV-1 *pol* evolves more slowly than does HIV-1 gp120, mutations in *pol* become more deeply rooted over time. Therefore, I reasoned that analysis of this gene would provide excellent evidence of compartmentalization if it occurred. To assess the degree of compartmentalization of FDC-trapped HIV-1 in different sLTs, I analyzed ~1100 bp of *pol* sequence cloned from the three different anatomical sites described in Figures 1-3, namely spleen, and right axillary and pancreatic LNs. Figure 4 is a Bayesian analysis of the sequence data sets described. This phylogenetic tree demonstrated that there was an even greater degree of compartmentalization of FDC-trapped *pol* sequences between sLTs, than of gp120 sequences from the same sLTs. Of particular note was the clear compartmentalization of all 17 *pol* sequences obtained from splenic FDCs in a monophyletic group on a branch with a Maximum Likelihood (ML) bootstrap value of 100. Because the region of *pol* sequence analyzed contained both the protease gene and the first 260 amino acids of the RT gene, I sought to determine whether compartmentalization was restricted to either protease or RT independently (Figures 5-6). Both protease and RT exhibited the same pattern of compartmentalization as *pol* taken as a whole, which suggested that the compartmentalization of *pol* sequences was not gene-specific. In summary, *pol* sequences were almost entirely compartmentalized into monophyletic groups based upon which sLT they were cloned from.

Because of the high degree of compartmentalization observed between FDC-trapped *pol* in three unrelated sLTs (i.e. spatially distal), I sought to determine what degree of compartmentalization existed between FDC-trapped sequences from three closely related sLTs. Therefore, in my next analysis, I included two more LNs from the same LN chain from where the first right axillary LN examined was taken (Figure 7). Most surprisingly, I observed a high degree of compartmentalization between the *pol* sequences obtained from the three LNs from the same chain. For example, all 18 sequences obtained from right axillary LN 3 clustered in a monophyletic group with a Bayesian Markov Chain Monte Carlo (BMCMC) inference value of 100. Similarly, 16 of the 19 sequences obtained from right axillary LN 1, and 14 of the 19 sequences obtained from right axillary LN 2, clustered in separate monophyletic groups, with BMCMC inference values 91 and 70, respectively. These data provided compelling evidence that not only was there compartmentalization between unrelated sLTs, but that FDC-trapped HIV-1 was compartmentalized even between LNs immediately adjacent to each other *in vivo*. Again, I noted the heterogeneity of the sequences sampled from each sLT, which indicated that I was not resampling a limited number of templates in my PCR. In addition, when I analyzed FDC-trapped *pol* from three sLTs from a second patient (patient N2_520) I observed a similar pattern (Figure 8). While sequences from FDC-trapped HIV-1 in two LNs were mixed, sequences from the third LN were completely compartmentalized.

Impact of compartmentalization of FDC-trapped HIV-1 on viral diversity

In order to assess the impact the observed compartmentalization may have had on the genotypic diversity of FDC-trapped HIV-1, I analyzed the sequence data sets using the LDhat program to generate estimates of Watterson's genetic diversity (θ_w) (Table 1). θ_w estimates the likelihood of finding a point mutation at a single site, where a value of $\theta_w = 1$ estimates a 100% likelihood. Therefore, the greater the value of θ_w is, the greater the estimated diversity. These results demonstrated that diversity of FDC-trapped HIV-1, as measured by analyzing viral sequences from one sLT, did not reflect the sequence diversity in multiple sLTs. For example, the estimated diversity for *pol* when analyzing sequences from the spleen alone was 0.00377; however, the estimated diversity for *pol* when three unrelated sLTs (including spleen) were analyzed, was over four times greater, i.e. 0.01612. Surprisingly, the same pattern was seen when analyzing the spatially related sLTs. The predicted diversity for *pol* if just the right axillary LN 3 were used was 0.00313; but the estimated diversity based on the analysis of three lymph nodes in a chain from the same site was over four times greater, i.e. 0.01423. These observations were confirmed in a second patient (N2_520) where the same pattern was seen (Table 1); that is, the predicted diversity of FDC-trapped *pol* when three sLTs were analyzed (i.e. LNs 1, 2, and 3), was over four times greater than that which was estimated when only LN 1 was analyzed. It was also interesting to note that the estimated viral diversity based on analysis of sequence from three related sLTs was comparable to that of three unrelated sLTs; in fact, in the case of FDC-trapped gp120, the estimated diversity was greater in the related sLTs.

Identification of sites under positive selection

Likelihood values and parameter estimates for different codon-substitution models of selection are shown in Tables 2 and 3. Diversifying selection ($\omega > 1$) dominated the evolution of FDC-trapped gp120 in the three different sLTs (Table 2). Although the one-ratio model (M0) did not reveal the existence of sites under positive selection in this gene ($\omega < 0.8$), M0 was rejected when compared with any of the more general models that allow for variable ω ratios among sites. All models that allow for positively selected sites did suggest the existence of such sites in gp120 in all three different sLTs. In fact, they all indicated the presence of a small proportion of sites (3% to 11%) under strong positive selection (ω ratio between 7.98 and 9.07). LRTs comparing M2 and M3 with M1 and M0 respectively, and M7 with M8 were all highly significant ($P < 0.001$). All the models tested in this gene provided consistent and significant evidence for the existence of positively selected nucleotide sites. The Bayesian approach identified 3, 4, and 7 positively selected sites in the pancreatic LN, the right axillary LN 1, and the spleen respectively, under the model M2; and 4, 5 and 7 nucleotide sites under positive selection in the pancreatic LN, the right axillary LN 1, and the spleen respectively, under the model M8. All sites found by model M2 were included in the model M8 (p$P < 0.95$). Therefore, even though these models were constructed differently, they produced congruent results for the identification of positively selected sites.

A different scenario was observed for the *pol* gene (Table 3). Only sequences isolated from FDCs from the pancreatic LN suggested a strong positive selection in this gene, with ω ratio ranging between 29.98 and 33.8 under the models M8 and M2 respectively. For the two other sLTs, $\omega = 1$ with both models. LRTs comparing M2 with

M1, and M7 with M8 were highly significant only for sequences from the pancreatic LN ($P < 0.001$). Two and three positively selected sites were identified by the Bayesian approach under the models M2 and M8 respectively in the *pol* gene for the pancreatic LN. All the sites detected by the model M8 were included in the model M2 ($pP < 0.95$).

I next analyzed which amino acid residues in gp120 trapped on FDCs were actually under positive selection (Table 4). Interestingly, the majority of residues under selection were different in the three different sLTs. For example, the residues under selection in the pancreatic LN were at positions 350, 381, and 406, while in the right axillary LN 1 they were at positions 318, 341, 359, and 430. This suggested the selective pressure was different in the two LNs. There were seven residues under selection in the spleen; all seven were different than the three residues under selection in the pancreatic LN. While three of the seven residues in the spleen correlated with sites under selection in the right axillary LN (i.e. 318, 359, and 430), the amino acids selected for at two of those sites were different (i.e. 318R and 430T). Analysis of the FDC-trapped *pol* data showed that only in the pancreatic LN was there a pressure sufficient to induce diversifying selection. Taken together, these data suggested that the pressure in all three sLTs examined was sufficiently different to select for different HIV-1 quasi-species.

FDC-trapped HIV-1 in different sLTs may be functionally different

Figures 1-8 demonstrated that FDC-trapped HIV-1 is highly compartmentalized between different sLTs. Identification of the sites under positive selection (Table 4) in the various sLTs also suggested that FDC-trapped HIV-1 may have been phenotypically different. Therefore, I sought to further test this hypothesis.

When FDC-trapped gp120 sequences were subjected to TCS network analysis (Figures 2-3) the sequences divided into two groups. This split was also apparent when the sequences were analyzed by phylogenetic methods (Figure 1), i.e. the topology of the tree consisted of two major branches. Reasoning that gp120 is responsible for the tropism of the virus (107-108), I postulated that the split of sequences into two groups may have been based on tropism. As the V3 loop appears to be the major determinant of cellular tropism (109-111), I looked more closely at the amino acids encoded by the sequenced nucleotides (Table 5).

A closer look at the V3 loop protein sequence revealed that all sequences in the upper branch of the tree in Figure 1 contained a basic residue (either a Lys or Arg) at position 25 of the V3 loop; all sequences in the lower branch contained the acidic Glu residue at the same position. Furthermore, 33 of the 35 sequences in the upper branch contained an in-frame insertion of three amino acids (Arg-Ile-Gly), that increased the length of the V3 loop to 38 residues and the net charge of the V3 loop by +1. In contrast, none of the 23 sequences in the lower branch contained the insertion. As a result of the difference in charge at position 25 and the in-frame insertion, the net charge of the V3 loop was approximately +3 greater for the sequences in the upper branch of the tree, compared with those in the lower branch. The V3 loop residues 19-22 also differed significantly between the two strains. The sequences in the lower branch contained the consensus SF162 (an R5 strain of HIV-1) sequence Ala-Phe-Tyr-Ala. However, for the sequences in the upper branch the dominant motif for residues 19-22 was Pro-Leu-Tyr-Val.

Interestingly, while sequences isolated from FDCs in the spleen and pancreatic LN were split approximately 1:1 between the two branches, sequences from the right axillary LN were found predominantly in the upper branch. Therefore, I expanded my analysis of the V3 loop to sequences isolated from FDCs in other sLTs, which included two other LNs from the right axillary site, a left axillary LN, and a mesenteric LN (Table 6). In the right axillary LNs there was a predominance (i.e. 90%) of quasi-species that contained a basic residue at position 25, coupled with the in-frame insertion. Additionally, the right axillary LNs were the only sites where I found a Lys at position 25 in the V3 loop in sequences trapped on FDCs. In all other sLTs tested there was an equal split between the two V3 loop motifs; 53% contained a basic residue at position 25, 47% an acidic residue at the same position.

I postulated that there may have been a selective pressure in the right axillary site that favored the predominance of the quasi-species with a more positively charged V3 loop. Flow cytometry data for the various sLTs demonstrated that there was a significant difference in the percentage of MØs in the right axillary LNs compared to all other sLTs examined (Figure 9). In right axillary LNs 1, 2, and 3, the $CD14^+$ population of cells ranged between 19.2 and 24.0 % (Figures 9a-9c). However, in the other four sLTs examined, the $CD14^+$ population of cells only ranged between 1.6 and 5.3 % (Figures 9d-9g). These data suggested that the selective pressures in different sLTs may have varied.

HIV-1 levels vary between FDCs, MØs, and T cells and different sLTs

Given the heterogeneous nature of HIV-1 trapped on FDCs, I investigated the differences in the virus between MØs and T cells isolated from different sLTs. Initially, I compared

differences in the amount of HIV-1 present in each site by assessing my ability to amplify the V1-V4 region of gp120 using nested PCR. As shown in Figure 10, there were striking differences in HIV-1 levels between MØs, T cells, and FDCs in an individual sLT. For example, in mesenteric LN 2 and the mediastinal LN, I amplified V1-V4 in the T cell population but not from either MØs or FDCs. However, in the renal/aortic LN, I amplified solely from the MØ fraction. These data suggested a restriction of virus flow between these three cell types, at least in some sLTs. All negative results were indicative of at least two independent experiments.

These data also revealed distinct differences in the pattern of HIV-1 levels between different sLTs. Perhaps of greatest interest were the differences observed when comparing sLTs within a LN chain. In the right axillary LN chain, I amplified V1-V4 from MØs in LNs 1 and 2, but not in LN 3; this despite the fact that these LNs were separated anatomically *in vivo* by a fraction of an inch. Also, in the two adjacent LNs obtained from the mesenteric site, I amplified V1-V4 in the T cells isolated from LN 2, but not in LN 1. My initial data demonstrated that FDC-trapped HIV-1 was compartmentalized (see Figures 1-8); these data suggested that the compartmentalization of HIV-1 may have been extended to other cell types in the sLTs.

Comparison of proviral gp120 sequences isolated from MØs in different sLTs

HIV-1 *env* sequences containing the C2-C3 regions from MØ cell lysates isolated from the spleen, right axillary LN 1, and the pancreatic LN were subjected to phylogenetic analyses (Figure 11). I observed that all sequences from the pancreatic LN MØs clustered on two branches of the tree. On one branch there were 8 clones, all of which were

sequences from the pancreatic LN. On the second branch there were 16 clones, 12 of which were sequences from the pancreatic LN.

I next sought to determine whether MØ sequences could be separated based on the residue at position 25 in the V3 loop (Table 7). Of the 58 sequences analyzed, all 19 sequences that contained the acidic Glu residue at position 25 clustered on the same branch, clearly separated from the remaining sequences. Interestingly, no sequences isolated from MØs in the pancreatic LN were found in this branch. The remaining 39 sequences all contained a basic residue (Lys or Arg) at position 25, and invariably, all contained the three amino acid in-frame insertion (Arg-Ile-Gly) in the V3 loop.

The MØ quasi-species that contained a basic residue at position 25 clustered on two separate branches (at the top and bottom of the tree). I sought to determine if a common motif separated these two branches. In the top branch 13 of the 14 sequences contained a Ser residue at position 9 in the V3 loop, while all sequences in the lower branch contained the consensus Arg at position 9. In addition, when I looked in the C3 region I observed that 13 of the 14 sequences in the upper branch contained a Q342K/R change and a G345E change. The phylogenetic tree data were supported by a TCS haplotype network analysis of the same sequence set (Figure 12).

Comparison of proviral gp120 sequences isolated from T cells in different sLTs

The *env* C2-C3 sequences from T cell lysates isolated from the spleen, right axillary LN 1, and the pancreatic LN were also subjected to phylogenetic analyses (Figure 13). Unlike FDC-trapped sequences and proviral sequences from MØs, T cell proviral sequences showed very little evidence of compartmentalization. Like FDC-trapped and MØ

sequences, T cell proviral sequences could be clearly divided based on the residue at position 25 in the V3 loop, and the presence or absence of the Arg-Ile-Gly insertion in the V3 loop (Table 8). Of the 58 sequences analyzed, 18 contained Glu at position 25 in the V3 loop. All 18 sequences were found in the bottom branch of the tree. The remaining 40 sequences all contained a basic residue (Lys or Arg) at position 25 and the three amino acid in-frame insertion (Arg-Ille-Gly) in the V3 loop. This insertion was absent in all 18 of the sequences found in the bottom branch of the phylogenetic tree.

Perhaps of greater significance was the unbalance of these two motifs in the two LNs when compared with the spleen. Of the 38 proviral sequences isolated from T cells in the pancreatic and right axillary LNs, 32 contained a basic residue at position 25 (i.e. 84%). However, in the spleen only 8 of the 20 sequences isolated from T cells contained a basic residue at position 25 (i.e. 40%). Again, the phylogenetic data were supported by haplotype network analysis of the same sequence set (Figure 14).

Comparison of HIV-1 in FDCs, MØs, and T cells from a single sLT

Having observed clear differences in the extent of compartmentalization of virus associated with FDCs, MØs, and T cells, I was interested in the genetic relationship of HIV-1 between the cell types in a single sLT. I first examined the relationship in right axillary LN1 (Figure 15). In this LN there was very little clustering of sequences based on cell type; in general it appeared that there was little restriction to the flow of virus between the three cell types in this sLT. This contrasted with the scenario in the pancreatic LN (Figure 16). In particular, the FDC-trapped sequences clustered together. For example, 11 of the 21 FDC sequences clustered to a single branch with just a little

mixing with T cell provirus and no mixing with MØ provirus. Several MØ proviral sequences also clustered together, i.e. haplotypes H47-H51. These results were demonstrated by both phylogenetic and haplotype network analyses (Figures 17-18). When I examined the relationship in the spleen, the difference when compared with right axillary LN 1 was even greater (Figure 19). In the spleen, 16 of the 17 sequences isolated from FDCs clustered on two branches with no mixing with sequences from either T cells or MØs. In addition, there was also some clustering of the MØ sequences, i.e. haplotypes H14-H17, H20, and H22. Again, these results were demonstrated by both phylogenetic and haplotype network analyses (Figure 20).

Comparison of FDC-trapped HIV-1 sequences with those isolated from a population of unfractionated cells from the same sLT

I reasoned that analysis of RNA from an unfractionated population of cells from a single sLT should primarily reflect cell-free virus particles and FDC-trapped virus in that same sLT. Therefore, I was interested to see how representative genetic sequences isolated from an unfractionated population of cells (referred to subsequently as "bulk sequences") were of FDC-trapped virus. In the pancreatic LN, I observed bulk sequences clustered with FDC-trapped sequences (Figure 21); although some FDC sequences appeared under-represented by bulk sequences, i.e. 1h3, 10e1, 8b5, 8b6, 6g8, 6h10, and 3d4. However, in the spleen there was a different pattern (Figure 22). All but one of the bulk sequences clustered on their own on a monophyletic branch of the tree, clearly separated from the FDC-trapped sequences.

It was also significant that almost all of the splenic bulk sequences (18 of 19) contained an acidic residue at position 25 in the V3 loop. This contrasted with the splenic FDC-trapped sequences where there were 10 sequences with an acidic residue and 9 with a basic residue at position 25.

Comparison of proviral sequences isolated from T cells and MØs with bulk sequences from the same sLT

I reasoned that analysis of DNA from an unfractionated population of cells from a single sLT should primarily reflect provirus from T cells and MØs from the same sLT. Therefore, I was interested to see how representative bulk sequences were of T cell and MØ provirus (Figures 23-24). My results demonstrated that a significant proportion of proviruses from fractionated cells were not represented by the bulk sequences. In the pancreatic LN there was a population of proviruses isolated from MØs, i.e. 6e7, 6e3, 6h10, 6g10, 6h8, 6h4, 6e4, and 6f9, which were unique and did not cluster with any bulk sequences. In the spleen there was a similar pattern that also included T cell proviruses. In fact, the majority of the bulk sequences from the spleen, i.e. 20, 23, 10, 18, 22, 1, 2, 7, 14, and 4, appeared to represent a population of cells that were different from the T cells and MØs isolated.

DISCUSSION

FDC-trapped HIV-1 is compartmentalized

FDCs trap antigens, including virus particles, opsonized with specific antibody and/or complement proteins. FDCs accomplish this by virtue of a high level of expression of the CD21 and CD32 cell surface receptors (44-45). Early work in this field demonstrates that when a host is challenged with a conventional protein antigen, the antigen is trapped in a highly localized manner to the follicles (GCs) of only the draining LNs (112). That is, with conventional, non-replicating antigen there appears to be a highly specific compartmentalization, so that antigens trapped on FDCs in one LN may be much different than those trapped in another LN.

However, HIV-1 is unlike conventional protein antigen. Shortly after infection HIV-1 disseminates throughout the lymphatic system and is trapped in enormous quantities on the FDC networks in sLTs (58). The virus in the sLTs appears to be in a highly dynamic state. In many cases, the initiation of HAART has an immediate impact on the viral burden in the sLTs (37). In addition, $CD4^+$ T cells and several other cells susceptible to HIV-1 infection are thought to circulate freely through the lymphatic system. There are no apparent restrictions on this circulation that would prevent these cells from being infected in one sLT, migrating to another unrelated sLT, where they could express new virus; this virus would be reflective of the virus in the first sLT in which the cell was initially infected. Therefore, the assumption has arisen that in contrast to conventional antigen, there is very little compartmentalization of HIV-1 between sLTs. As a result, it is believed that virus trapped in one LN is to a large degree homologous

with virus trapped in another LN; and by inference, that the genetic diversity of HIV-1 in one LN is indicative of the diversity in all sLTs.

However, a number of studies suggest that this may be an overly simplistic view of the situation. For some time it has been recognized that HIV-1 is compartmentalized between different tissues including brain, lungs, sLTs as a whole, gastrointestinal and genital tracts, and blood (15, 69-80). It is postulated that selective pressures imposed by the immune system, drug therapy, and/or cellular tropism, vary between the different tissues, and that these differing pressures give rise to sites of independent viral evolution. Of note, these studies also include evidence that virus in the blood, which is intimately connected with the lymphatic system, may not represent virus in sLTs (85).

Of greater significance to this present study, is evidence that subpopulations of HIV-1 exist within a single tissue. Genetically distinct quasi-species appear to exist in different GCs in the spleen, so that each splenic white pulp appears to be a unique site of viral evolution (69, 73, 113). In addition, HIV-1 appears to compartmentalize within the brain, so that distinct quasi-species can be detected in different parts of the brain such as the frontal lobe, basal ganglia, and medial and nonmedial temporal lobes (79). All this evidence suggests that even within a tissue compartment there may be a restriction to the viral genetic flow. Finally, because of the ability of FDCs to retain infectious virus on their surface for long periods of time (54, 60), coupled with the sessile nature of FDCs, I reasoned that viral information may not flow freely from one LN to another; at least not that information which is trapped on FDCs.

In this study, I carried out an extensive investigation into the genetic diversity of HIV-1 that exists between different sLTs. My initial studies focused more specifically on

the relatedness of virus trapped on FDCs in those sLTs. To my knowledge, this is the first study of its kind, in which not only were multiple single sLTs examined (both related and unrelated), but also where FDCs were isolated from the various sLTs for comparison. By examining multiple genetic sequences from each site, I sought to determine whether there is compartmentalization of HIV-1 between sLTs. In this report I have shown clear evidence that there is in fact a high degree of compartmentalization of HIV-1 trapped on FDCs. Examination of sequences obtained from three different sLTs indicated that the majority of sequences clustered with other sequences from the same sLT. For example, in Figure 2, haplotypes 15-23 (pancreatic LN) were more closely related to each other than to any sequences from a different sLT. This was also true for haplotypes 4-11 and 45-51 from the spleen. This suggests that most of these sequences have evolved from virus within the same sLT, and that therefore there was a restriction to the viral genetic flow between these sites. It is also interesting to note that there were many long branches in this network, especially when V1-V4 sequences were analyzed (Figure 3). These data suggest great diversity among the sequences in this haplotype network. The sequences at the ends of the branches most likely represent the most recent virus that was present in a given sLT; those sequences from which they appear to have evolved likely represent what was archived virus. This is significant because one of the hallmarks of a viral reservoir is that sequences sampled from a reservoir exhibit a greater degree of diversity when compared to sequences sampled from a non-reservoir, reflecting both recent and historical virus (64). Previously, our laboratory has shown evidence which demonstrates that the FDC is a long-term reservoir of infectious HIV-1 particles (54, 60). Based on these new data, I postulate that FDCs in different sLTs are independent sites where there

is continual trapping of a constantly evolving virus over a long period of time. This haplotype network provides good evidence that FDCs in different sLTs are acting as distinct and separate viral reservoirs.

Bayesian phylogenetic analysis of the relationship of *pol* sequences in five different sLTs, three of which were LNs in the same chain taken from the right axillary site, indicated that all 17 *pol* sequences in the spleen clustered in a monophyletic group and exhibited no mixing with sequences taken from the other sLTs (Figure 7). Therefore, FDC-trapped *pol* sequences in the spleen exhibited even greater compartmentalization than did gp120 sequences.

Natural selection is the process whereby beneficial alleles predominate in the population over time. In contrast, genetic drift is the tendency of an allele to vary randomly in frequency due to statistical variation alone. Unlike gp120, FDC-trapped *pol* sequences from the spleen appear to have been under no selective pressure. Therefore, I reason that these sequences were compartmentalized as a result of genetic drift as opposed to differing selective pressures in the tissues.

Given that the spleen filters blood as opposed to the LNs which drain lymph, the complete lack of mixing of splenic *pol* sequences with those in the LNs suggests there may be a barrier preventing the free flow of virus between the blood and the lymph. Relative to this hypothesis, Rosenberg and Janossy have suggested that changes in the blood may be a poor predictor of what is occurring in the tissues (115). Clearly the FDC-trapped HIV-1 in the spleen differed from that trapped in other sLTs; both gp120 and *pol* sequence data support this conclusion. Perhaps of greater significance, these data also demonstrated that there is clear compartmentalization of FDC-trapped *pol* sequences

even among related sLTs, i.e. LNs taken from the same LN chain. This suggests that there may also be a significant restriction to the flow of virus between two very similar sLTs, even in the same anatomical site, a fact not previously appreciated.

Compartmentalization creates a more diverse viral population

I analyzed what effect the observed compartmentalization had on the diversity of HIV-1 trapped in sLTs. My results demonstrated that FDC-trapped HIV-1 taken from just three sLTs is considerably more diverse than HIV-1 taken from a single sLT, even when the three sLTs are taken from the same anatomical site (Table 1). The FDC networks in different sLTs appear to be sites of independent virus evolution. By evolving in independent sites, the population of HIV-1 becomes genetically diverse. With such diversity, the virus population possesses a greater ability to respond more effectively to immune pressure, therapy, or in the latter stages of disease, the depletion of target cells required for continued infection. Currently, much of the information regarding HIV-1 in sLTs is inferred by analyzing the virus in just a single sLT (71, 80-88), or even the blood (89-91). Recognizing that there are approximately 500 LNs in the body, these data suggest that estimating viral diversity based on sequences from a single sLT may greatly underestimate the total viral diversity in all sLTs in an infected individual.

Compartmentalized virus may be functionally distinct

The data presented gave a clear indication that FDC-trapped HIV-1 was genetically distinct between sLTs. However, it is a harder proposition to determine whether FDC-trapped virus was also functionally distinct based purely on DNA sequence. In spite of

this, a few findings suggest it may have been. First, in an earlier study conducted in our laboratory, it was demonstrated in one patient that a major non-nucleoside RT inhibitor resistance mutation, K103N, was found in 18 of 18 sequences cloned from FDC-trapped HIV-1 in a single LN, but in 0 of 10 sequences trapped on splenic FDCs (unpublished data). These data suggested that while some specific drug-resistant virus may be present in LNs, it may not necessarily be detected on splenic FDCs. Second, PAML analysis of FDC-trapped HIV-1 in sLTs from patient N1_205 indicated that gp120 in all sLTs studied was under positive selection, and that the amino acid residues selected for, varied between sLTs (Table 4). In addition, *pol* in the pancreatic LN was also under positive selection, in spite of the fact that this patient was therapy naïve. Presumably, amino acid residues that have been positively selected for confer some functional benefit to the virus. In the case of Env protein, this benefit is likely to be immune escape or perhaps altered infectivity. The fact that different residues were selected for in different sLTs suggests that these quasi-species were functionally different.

The third finding that suggests there may be functional differences in FDC-trapped HIV-1 comes from the analysis of the V3 loop. My results demonstrated that in patient N1_205, in all sLTs examined, *env* sequences cluster based on two V3 loop motifs common to the single patient. The first motif exhibited a great deal of homology with the V3 loop of SF162, an R5 strain of HIV-1. Notably, position 25 in this motif was invariably the acidic residue Glu. Interestingly, a number of reports suggest that a negative charge at position 25 in the V3 loop is a good predictor of R5 tropism (6, 8, 11). In contrast, the second motif invariably contained a basic residue at position 25 (either Lys or Arg). Numerous investigations have confirmed that in many cases the mutation of

a negatively charged residue at position 25 in the V3 loop to a positively charged one, converts an R5 strain into an X4 strain (9-11). In addition, in this patient in almost all instances, the change to a basic residue at position 25 was accompanied by an in-frame insertion of three amino acids (Arg-Ile-Gly). As a result of the difference in charge at position 25 and the in-frame insertion, the net charge of the V3 loop was approximately 3-plus greater for the quasi-species that contained a basic residue at position 25. Several reports also demonstrate that increased net charge in the V3 loop is a hallmark of X4 tropic HIV-1 (6, 8-12). Finally, this second motif regularly contained three more amino acid changes in the V3 crown compared with the first motif, which may conceivably have affected cellular tropism. The phylogenetic trees and TCS networks showed clear separation based on these V3 loop motifs. Most notably, the branches in the various trees and networks, although generated from approximately 570 bp, could in all cases, be cleanly separated based on a difference at just one amino acid, i.e. position 25 in the V3 loop. Taken together these data suggested that the major branches of the phylogenetic trees and haplotype networks represented isolates of virus with differing tropism.

With this background, it is interesting then, that in all the right axillary LNs examined, FDC-trapped HIV-1 predominantly contained the more positively charged V3 loop motif. This was in contrast to all the other sLTs examined, where I observed an approximate 1:1 ratio of the two strains. If the two V3 loop motifs really do represent functionally different virus, it would appear that in this patient, FDC-trapped viruses in right axillary LNs, taken as a whole, were functionally different from FDC-trapped virus in other sLTs.

Possible explanations for compartmentalization of FDC-trapped HIV-1

The circumstances surrounding the trapping of HIV-1 on FDCs are still poorly understood. For example, it is unknown which cell type(s) is producing the bulk of the trapped virus. Therefore, it is difficult to postulate what is causing the compartmentalization of FDC-trapped virus. However, the data may give a clue as to the nature of the cell that produces the virus trapped by FDCs, and in turn why compartmentalization occurs.

The data may suggest that FDC-trapped virus is infecting a cell that is held in a specific germinal center (GC) for an extended period of time, where it is both infected and subsequently expresses new virus in the same GC. Presumably, this newly expressed virus could be trapped on the same local FDCs that presented the virus that caused the initial infection. The infected cell may then either die without leaving the site, or migrate from the GC without passing through anymore sLTs. This postulate finds support in a recent study that demonstrates that, in the spleen at least, the majority of FDC-trapped HIV-1 viral particles are produced locally, rather than from trapping circulating viruses or immune complexes (116). These conditions would seem to allow for the independent evolution of HIV-1 in different sLTs, which is necessary to explain the observed compartmentalization.

Germane to this argument, GC T cells, which are found in close proximity to FDCs, have recently been shown to have up-regulated CXCR4 expression (117). This increased CXCR4 expression renders the GC T cell more susceptible to infection by X4 isolates of HIV-1. Yet a follow-up study demonstrates that GC T cells actually exhibit a decreased ability to migrate to SDF-1, the natural ligand for CXCR4 (118). Therefore, the GC T cell

can be characterized as a cell that is susceptible to infection by FDC-trapped HIV-1, which at the same time is trapped in the GC microenvironment for an extended period of time.

The other, perhaps more obvious, explanation for why FDC-trapped HIV-1 is compartmentalized is that selective pressures in sLTs vary, creating unique environments that drive the differences in viral evolution. In support of this idea is the significant difference in the percentage of MØs in the right axillary LNs when compared with the other sLTs (Figure 9). These data suggest that the immune pressures in the right axillary LNs of this patient may have been significantly different to those in other sLTs. I imagine it is possible that the state of immune activation, the cellular mix, cytokine production, and other additional immune pressures may all vary significantly between different sLTs. Also relevant to this idea are the findings that the mechanism of trapping and/or retaining ICs by FDCs in the spleen may be different than that in LNs (114). Given that complement is so abundant in the blood, it may be that trapping in the spleen is more complement-dependent than it is in the LNs. If this were the case, it may allow the selection of a variant HIV-1 Env in the spleen that more readily binds complement. I reason that differences in the mechanisms of viral trapping may also drive the evolution of a spleen-specific virus, or at least spleen-specific Env proteins.

These two postulates need not be mutually exclusive. The selection data presented in Table 4 and already discussed above would seem to support the idea that there were different pressures in the different sLTs driving the positive selection of different residues in gp120; e.g. 6 of the 7 residues under positive selection on FDCs in the spleen were not selected for in the other sLTs. However, it appears for the most part that FDC-trapped *pol*

was not under positive selection. As mentioned above, compartmentalization of *pol* may have been due to genetic drift rather than a selective environment. Therefore, a restricted migration of the principal HIV-1 producer cell in the GC may explain *pol* compartmentalization, while differing selective environments may explain gp120 compartmentalization.

MØ and T cell provirus studies

Phylogenetic and haplotype network analyses revealed that MØ provirus was compartmentalized to a degree (Figures 11 and 12), though not to the same extent as FDC-trapped HIV-1. Interestingly, in the FDC study, sequences isolated from splenic FDCs showed the greatest degree of compartmentalization; in the MØ study, provirus from MØs isolated from the pancreatic LN showed the greatest degree of compartmentalization. This would seem to suggest that the factors that affected the compartmentalization of FDC-trapped HIV-1 were different, at least to some degree, to those that were driving MØ provirus compartmentalization. In contrast to FDC-trapped HIV-1 and MØ provirus, it appears as though there was very little compartmentalization of T cell provirus (Figures 13 and 14); although haplotypes 39-45 (spleen) showed some clustering.

The differences in the degree of compartmentalization for the three cell types may thus be summarized as follows: FDC-trapped HIV-1 > MØ provirus > T cell provirus. This order may in part be a reflection of the mobility of the three cell types within the lymphoid system; FDCs being sessile in nature, T cells presumably having the greatest

degree of freedom to migrate through different sLTs, and MØs having a degree of mobility somewhere in between the two.

The question of whether MØ and T cell provirus was functionally different in different sLTs was approached by using one of the ideas used to address FDC-trapped virus functionality, i.e. differences in the V3 loop motifs. Table 7 summarized the MØ provirus V3 loop sequence data. In the pancreatic LN, all 20 sequences isolated contained the more positively charged V3 loop motif. In the spleen and right axillary LN 1, there was an approximate 1:1 ratio between the two motifs. Therefore, if the two V3 loop motifs represent different Env phenotypes, MØ provirus in the pancreatic LN of this patient may have been functionally different than that in other sLTs.

In the T cells I saw a predominance of the more positively charged V3 loop motif in provirus isolated from the LNs. In contrast, the majority of infected T cells from the spleen harbored provirus with an acidic residue at position 25 in the V3 loop (Table 8). Again, if the two V3 loop motifs represent genuinely different phenotypes, given that $CD4^+$ T cells are the main producers of HIV-1, these data indicated that there may have been significant differences in the functionality of the virus produced in the LNs versus the spleen.

Sequences from an unfractionated population of cells fail to adequately reflect all quasi-species in sLTs

The majority of studies into sLT-associated HIV-1 take the straightforward approach of isolating RNA and/or genomic DNA from a tissue homogenate (71, 80-88). My results suggested that this approach may miss important populations of quasi-species. I reasoned

that isolating RNA should primarily represent either FDC-trapped HIV-1, or cell-free virions in the lymph or the blood. When I compared sequences isolated from an unfractionated cell population from the spleen ("bulk" or unfractionated sequences), with specific FDC-trapped sequences from the spleen, I found that 18 of the 19 bulk sequences clustered on a single branch without any mixing with the FDC-trapped sequences (Figure 22). I postulate that this population (i.e. the bulk sequences) is representative of cell-free virions in the blood, rather than FDC-trapped virus particles. This would also be consistent with reports in the mouse that tissue homogenization destroys FDCs. This being the case, the nature of these bulk sequences becomes very interesting. When I analyzed what V3 loop motif was common among the 18 bulk sequences in the monophyletic branch, I found that they all exhibited the motif containing an acidic residue at position 25, perhaps indicating an R5 tropic strain of virus. This may suggest that the virus present in the blood of this patient at the time of death was predominantly R5 in nature. Yet in the sLTs I observed a mix of both V3 loop motifs. In fact, as has already been shown, in some sLTs the more positively charged motif predominated in some cell types. If my postulates regarding tropism are correct, this may indicate that the blood may not always be an accurate predictor of whether a tropism shift in a patient has occurred or not. Figure 21 demonstrates that in the LNs as well, bulk RNA sequences may under-represent populations of FDC-trapped quasi-species. In this phylogenetic tree it can be seen that 7 FDC-trapped sequences on one monophyletic branch are represented by only one bulk sequence.

It appears that just as bulk RNA sequences may be an inadequate representation of FDC-trapped HIV-1, bulk DNA sequences from a single sLT may fail to fully represent

the genetic variation of proviruses in MØs and T cells (Figures 23-24). In the pancreatic LN there was a population of 8 MØ proviruses that clustered on a monophyletic branch. These sequences exhibited no mixing with the bulk DNA sequences from the pancreatic LN. In the spleen there was a population of 9 MØ proviruses and 12 T cell proviruses that clustered on a monophyletic branch. This significant population (i.e. more than 50% of the MØ and T cell proviruses analyzed) was only represented by one of the bulk DNA sequences. The data from these two sLTs (one LN and the spleen) suggest that sequencing virus isolated from a tissue homogenate may miss significant populations of quasi-species in MØs and T cells.

In summary; shortly following infection of an individual with HIV-1, the virus is trapped on FDCs in massive quantities (58). Contrary to common assumptions, I have shown that the nature of this trapped virus may be highly compartmentalized. It also appears that this compartmentalization has a significant impact on viral diversity in sLTs. I have also shown that this compartmentalization may be extended to other cells found in sLTs, and that sequencing unfractionated cells may poorly represent the diversity of quasi-species in sLTs.

I believe my data demonstrate that the viral dynamics in sLTs are far more complex than currently appreciated. Presently, HIV-1 disease prognosis is evaluated based on the nature of virus in the blood, or occasionally virus isolated from a single sLT biopsy homogenate. These studies suggest that important quasi-species in the sLTs may never be detected in the blood. In particular, my data raise the possibility that while a tropism switch from an R5 to an X4 strain of virus may occur in the sLTs, this major marker of disease progression may never be detected in blood samples. In addition, these studies

support the hypothesis that FDCs are a dangerous, long-term reservoir of HIV-1. I believe that therapeutic strategies designed to eliminate virus from the host need to give far greater consideration to the significant contributions made by FDCs to HIV-1 pathogenesis.

ABBREVIATIONS

Ab, antibody; **AIDS**, acquired immunodeficiency syndrome; **BMCMC**, Bayesian Markov Chain Monte Carlo; **bp**, base pairs; **C**, constant region domain of HIV-1 Env; **CCR5**, CC chemokine receptor 5; **CNS**, Central Nervous System; **CR2**, complement receptor 2; **CXCR4**, CXC chemokine receptor 4; **ds**, double stranded; **Env**, gp160 envelope protein; **FcγRII**, Fcγ receptor II; **FDCs**, follicular dendritic cells; **GC**, germinal center; **GC T cells**, germinal center $CD4^+/CD57^+$ T cells; **HAART**, Highly Active Anti-Retroviral Therapy; **HIV**, human immunodeficiency virus; **ICs**, immune complexes; **Ig**, immunoglobulin; **LNs**, lymph nodes; **LRT**, Likelihood Ratio Test; **ML**, Maximum Likelihood; **MØs**, macrophages; **PCR**, polymerase chain reaction; **pol**, HIV-1 polymerase; **R5**, CCR5 tropic strain of HIV-1; SDF-1, stromal-cell derived factor 1; **RT**, HIV-1 reverse transcriptase; **RT-PCR**, reverse transcription-PCR; **sLTs**, secondary lymphoid tissues; **V**, variable region domain of HIV-1 Env; **V3 loop**, variable region 3 domain of HIV-1 Env; **X4**, CXCR4 tropic strain of HIV-1; **X4R5**, dual tropic strain of HIV-1.

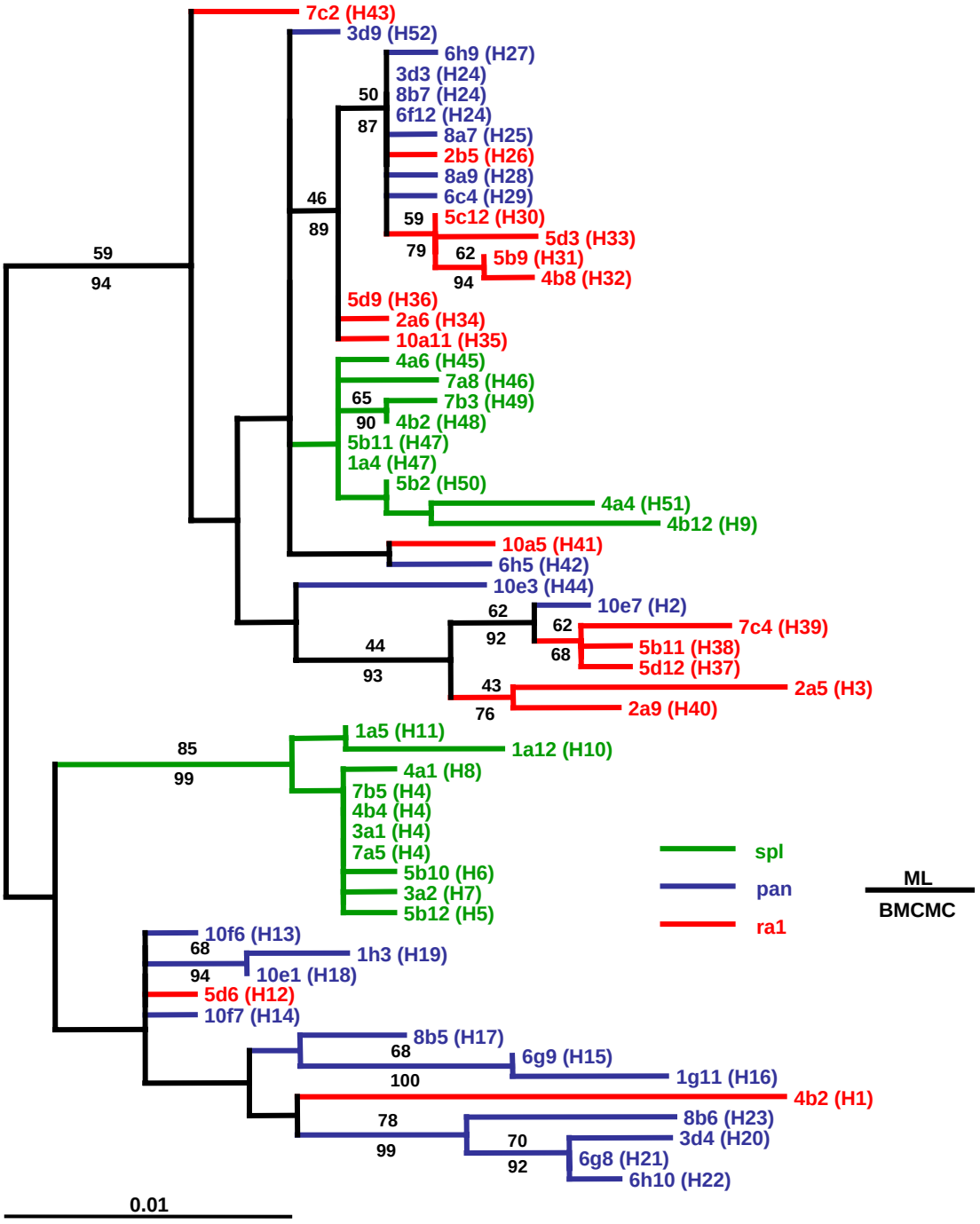

Figure 1. FDC-trapped gp120 is compartmentalized between different sLTs. gp120 C2-C3 sequences from FDCs isolated from a splenic fragment (**spl**), and pancreatic (**pan**) and right axillary (**ra1**) LNs were subjected to both Maximum Likelihood and Bayesian phylogenetic analyses. Maximum Likelihood bootstrap values (**ML**) appear above the branches and Bayesian Markov Chain Monte Carlo (**BMCMC**) inference values below the branches. Haplotype designations from the corresponding TCS network (Figure 2) appear in brackets (H) following the clone label at the end of branches. See also Table 5.

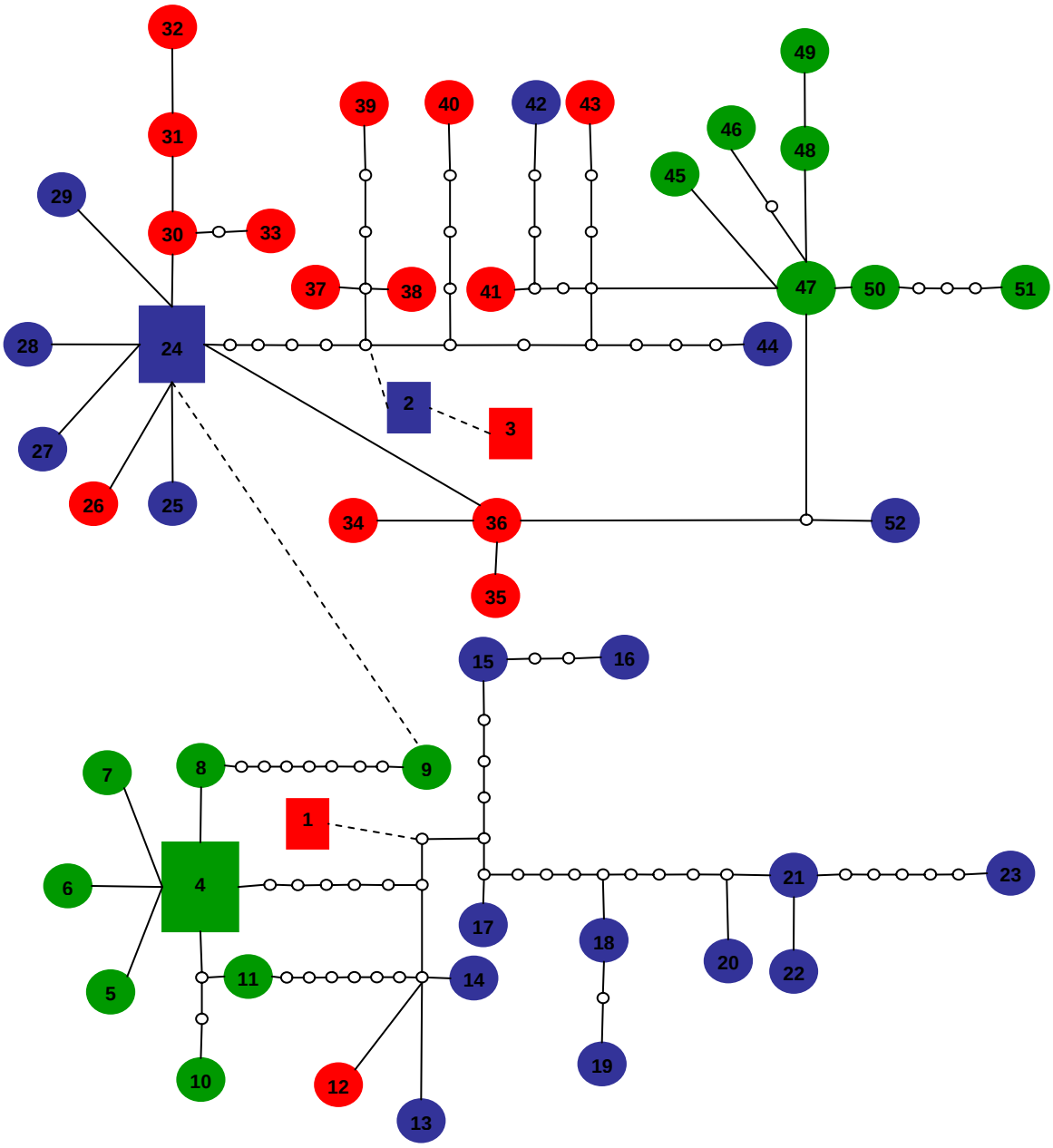

Figure 2. FDC-trapped gp120 is compartmentalized between different sLTs. C2-C3 sequences from FDCs isolated from a splenic fragment (**spl**), and pancreatic (**pan**) and right axillary (**ra1**) LNs were subjected to TCS network analysis. Colored squares (putative out groups) and circles represent actual cloned sequences, the sizes of which are proportional to the number of clones with the same sequence. Each open circle represents a putative quasi-species in the evolutionary pathway. The solid lines connecting a network suggest two quasi-species can be connected with at least a 95% degree of confidence. The dashed lines in a network represent a more tenuous connection. Haplotype designations are arbitrary and correspond to the numbers in brackets (H) in the corresponding phylogenetic tree (Figure 1).

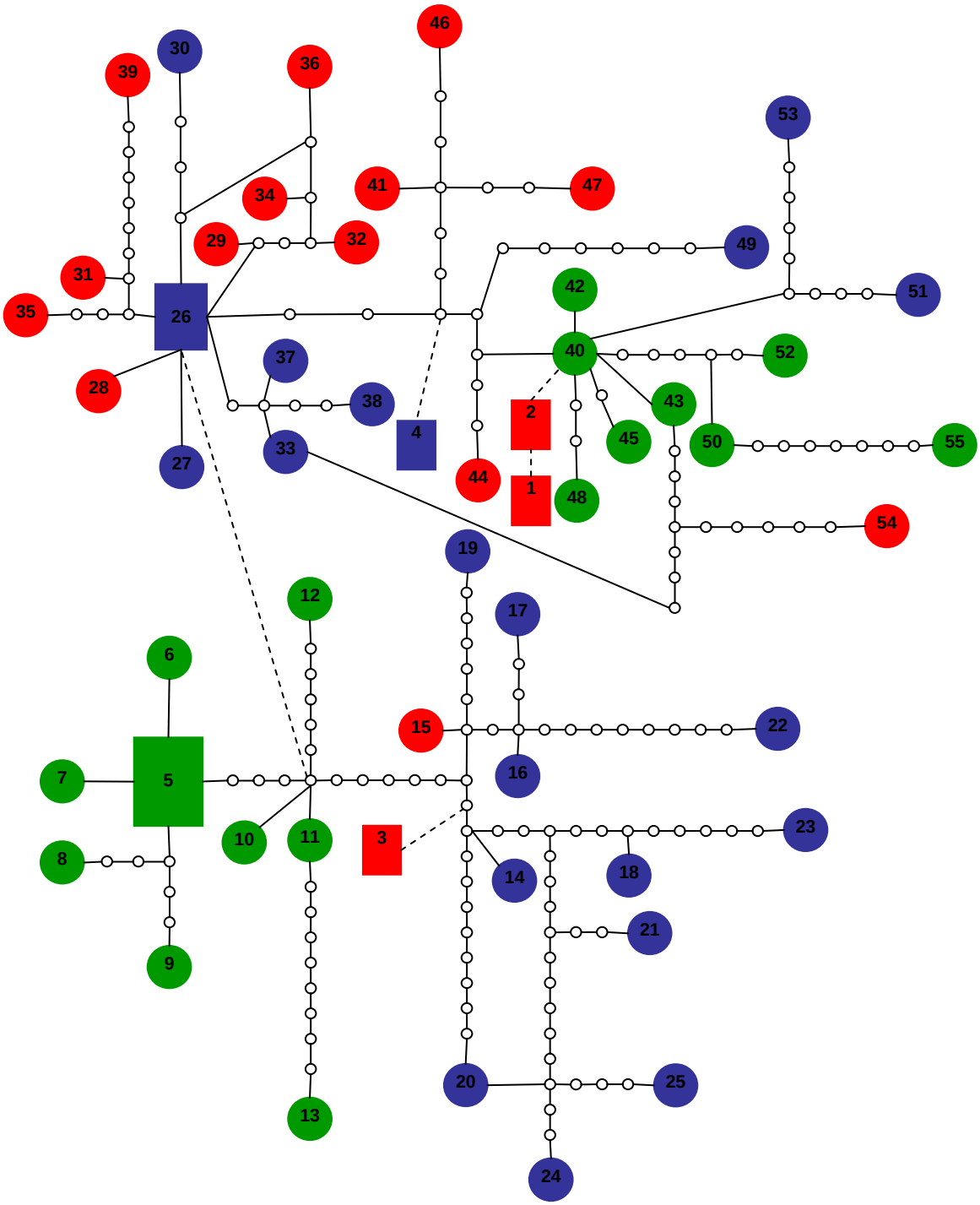

Figure 3. FDC-trapped gp120 is compartmentalized between different sLTs and highly diverse. V1-V4 sequences from FDCs isolated from a splenic fragment (**spl**), and pancreatic (**pan**) and right axillary (**ra1**) LNs were subjected to TCS network analysis. Details of how to read the TCS network can be found in the materials and methods chapter and more briefly in the Figure 2 legend. Haplotype designations are arbitrary.

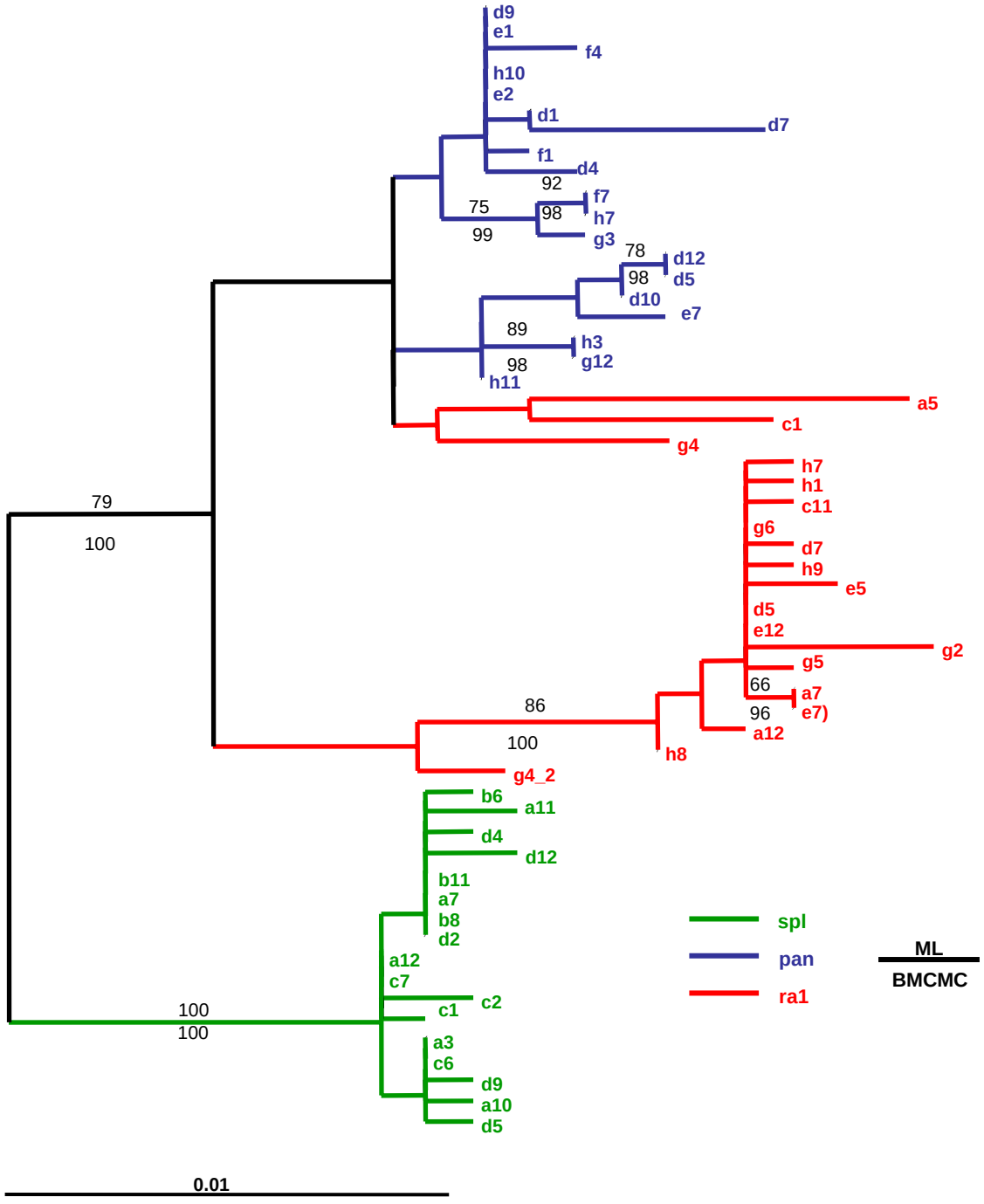

Figure 4. FDC-trapped HIV-1 *pol* is highly compartmentalized between different sLTs. *pol* sequences from FDCs isolated from a splenic fragment (**spl**), and pancreatic (**pan**) and right axillary (**ra1**) LNs were subjected to both Maximum Likelihood and Bayesian phylogenetic analyses. Maximum Likelihood bootstrap values (**ML**) appear above the branches and Bayesian Markov Chain Monte Carlo (**BMCMC**) inference values below the branches.

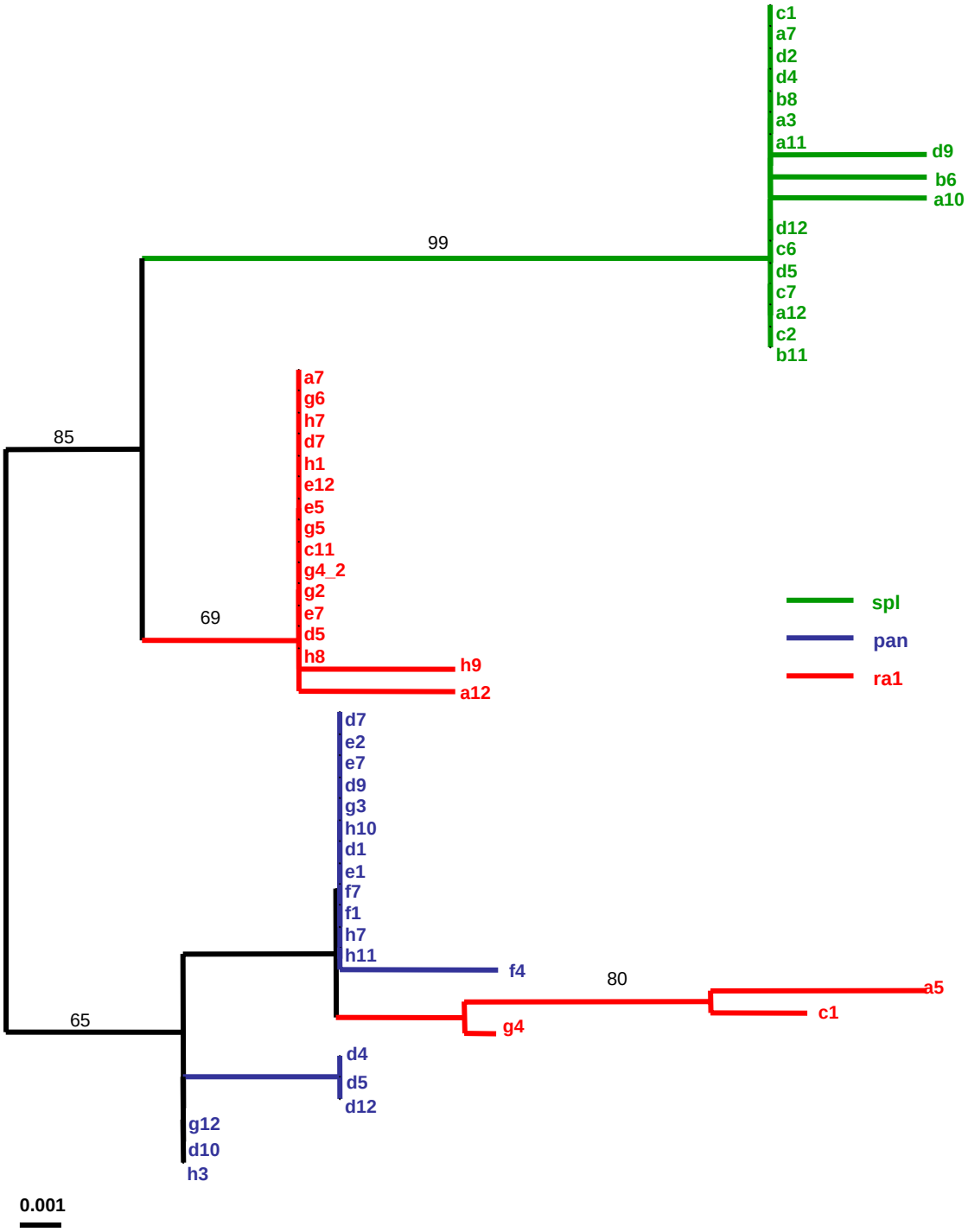

Figure 5. FDC-trapped HIV-1 protease is highly compartmentalized between different sLTs. Protease sequences from FDCs isolated from a splenic fragment (**spl**), and pancreatic (**pan**) and right axillary (**ra1**) LNs were subjected to Neighbor Joining phylogenetic analyses. Neighbor Joining bootstrap values appear above the branches. Clone designations correspond to clones in Figures 4 and 6.

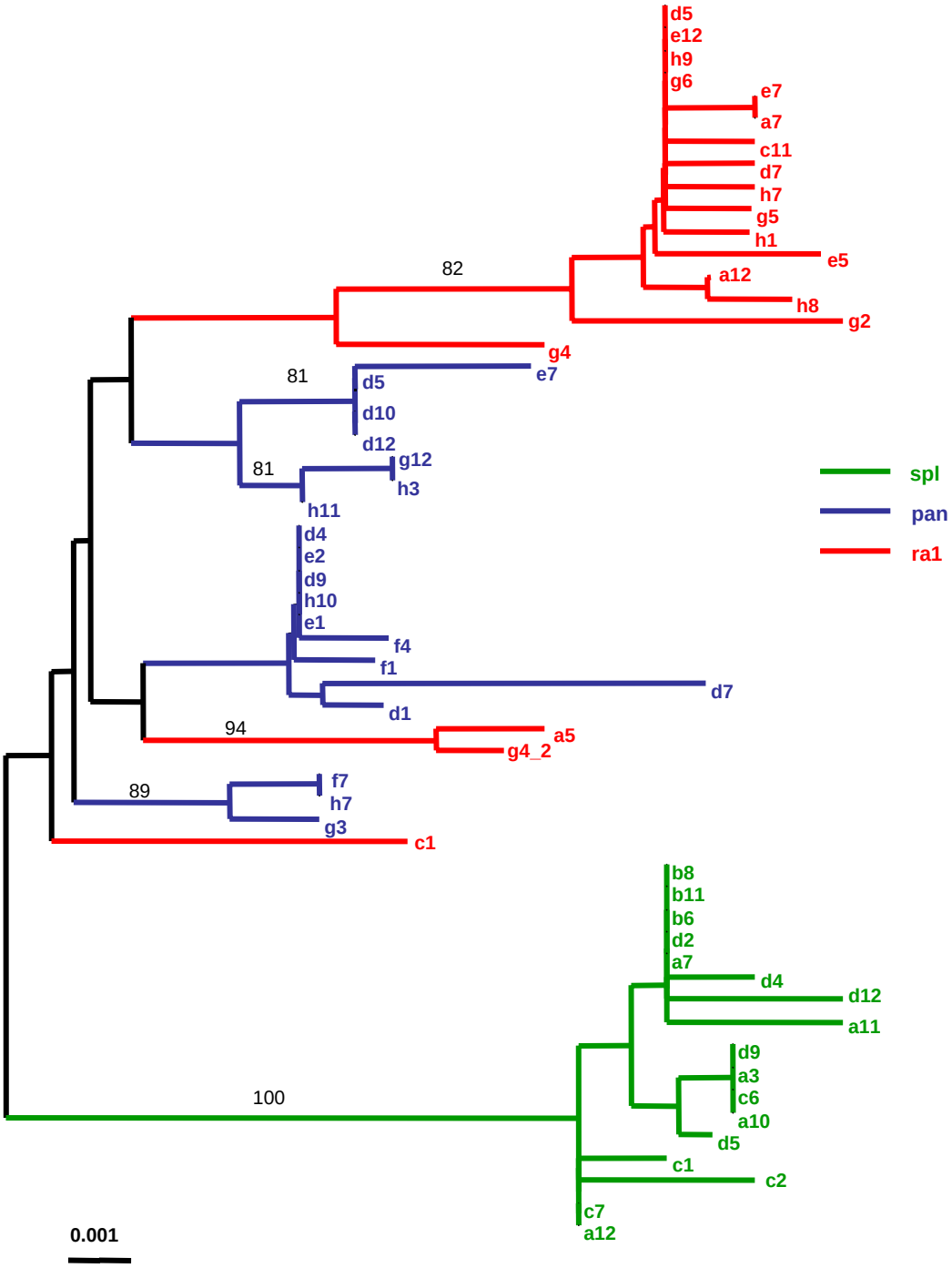

Figure 6. FDC-trapped HIV-1 RT is highly compartmentalized between different sLTs. RT sequences from FDCs isolated from a splenic fragment (**spl**), and pancreatic (**pan**) and right axillary (**ra1**) LNs were subjected to Neighbor Joining phylogenetic analyses. Neighbor Joining bootstrap values appear above the branches. Clone designations correspond to clones in Figures 4 and 5.

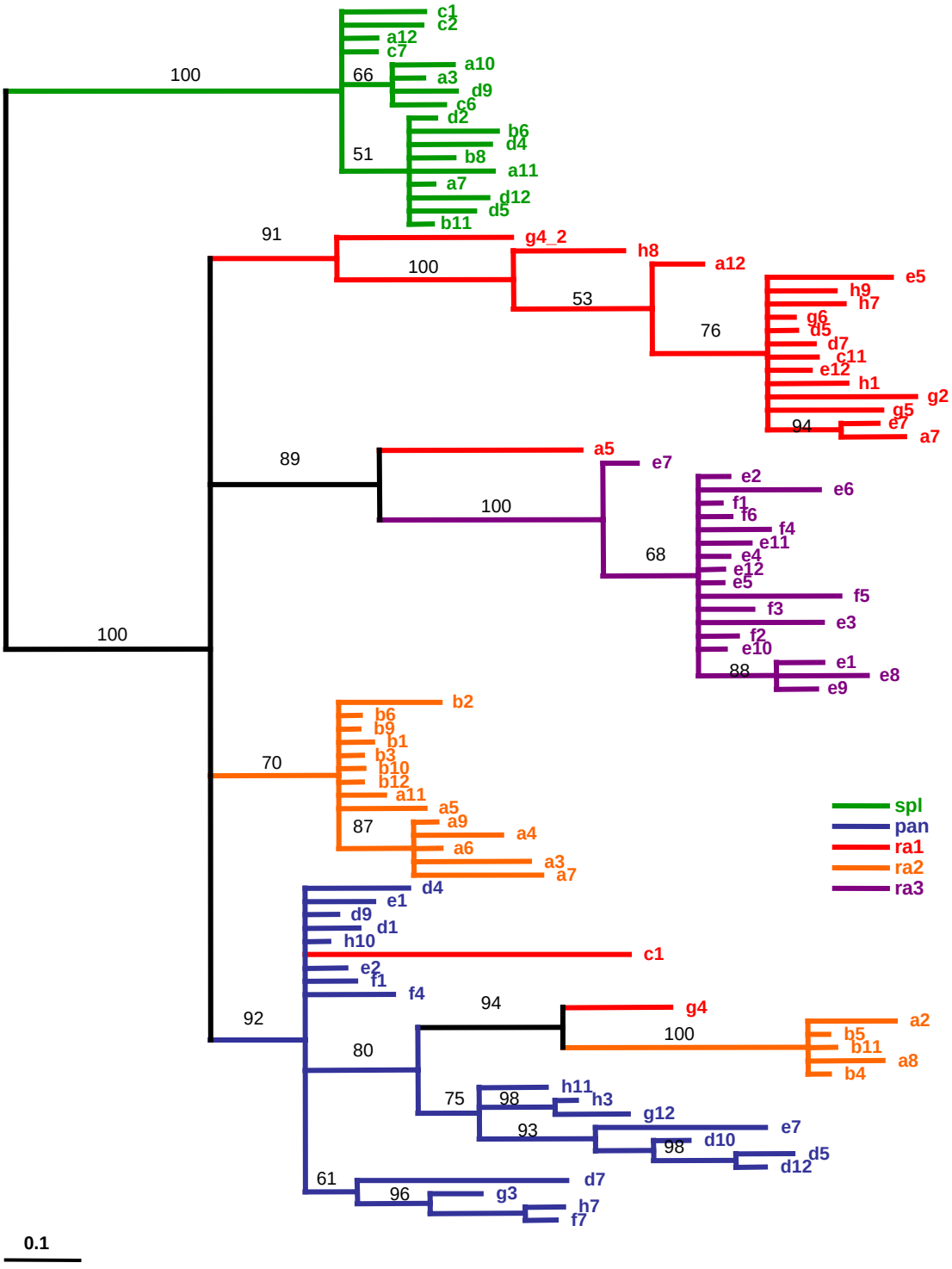

Figure 7. FDC-trapped HIV-1 *pol* is highly compartmentalized between related sLTs. *pol* sequences from FDCs isolated from a splenic fragment (**spl**), and right axillary 1 (**ra1**), right axillary 2 (**ra2**), right axillary 3 (**ra3**), and pancreatic (**pan**) LNs were subjected to Bayesian phylogenetic analysis. Bayesian Markov Chain Monte Carlo inference values appear above the branches.

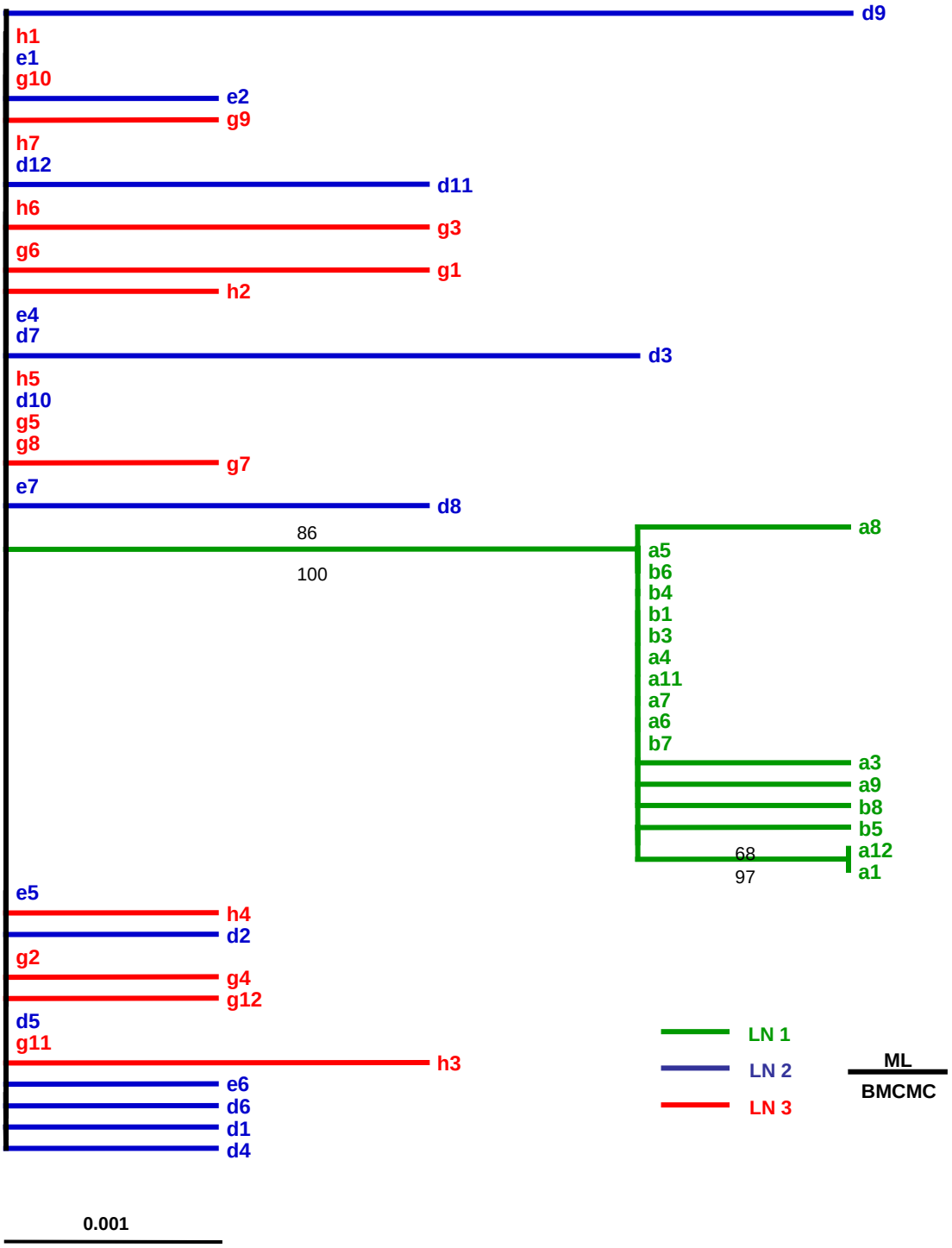

Figure 8. FDC-trapped HIV-1 *pol* in a second patient (N2_520) is compartmentalized between different sLTs. *pol* sequences from FDCs isolated from three LNs (**LN 1**), (**LN 2**), and (**LN 3**) were subjected to both Maximum Likelihood and Bayesian phylogenetic analyses. Maximum Likelihood bootstrap values (**ML**) appear above the branches and Bayesian Markov Chain Monte Carlo (**BMCMC**) inference values below the branches.

Table 1. Estimates of Watterson's genetic diversity (θ_w) calculated for sequences cloned from FDCs in various sLTs.

Source of FDCs	Region of HIV-1	
	pol	gp120
N1 205		
Right axillary LN 1	0.01079	0.01993
Pancreatic LN	0.00591	0.01594
Spleen	0.00377	0.01044
3 sLTs combined	**0.01612**	**0.02430**
Right axillary LN 1	0.01079	0.01993
Right axillary LN 2	0.00677	0.01964
Right axillary LN 3	0.00313	0.01551
3 sLTs combined	**0.01423**	**0.03043**
N2 521		
LN 1	0.00173	-
LN 2	0.00483	-
LN 3	0.00335	-
3 sLTs combined	**0.00802**	-

Table 2. Log-likelihood values and ML estimates of parameters ω (dN/dS), p (proportion of sites), and n (number of positively selected sites) for FDC-trapped gp120 in patient N1 205.

	Source of FDC-trapped gp120			
	Panc LN	Rt Ax LN1	Spleen	3 sLTs combined
MO lnL	-1672.74	-1798.05	-1498.11	-2410.32
ω	0.4351	0.3874	0.7664	0.4046
M1 lnL	-1646.70	-1766.62	-1485.00	-2333.92
M2 lnL	-1632.82	-1751.40	-1468.50	-2300.03
ω	7.9768	8.4174	8.4146	7.3430
p2	0.0524	0.0364	0.1164	0.0423
n	3 (3)	4 (4)	24 (7)	7 (7)
M3 lnL	-1632.63	-1750.53	-1468.50	-2299.98
ω	9.2336	13.6554	8.4146	7.1584
p2	0.0411	0.0175	0.1164	0.0432
n	30	21	24	7
M7 lnL	-1646.98	-1766.62	-1485.86	-2334.59
M8 lnL	-1632.84	-1751.49	-1468.50	-2300.25
ω	8.2564	9.0749	8.4146	7.1475
p1	0.0504	0.0332	0.1164	0.0432
n	3 (4)	3 (5)	24 (7)	7 (8)

Table 3. Log-likelihood values and ML estimates of parameters ω (dN/dS), p (proportion of sites), and n (number of positively selected sites) for FDC-trapped *pol* in patient N1 205.

	Source of FDC-trapped *pol*			
	Panc LN	Rt Ax LN1	Spleen	3 sLTs combined
MO lnL	-1545.11	-1666.13	-1439.93	-2103.63
ω	0.5705	0.1035	0.6273	0.2371
M1 lnL	-1539.39	-1663.91	-1439.92	-2085.11
M2 lnL	-1530.01	-1663.91	-1439.93	-2077.27
ω	33.7976	1	1	6.0180
p2	0.0152	0.0436	0	0.0268
n	2 (2)	0 (0)	0 (0)	4 (3)
M3 lnL	-1529.59	-1663.82	-1439.93	-2078.02
ω	53.2734	0.7097	0.6274	5.8636
p2	0.0090	0.1453	0.2859	0.0280
n	0	0	4	12
M7 lnL	-1539.65	-1663.87	-1439.93	-2085.34
M8 lnL	-1530.18	-1663.85	-1440.81	-2078.10
ω	25.9778	1	1	5.8542
p1	0.0210	0.0414	0	0.0281
n	3 (3)	0 (0)	0 (0)	4 (4)

Table 4. Estimates of parameters ω (dN/dS ratio), n (number of positively selected sites), and identification of selected sites for FDC-trapped HIV-1 in patient N1 205.

FDC Source	ω2 (M2) gp120	n (M2) gp120	Positively selected sites in gp120 (M2, BEB Analysis: P>95%)
Panc LN	7.9768	3	350S; 381D; 406R
Rt Ax LN 1	8.4174	4	318E; 341M; 359H; 430R
Spleen	8.4146	7	238Q; 275F; 318R; 359H; 364D; 401N; 430T

FDC Source	ω2 (M2) pol	n (M2) pol	Positively selected sites in *pol* (M2, BEB Analysis: P>95%)
Panc LN	33.7976	2	37N; 197L
Rt Ax LN 1	1	0	N/A
Spleen	1	0	N/A

Note: Amino acid residues are numbered according to SF162 env, pro, and RT sequence.

Table 5. Amino acid sequence of the V3 loop for FDC-trapped HIV-1 Env in three different sLTs.

FDC source	Clone	V3 loop amino acid sequence[a]
	SF162	C T R P N N N T R K S I T I G P G R A F Y A T G **D** I I G D I R Q A H C
Spleen	*	- - - - S - - - - - - - H - - - - - - - - - - - **E** - T - - - - - - - -
	4b12	- - - - S - - - - - - - H - - - - - P L - - - - **R** - T - - - - - - - -
	7a8	- - - - S - - - - - - - R I G H - - L - - P L - V - - **R** - T - - - - - - - -
	†	- - - - S - - - - - - - R I G H - - - - - P L - V - - **R** - T - - - - - - - -
Panc	§	- - - - S - - - - - - - H - - - - - - - - - - - **E** - T - - - - - - - -
LN	1h3	- - - - S - - - K - - - H - - - - - - - - - - - **E** - T - - - - - - - -
	‡	- - - - S - - - - - - - R I G H - - - - - P L - V - - **R** - T - - - - - - - -
Rt Ax	5d6, 4b2	- - - - S - - - - - - - H - - - - - - - - - - - **E** - T - - - - - - - -
LN 1	2a5	- - - - S - - - - - - - H - - L - - P L - - - - **K** - T - - - - - - - -
	7c2	- - - - S - - - - - - - R I G H - - - - - P L - V - - **K** - T - - - - - - - -
	2a9	- - - - S - - - S - - - R I G H - - - - - P L - V - - **R** - T - - - - - - - -
	∞	- - - - S - - - - - - - R I G H - - - - - P L - V - - **R** - T - - - - - - - -

Note: [a] Amino acid position 25 (using SF162 amino acid positions) is in boldface. Conserved three amino acid insertion (RIG) in a subpopulation of HIV-1 is underlined.

Spleen * - 10 clones: 1a5, 1a12, 4a1, 7b5, 4b4, 3a1, 7a5, 5b10, 3a2, 5b12.
Spleen † - 7 clones: 4a6, 7b3, 4b2, 5b11, 1a4, 5b2, 4a4.

Panc LN § - 10 clones: 10f6, 10e1, 10f7, 8b5, 6g9, 1g11, 8b6, 3d4, 6g8, 6h10.
Panc LN ‡ - 11 clones: 3d9, 6h9, 3d3, 8b7, 6f12, 8a7, 8a9, 6c4, 6h5, 10e3, 10e7.

Rt Ax LN 1 ∞ - 12 clones: 2b5, 5c12, 5d3, 5b9, 4b8, 5d9, 2a6, 10a11, 10a5, 7c4, 5b11, 5d12.

Table 6. Amino acid sequence of the V3 loop for FDC-trapped HIV-1 Env in four different sLTs.

FDC source	Clone	V3 loop amino acid sequence[a]
	SF162	C T R P N N N T R K S I T I G P G R A F Y A T G **D** I I G D I R Q A H C
Mesn	*	- - - - S - - - - - - - H - - - - - - - - - - - **E** - T - - - - - - - -
LN 1	3e7	R - - - S - - - - - - - R I G H - - - - - P L - V - - **A** - T - - - - - - - -
	3f3	- - - - S - - - - - - - R I G H - - - - - P L - V - - **R** - T - - - - - - - -
	6f5	- - - - S - - - - - - - R I G H - - - - - P L - V - - **R** - T - - - - - - - -
	†	- - - - S - - - - - - - R I G H - - - - - P L - V - - **R** - T - - - - - - - -
Lt Ax	§	- - - - S - - - - - - - H - - - - - - - - - - - **E** - T - - - - - - - -
LN	8g6	- - - - S - - - - - - V H - - - - - - - - - - - **E** - T - - - - - - - -
	‡	- - - - S - - - - - - - R I G H - - - - - P L - V - - **R** - T - - - - - - - -
Rt Ax	∞	- - - - S - - - - - - - H - - - - - - - - - - - **E** - T - - - - - - - -
LN 2	7e5, 7d2	- - - - S - - - - - - - R I G H - - - - - P L - V - - **R** - T - - - - - - - -
	1c2, 5d8	- - - - S - - - S - - - R I G P - - - - - P L - V - - **R** - T - - - - - - - -
	ζ	- - - - S - - - S - - - R I G H - - - - - P L - V - - **R** - T - - - - - - - -
	Ж	- - - - - - - - - - - - R I G H - - - - - P L - V - - **K** - T - - - - - - - -
Rt Ax	ф	- - - - S - - - - - - - R I G H - - - - - P L - V - - **R** - T - - - - - - - -
LN 3	8f2, 4f4	- - - - S - - - - - - - R I G H - - - - - P L - V - - **K** - T - - - - - - - -
	¥	- - - - - - - - - - - - R I G H - - - - - P L - V - - **K** - T - - - - - - - -
	8f5	- - - - - - - - - - - - R I G H - - L - - P L - V - - **K** - T - - - - - - - -
	8g11	- - - - - - - - - - - - R I G H - E - - - P L - V - - **K** - T - - - - - - - -
	8h5	- - - - - - - - - - - - R I G H - - - - - P L - V I - **K** - T - - - - - - - -
	8e11	- - - - - - - A - - - - R I G H - - - - - P L - V - - **K** - T - - - - - - - -
	¶	- - - - S - - - S - - - R I G H - - - - - P L - V - - **K** - T - - - - - - - -

Note: [a] Amino acid position 25 (using SF162 amino acid positions) is in boldface. Conserved three amino acid insertion (RIG) in a subpopulation of HIV-1 is underlined.

Mesn 1 LN * - 7 clones: 7g10, 10a12, 10a10, 6g11, 6f10, 10a7, 8h2.
Mesn 1 LN † - 10 clones: 10a9, 10a8, 3e2, 10a6, 3e3, 7g6, 7g5, 7e7, 7g8, 6f8.

Lt Ax LN § - 9 clones: 8c2, 8f10, 1e8, 8g12, 8e3, 8h10, 4f12, 8g6, 1f11.
Lt Ax LN ‡ - 13 clones: 8h3, 1f2, 1e9, 1e5, 4e5, 8g7, 4e4, 8f12, 8h11, 8f8, 3e3, 4f4, 8c9.

Rt Ax 2 LN ∞ - 6 clones: 10c5, 9a12, 9a4, 9a9, 10b4, 9a11.
Rt Ax 2 LN ζ - 4 clones: 10b6, 10b2, 10b7, 9a10.
Rt Ax 2 LN Ж - 5 clones: 1c1, 3c8, 3c12, 7d12, 5d7.

Rt Ax 3 LN ф - 3 clones: 2e1, 3e2, 4f5.
Rt Ax 3 LN ¥ - 4 clones: 8e5, 8f6, 8h8, 8g10.
Rt Ax 3 LN ¶ - 6 clones: 8e10, 8f11, 8h6, 8e8, 8e9, 8f8.

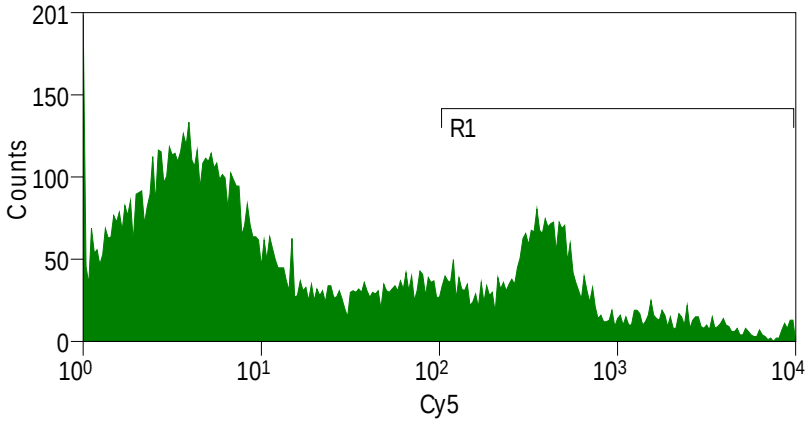

Figure 9a. MØ population in right axillary LN 1. Post-enzymatic digest cells were stained with CD14-Cy5. Cells were gated to select for live cells based on forward and side scatter. The area under the R1 gate is 19.2 %.

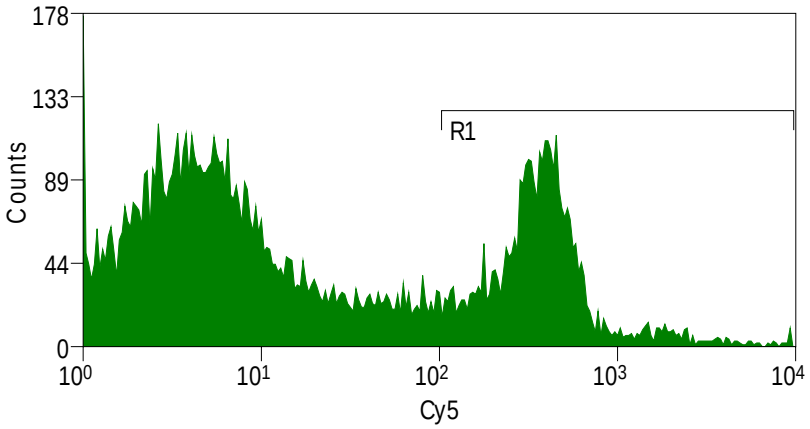

Figure 9b. MØ population in right axillary LN 2. Post-enzymatic digest cells were stained with CD14-Cy5. Cells were gated to select for live cells based on forward and side scatter. The area under the R1 gate is 21.9 %.

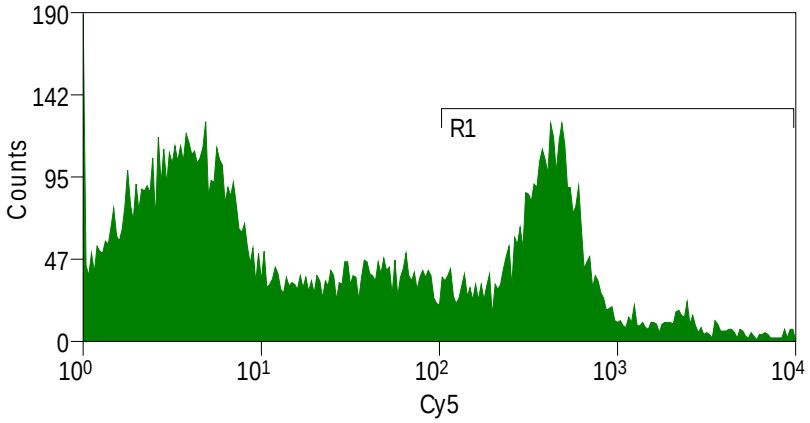

Figure 9c. MØ population in right axillary LN 3. Post-enzymatic digest cells were stained with CD14-Cy5. Cells were gated to select for live cells based on forward and side scatter. The area under the R1 gate is 24.0 %.

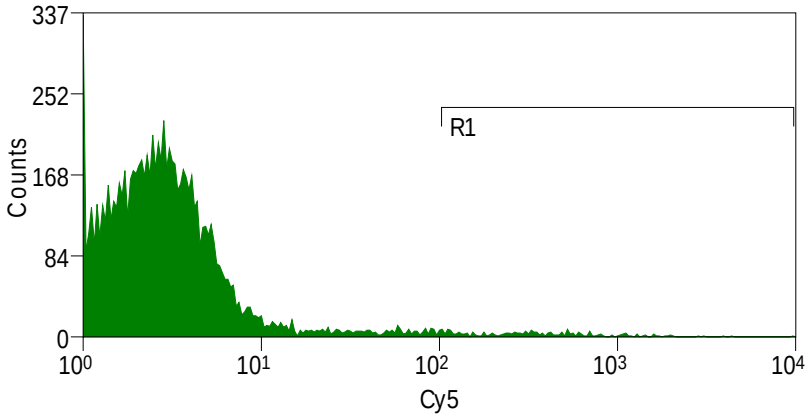

Figure 9d. MØ population in the splenic fragment. Post-enzymatic digest cells were stained with CD14-Cy5. Cells were gated to select for live cells based on forward and side scatter. The area under the R1 gate is 1.6 %.

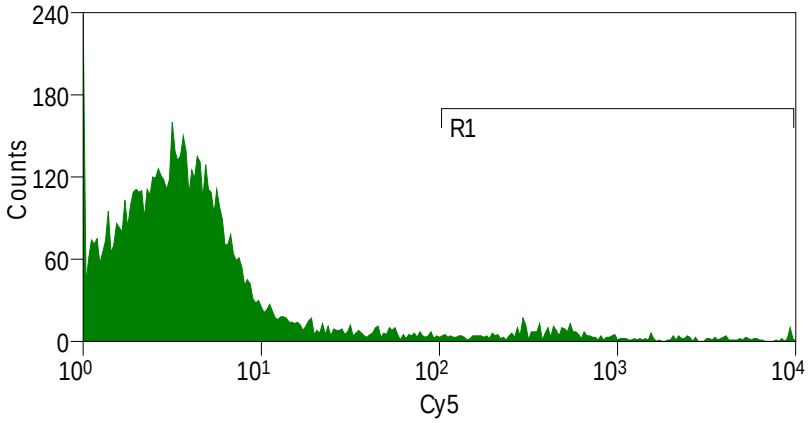

Figure 9e. MØ population in the pancreatic LN. Post-enzymatic digest cells were stained with CD14-Cy5. Cells were gated to select for live cells based on forward and side scatter. The area under the R1 gate is 3.4 %.

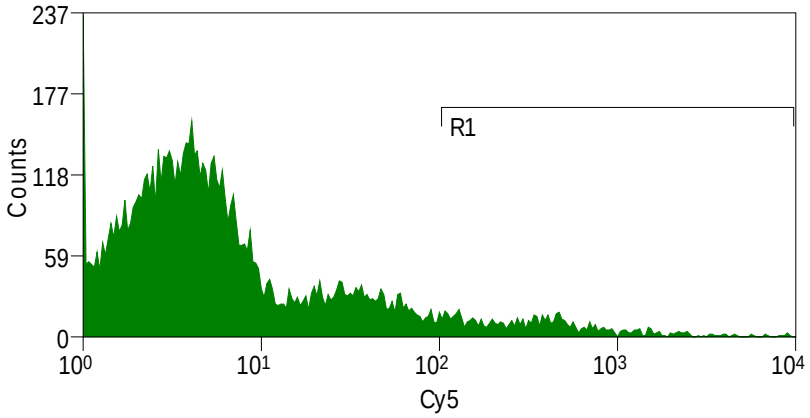

Figure 9f. MØ population in mesenteric LN 1. Post-enzymatic digest cells were stained with CD14-Cy5. Cells were gated to select for live cells based on forward and side scatter. The area under the R1 gate is 5.3 %.

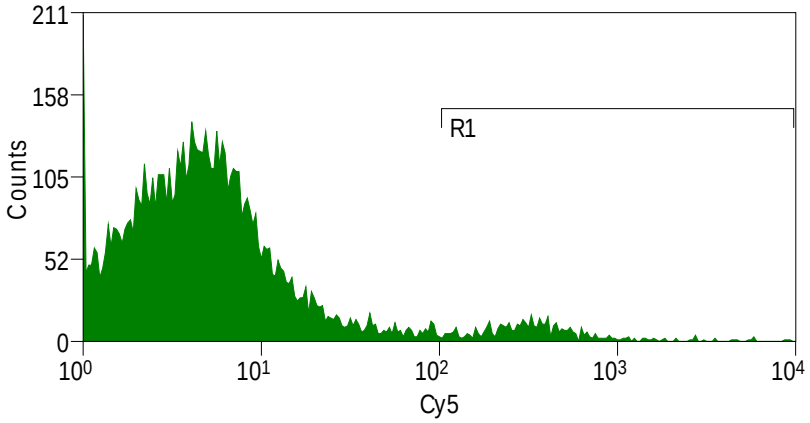

Figure 9g. MØ population in the left axillary LN. Post-enzymatic digest cells were stained with CD14-Cy5. Cells were gated to select for live cells based on forward and side scatter. The area under the R1 gate is 3.4 %.

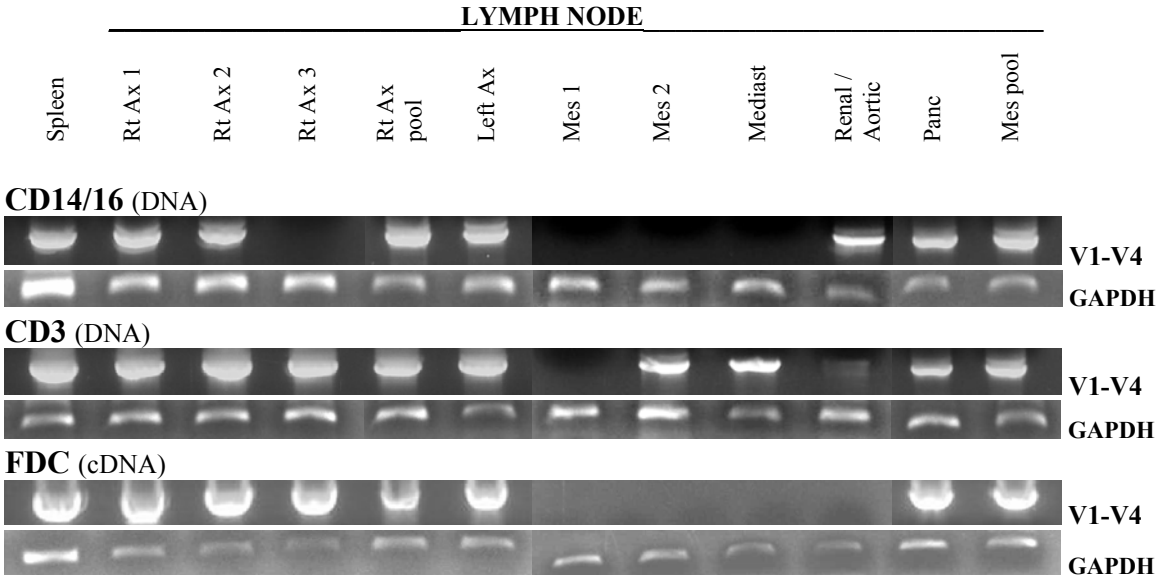

Figure 10. HIV-1 levels vary between different cell types and different sLTs. PCR HIV-1 Env (V1-V4) amplimers are shown from MØ (CD14/16), T cells (CD3) and FDCs from different intra-patient sLTs. Differential HIV-1 levels are observed both within and between sLTs. For example, in the right axillary LN chain HIV-1 is detected in MØs in LN 1 and LN 2 but not in LN 3; in the mediastinal LN HIV-1 is detected in T cells but not in macrophages or FDCs. All negative results are indicative of at least two independent experiments.

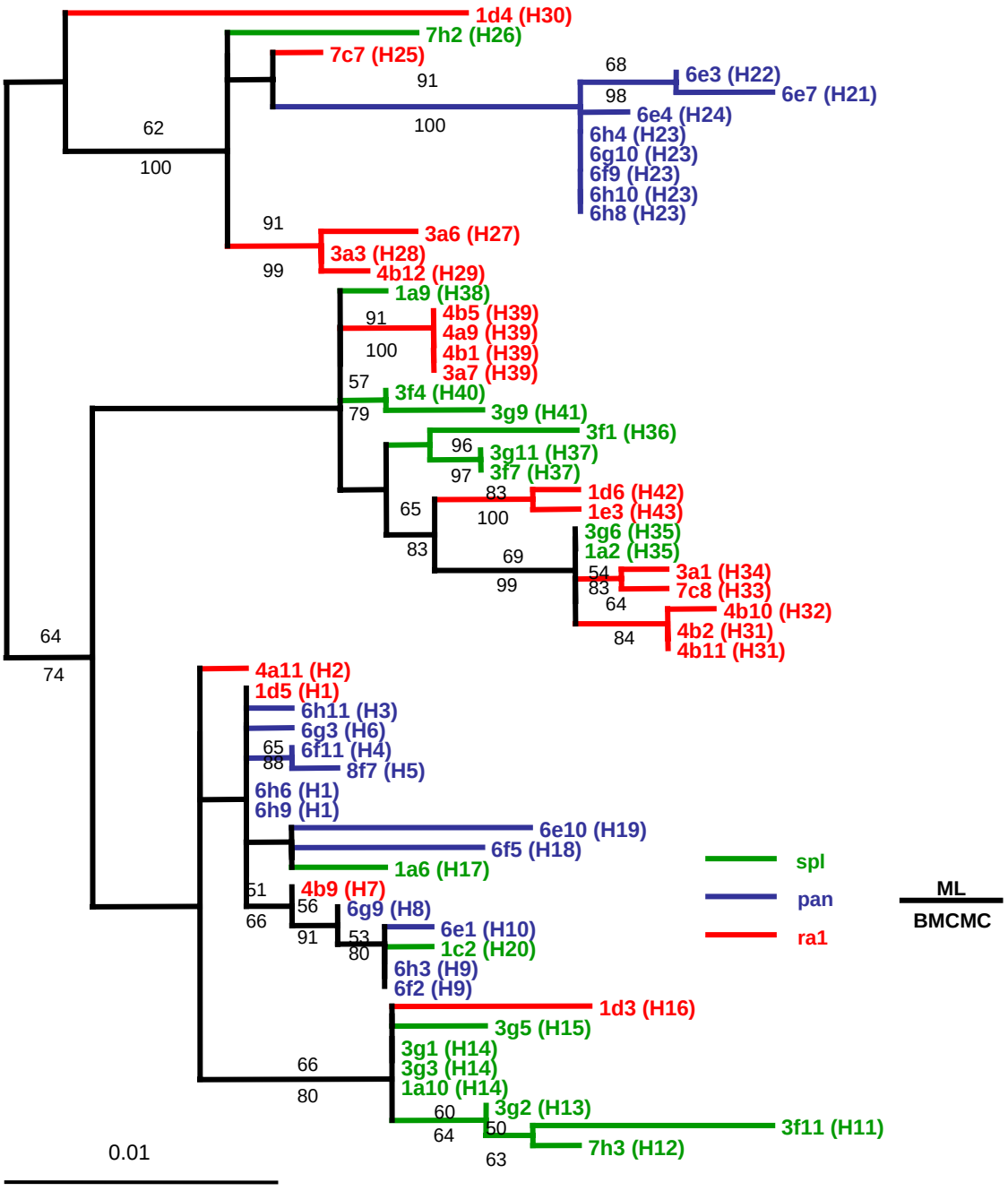

Figure 11. HIV-1 gp120 isolated from MØs in different sLTs is partially compartmentalized. C2-C3 sequences from MØs isolated from a splenic fragment (**spl**), and pancreatic (**pan**) and right axillary (**ra1**) LNs were subjected to both Maximum Likelihood and Bayesian phylogenetic analyses. Maximum Likelihood bootstrap values (**ML**) appear above the branches and Bayesian Markov Chain Monte Carlo (**BMCMC**) inference values below the branches. Haplotype designations from the corresponding TCS network (Figure 12) appear in brackets (H) following the clone label at the end of branches. See also Table 7.

Table 7. Amino acid sequence of the V3 loop for HIV-1 Env provirus isolated from MØs in different sLTs.

FDC source	Clone	V3 loop amino acid sequence[a]
	SF162	C T R P N N N T R K S I T I G P G R A F Y A T G **D** I I G D I R Q A H C
Spleen	*	- - - - S - - - - - - - H - - - - - - - - - - - - **E** - T - - - - - - - -
	3f1	- - - - S - I - - - - - H - - - - - - - - - - - - **E** - T - - - - - - - -
	7h2	- - - - S - - - S - - - R I G H - - - - - P L - V - - **R** - T - - - - - - - -
	7h3	- - - - S - I - - - - - R I G H - - - - - P L - V - - **R** - T - - - - - - - -
	†	- - - - S - - - - - - - R I G H - - - - - P L - V - - **R** - T - - - - - - - -
Panc LN	§	- - - - S - - - - - - - R I G H - - - - - P L - V - - **R** - T - - - - - - - -
	6f5	- - - - S - - - - - - - R I G H - - - - - P L - V A - **R** - T - - - - - - - -
	6e1	- - - - S - A - - - - - R I G H - - - - - P L - V - - **R** - T - - - - - - - -
	6e10	- - - - S - - - S - - - R I G H - - - - - P L - V - - **R** - T - - - - - - - -
	‡	- - - - S - - - S - - - R I G H - - - - - P L - V - - **K** - T - - - - - - - -
Rt Ax LN 1	ζ	- - - - S - - - - - - - H - - - - - - - - - - - - **E** - T - - - - - - - -
	7c7	- - - - S - - - S - - - R I G H - - - - - P L - V - - **K** - T - - - - - - - -
	Ж	- - - - S - - - S - - - R I G H - - - - - P L - V - - **R** - T - - - - - - - -
	∞	- - - - S - - - - - - - R I G H - - - - - P L - V - - **R** - T - - - - - - - -

Note: [a] Amino acid position 25 (using SF162 amino acid positions) is in boldface. Conserved three amino acid insertion (RIG) in a subpopulation of HIV-1 is underlined.

Spleen * - 7 clones: 1a9, 3f4, 3g9, 3g11, 3f7, 3g6, 1a2.
Spleen † - 8 clones: 1a6, 1c2, 3g5, 3g1, 3g3, 1a10, 3g2, 3f11.

Panc LN § - 9 clones: 6h11, 6g3, 6f11, 8f7, 6h6, 6h9, 6g9, 6h3, 6f2.
Panc LN ‡ - 8 clones: 6e3, 6e7, 6e4, 6h4, 6g10, 6f9, 6h10, 6h8.

Rt Ax LN 1 ζ - 11 clones: 4b5, 4a9, 4b1, 3a7, 1d6, 1e3, 3a1, 7c8, 4b10, 4b2, 4b11.
Rt Ax LN 1 Ж - 3 clones: 3a6, 3a3, 4b12.
Rt Ax LN 1 ∞ - 5 clones: 1d4, 4[a]11, 1d5, 4b9, 1d3.

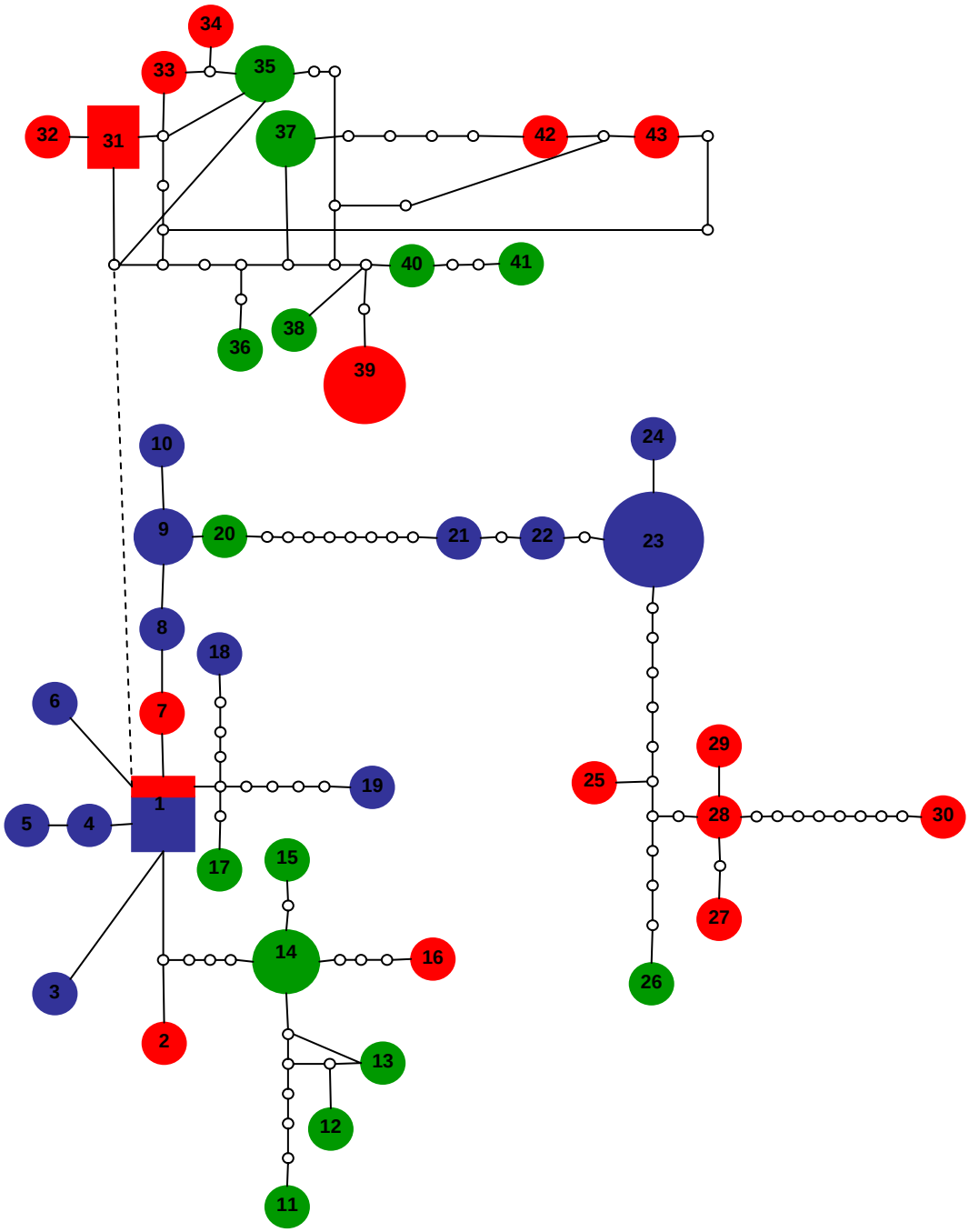

Figure 12. HIV-1 gp120 isolated from MØs in different sLTs is partially compartmentalized. C2-C3 sequences from MØs isolated from a splenic fragment (**spl**), and pancreatic (**pan**) and right axillary (**ra1**) LNs were subjected to TCS network analysis. Details of how to read the TCS network can be found in the materials and methods chapter and more briefly in the Figure 2 legend. Haplotype designations are arbitrary correspond to the numbers in brackets (H) in the corresponding phylogenetic tree (Figure 11).

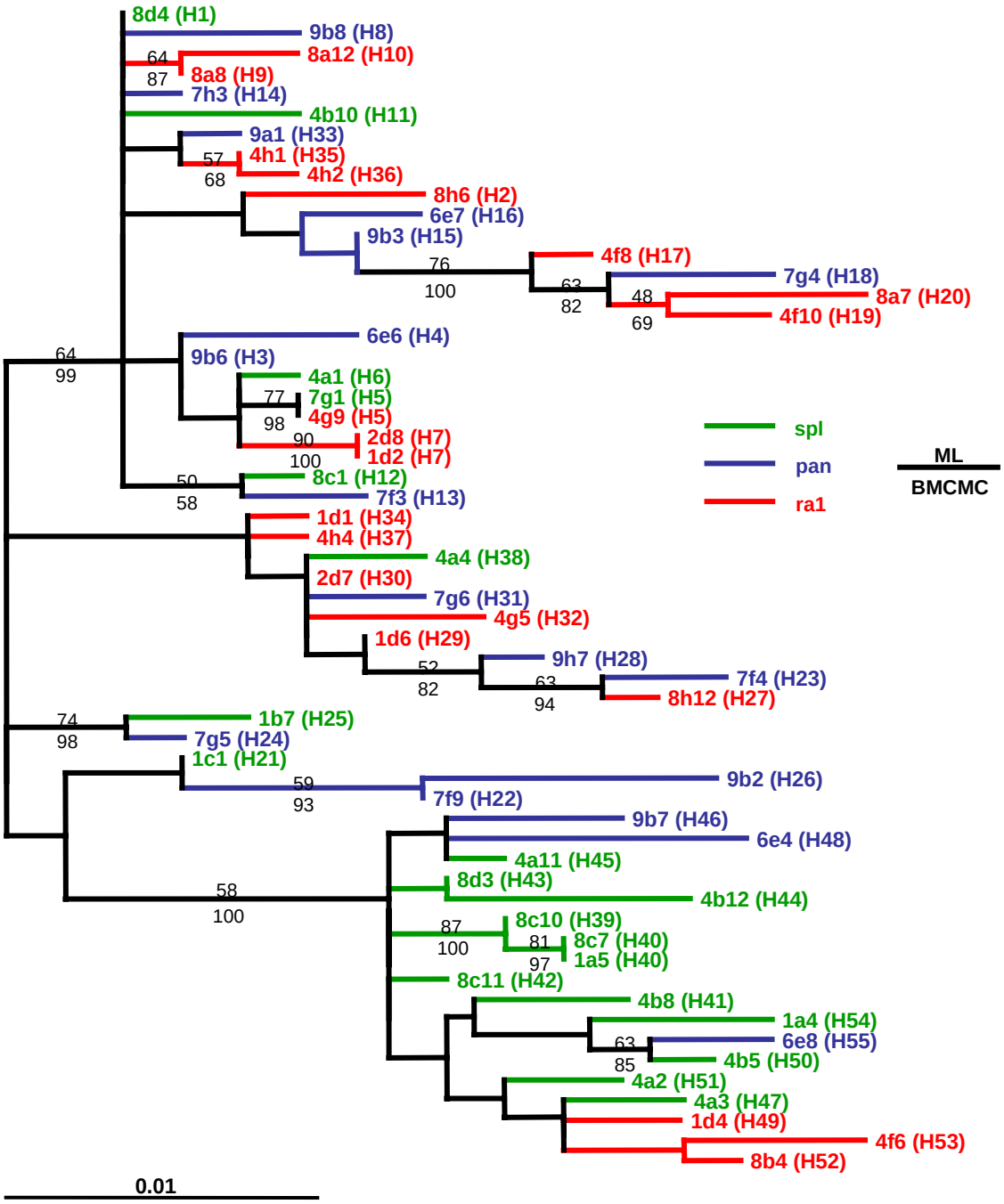

Figure 13. HIV-1 gp120 isolated from T cells in different sLTs is not compartmentalized. C2-C3 sequences from T cells isolated from a splenic fragment (**spl**), and pancreatic (**pan**) and right axillary (**ra1**) LNs were subjected to both Maximum Likelihood and Bayesian phylogenetic analyses. Maximum Likelihood bootstrap values (**ML**) appear above the branches and Bayesian Markov Chain Monte Carlo (**BMCMC**) inference values below the branches. Haplotype designations from the corresponding TCS network (Figure 14) appear in brackets (H) following the clone label at the end of branches. See also Table 8.

Table 8. Amino acid sequence of the V3 loop for HIV-1 Env provirus isolated from T cells in different sLTs.

FDC source	Clone	V3 loop amino acid sequence[a]
	SF162	C T R P N N N T R K S I T I G P G R A F Y A T G **D** I I G D I R Q A H C
Spleen	*	- - - - S - - - - - - - H - - - - - - - - - - - **E** - T - - - - - - - -
	4b10	- - - - S - - - - - - - R I G R - - - - - P L - V - - **R** - T - - - - - - - -
	4a4	- - - - S - - - - - - - R I G H - - - - - P L - V - - **R** - T E - - - - - - -
	1b7	- - - - - - - - - - - - R I G H - - - - - P L - V - - **K** - T - - - - - - - -
	†	- - - - S - - - - - - - R I G H - - - - - P L - V - - **R** - T - - - - - - - -
Panc	§	- - - - S - - - - - - - H - - - - - - - - - - - **E** - T - - - - - - - -
LN	7g4	- - - - S - - - S - - - R I G H - - - - - P L - V - - **K** - T - - - - - - - -
	7f3	- - - - S - - - - - - M R I G H - - - - - P L - V - - **R** - T - - - - - - - -
	7g5	- - - - - - - - - - - - R I G H - - - - - P L - V - - **K** - T - - - - - - - -
	‡	- - - - S - - - S - - - R I G H - - - - - P L - V - - **R** - T - - - - - - - -
	ζ	- - - - S - - - - - - - R I G H - - - - - P L - V - - **R** - T - - - - - - - -
Rt Ax 1	1d4, 8b4	- - - - S - - - - - - - H - - - - - - - - - - - **E** - T - - - - - - - -
LN	4f6	- - K L S - - - - - - - H - - - - - - - - - - - **E** - T - - - - - - - -
	8a7	- - G - S - - - S - - - R I G H - - - - - P L - V - - **K** - T - - - - - - - -
	8h6	- - - - S - - - - - - - R I G H - - - - - P L - V - - **K** - T - G - - - - - -
	Ж	- - - - S - - - S - - - R I G H - - - - - P L - V - - **R** - T - - - - - - - -
	∞	- - - - S - - - - - - - R I G H - - - - - P L - V - - **R** - T - - - - - - - -

Note: [a] Amino acid position 25 (using SF162 amino acid positions) is in boldface. Conserved three amino acid insertion (RIG) in a subpopulation of HIV-1 is underlined.

Spleen * - 12 clones: 4a11, 8d3, 4b12, 8c10, 8c7, 1a5, 8c11, 4b8, 1a4, 4b5, 4a2, 4a3.
Spleen † - 5 clones: 8d4, 4a1, 7g1, 8c1, 1c1.

Panc LN § - 3 clones: 9b7, 6e4, 6e8.
Panc LN ‡ - 3 clones: 6e7, 9b3, 6e6.
Panc LN ζ - 9 clones: 9b8, 7h3, 9a1, 9b6, 7g6, 9h7, 7f4, 9b2, 7f9.

Rt Ax 1 LN Ж - 4 clones: 4h1, 4h2, 4f8, 4f10.
Rt Ax 1 LN ∞ - 11 clones: 8a12, 8a8, 4g9, 2d8, 1d2, 1d1, 4h4, 2d7, 4g5, 1d6, 8h12.

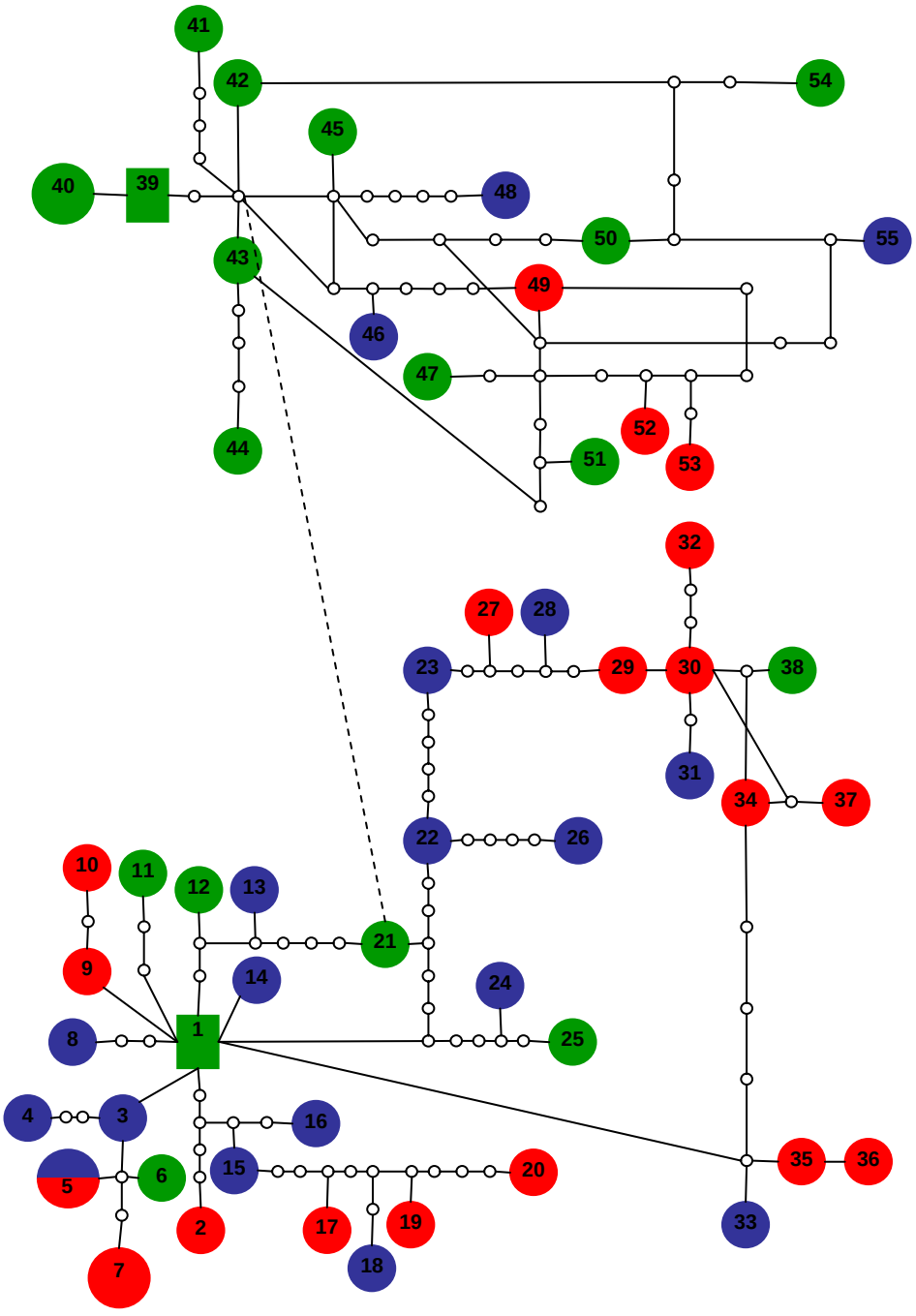

Figure 14. HIV-1 gp120 isolated from T cells in different sLTs is not compartmentalized. C2-C3 sequences from T cells isolated from a splenic fragment (**spl**), and pancreatic (**pan**) and right axillary (**ra1**) LNs were subjected to TCS network analysis. Details of how to read the TCS network can be found in the materials and methods chapter and more briefly in the Figure 2 legend. Haplotype designations are arbitrary correspond to the numbers in brackets (H) in the corresponding phylogenetic tree (Figure 13).

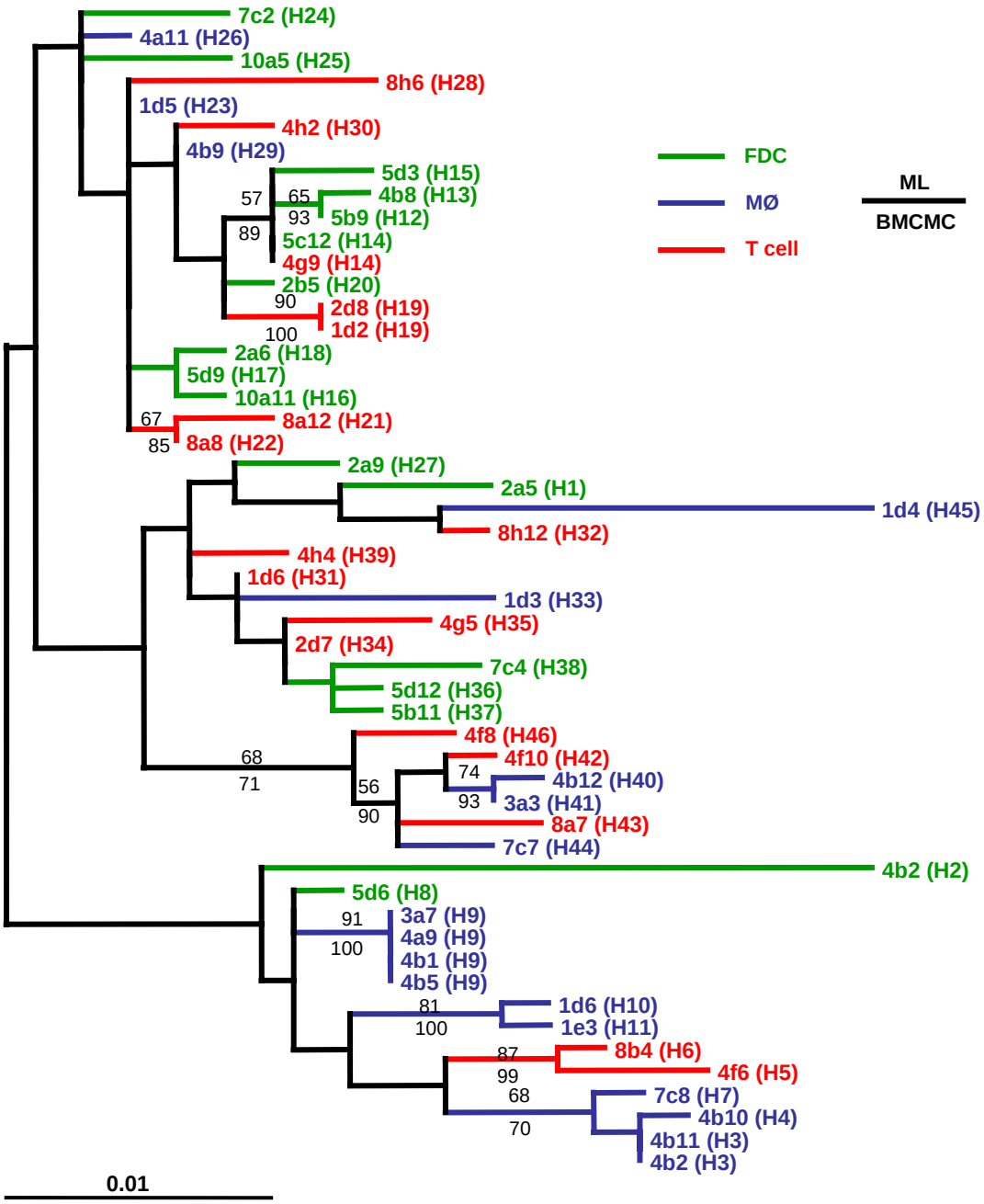

Figure 15. HIV-1 gp120 is not compartmentalized between cells in the right axillary LN. C2-C3 sequences isolated from **T cells**, **MØs**, and **FDCs** from the right axillary LN were subjected to both Maximum Likelihood and Bayesian phylogenetic analyses. Maximum Likelihood bootstrap values (**ML**) appear above the branches and Bayesian Markov Chain Monte Carlo (**BMCMC**) inference values below the branches. Haplotype designations from the corresponding TCS network (Figure 17) appear in brackets (H) following the clone label at the end of branches.

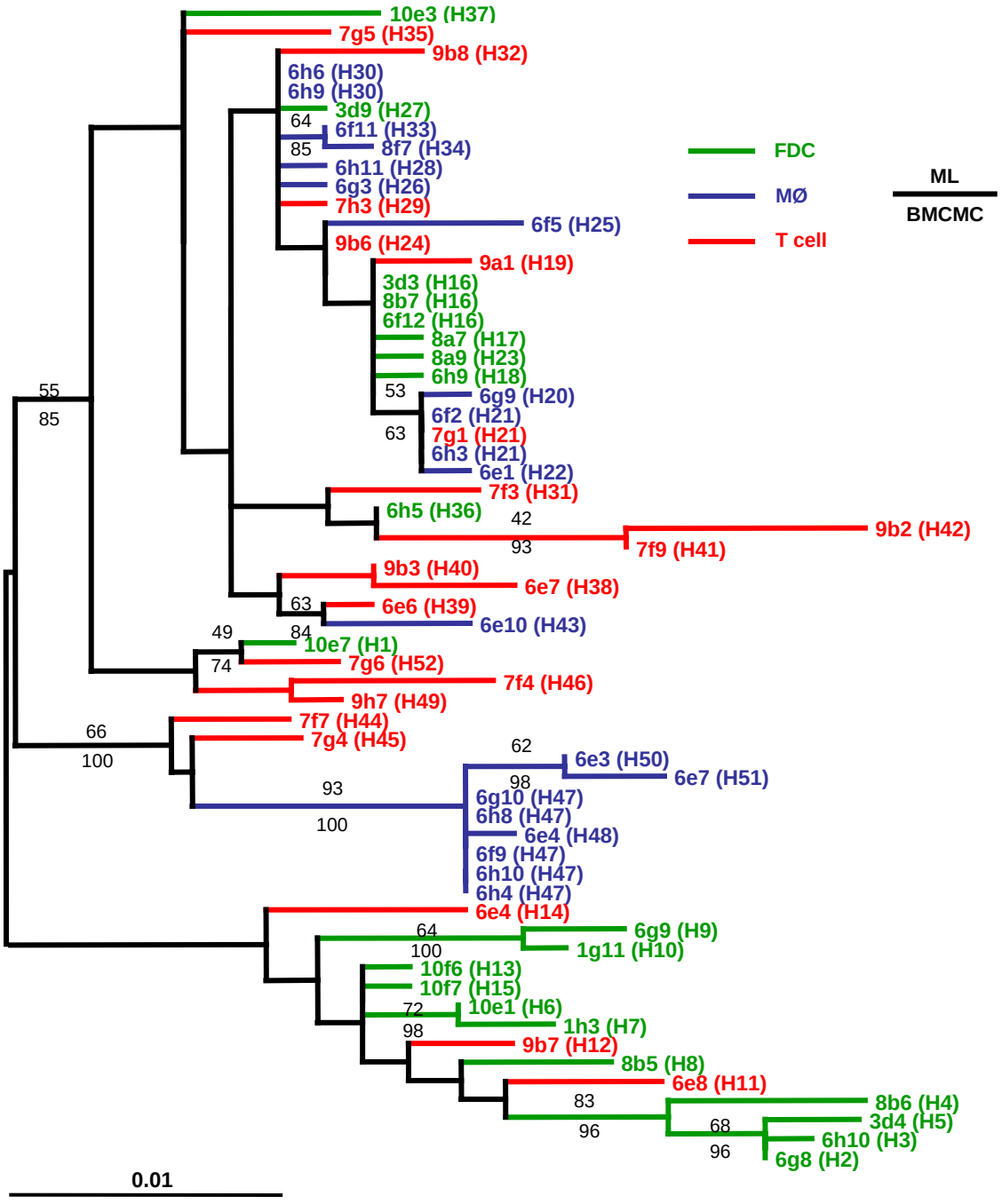

Figure 16. HIV-1 gp120 is partially compartmentalized between cells in the pancreatic LN. C2-C3 sequences isolated from **T cells**, **MØs**, and **FDCs** from the pancreatic LN were subjected to both Maximum Likelihood and Bayesian phylogenetic analyses. Maximum Likelihood bootstrap values (**ML**) appear above the branches and Bayesian Markov Chain Monte Carlo (**BMCMC**) inference values below the branches. Haplotype designations from the corresponding TCS network (Figure 18) appear in brackets (H) following the clone label at the end of branches.

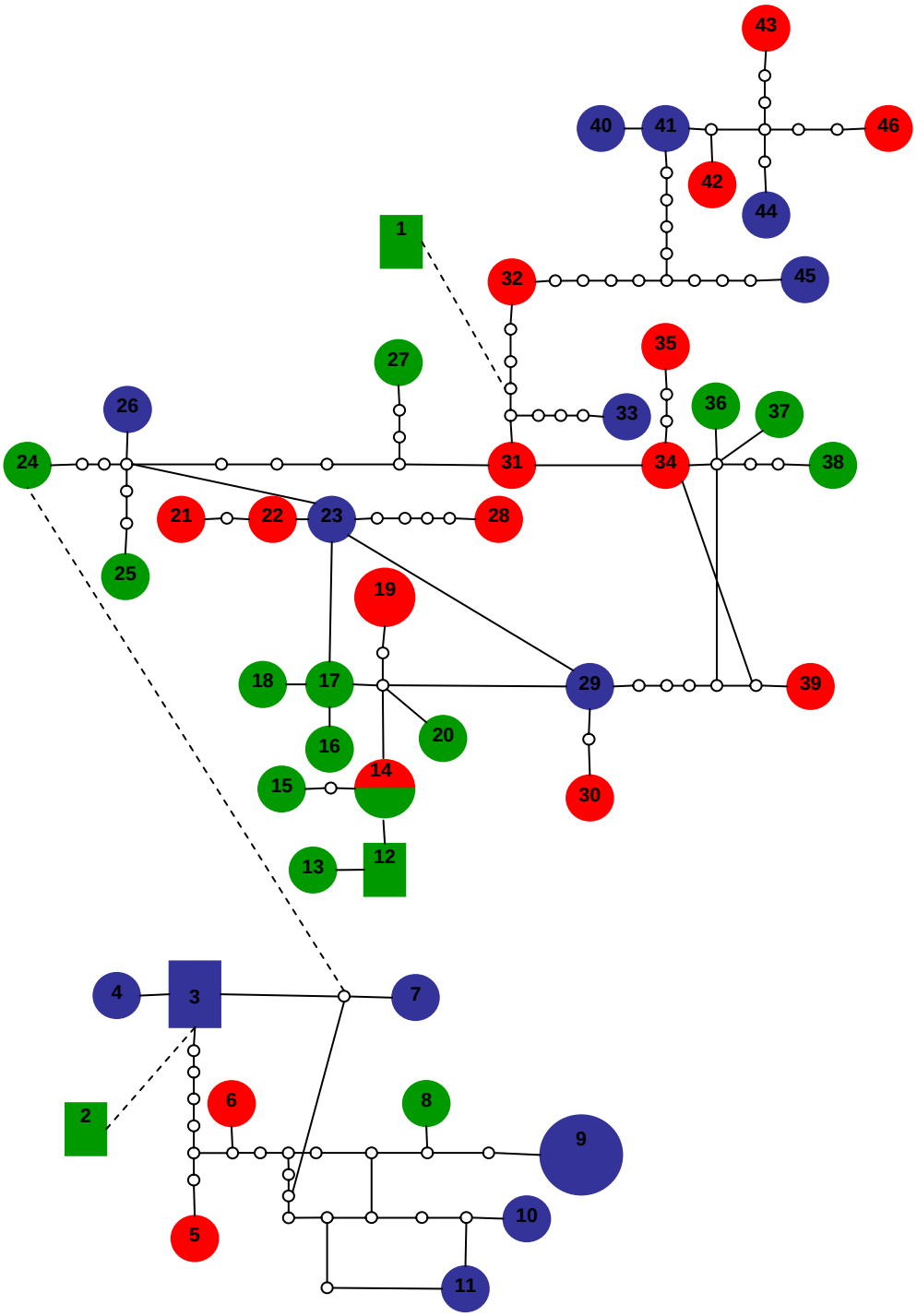

Figure 17. HIV-1 gp120 is not compartmentalized between cells in the right axillary LN. C2-C3 sequences isolated from **T cells**, **MØs**, and **FDCs** from the right axillary LN were subjected to TCS network analysis. Details of how to read the TCS network can be found in the materials and methods chapter and more briefly in the Figure 2 legend. Haplotype designations are arbitrary correspond to the numbers in brackets (H) in the corresponding phylogenetic tree (Figure 15).

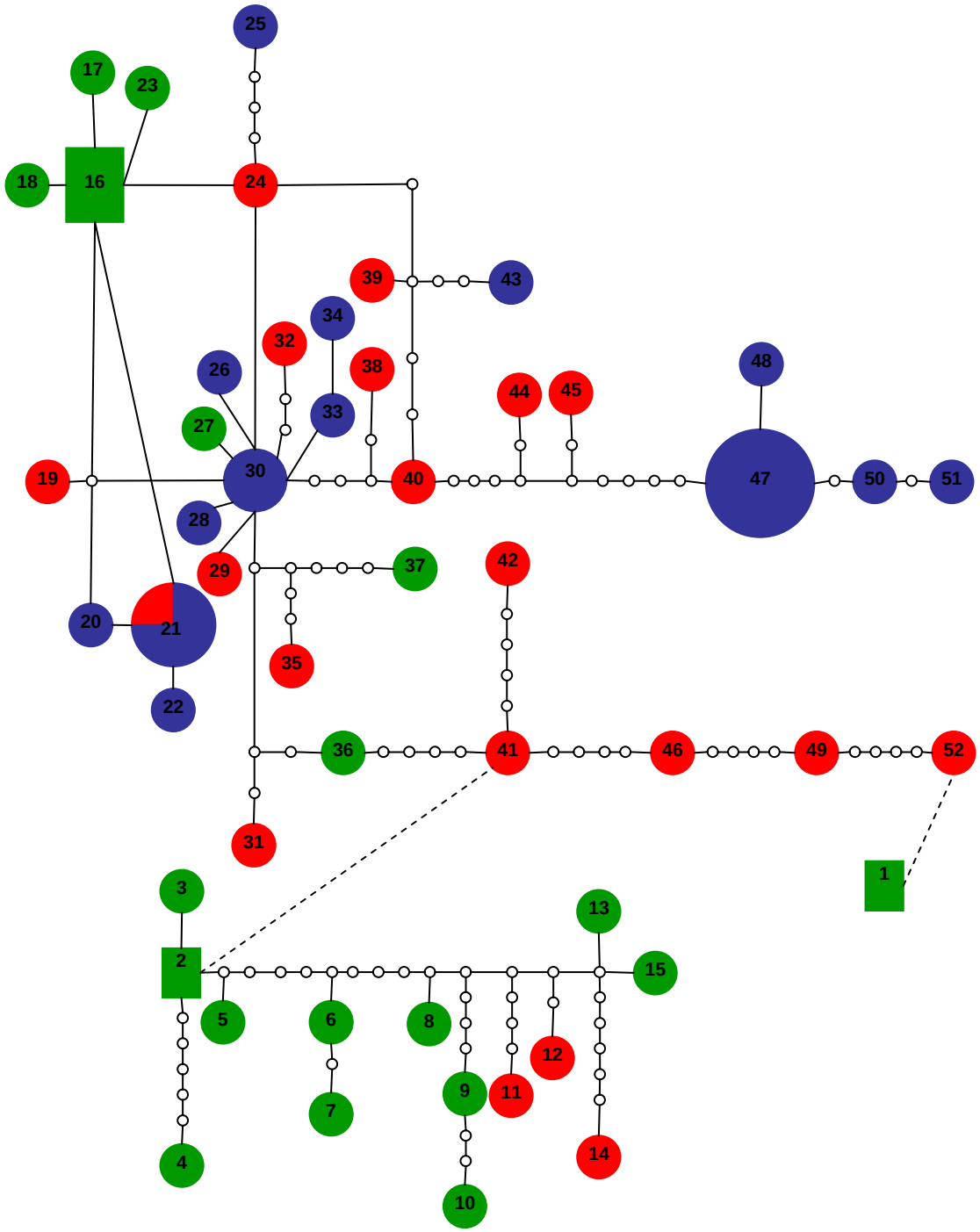

Figure 18. HIV-1 gp120 is partially compartmentalized between cells in the pancreatic LN. C2-C3 sequences isolated from **T cells**, **MØs**, and **FDCs** from the pancreatic LN were subjected to TCS network analysis. Details of how to read the TCS network can be found in the materials and methods chapter and more briefly in the Figure 2 legend. Haplotype designations are arbitrary correspond to the numbers in brackets (H) in the corresponding phylogenetic tree (Figure 16).

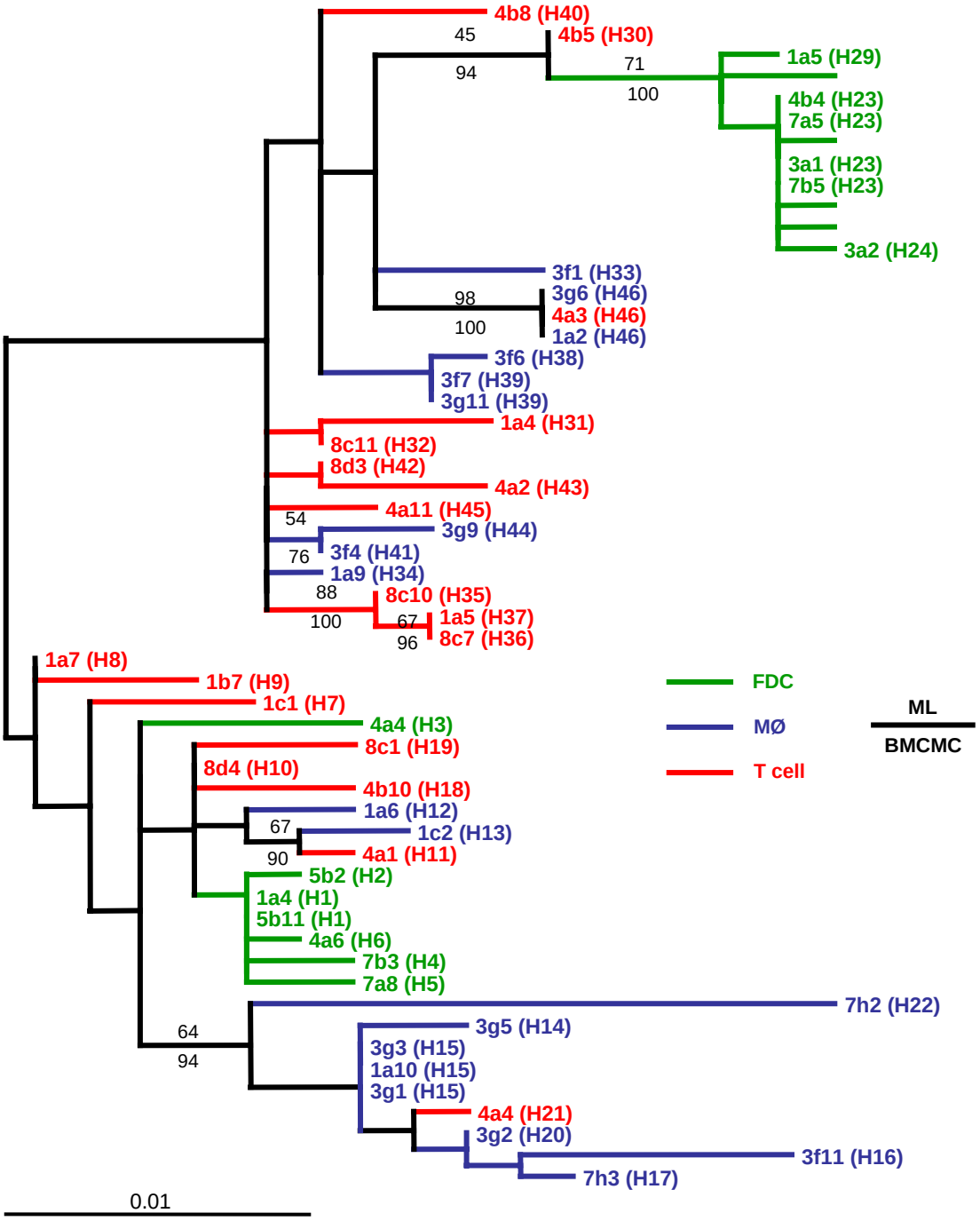

Figure 19. FDC-trapped HIV-1 gp120 is compartmentalized from T cells and MØs in the spleen. C2-C3 sequences isolated from **T cells**, **MØs**, and **FDCs** from the spleen were subjected to both Maximum Likelihood and Bayesian phylogenetic analyses. Maximum Likelihood bootstrap values (**ML**) appear above the branches and Bayesian Markov Chain Monte Carlo (**BMCMC**) inference values below the branches. Haplotype designations from the corresponding TCS network (Figure 20) appear in brackets (H) following the clone label at the end of branches.

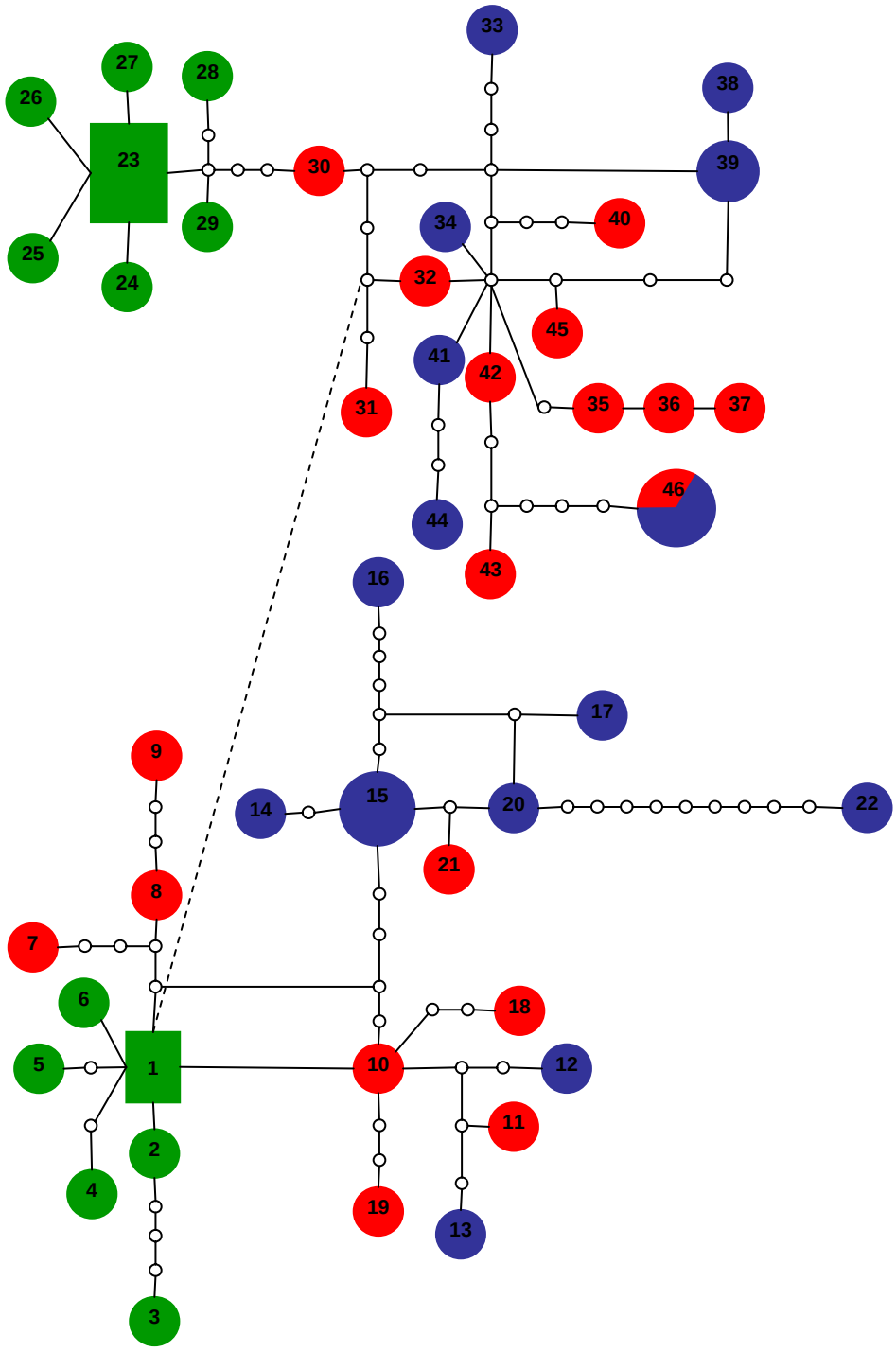

Figure 20. FDC-trapped HIV-1 gp120 is compartmentalized from T cells and MØs in the spleen. C2-C3 sequences isolated from **T cells**, **MØs**, and **FDCs** from the spleen were subjected to TCS network analysis. Details of how to read the TCS network can be found in the materials and methods chapter and more briefly in the Figure 2 legend. Haplotype designations are arbitrary correspond to the numbers in brackets (H) in the corresponding phylogenetic tree (Figure 19).

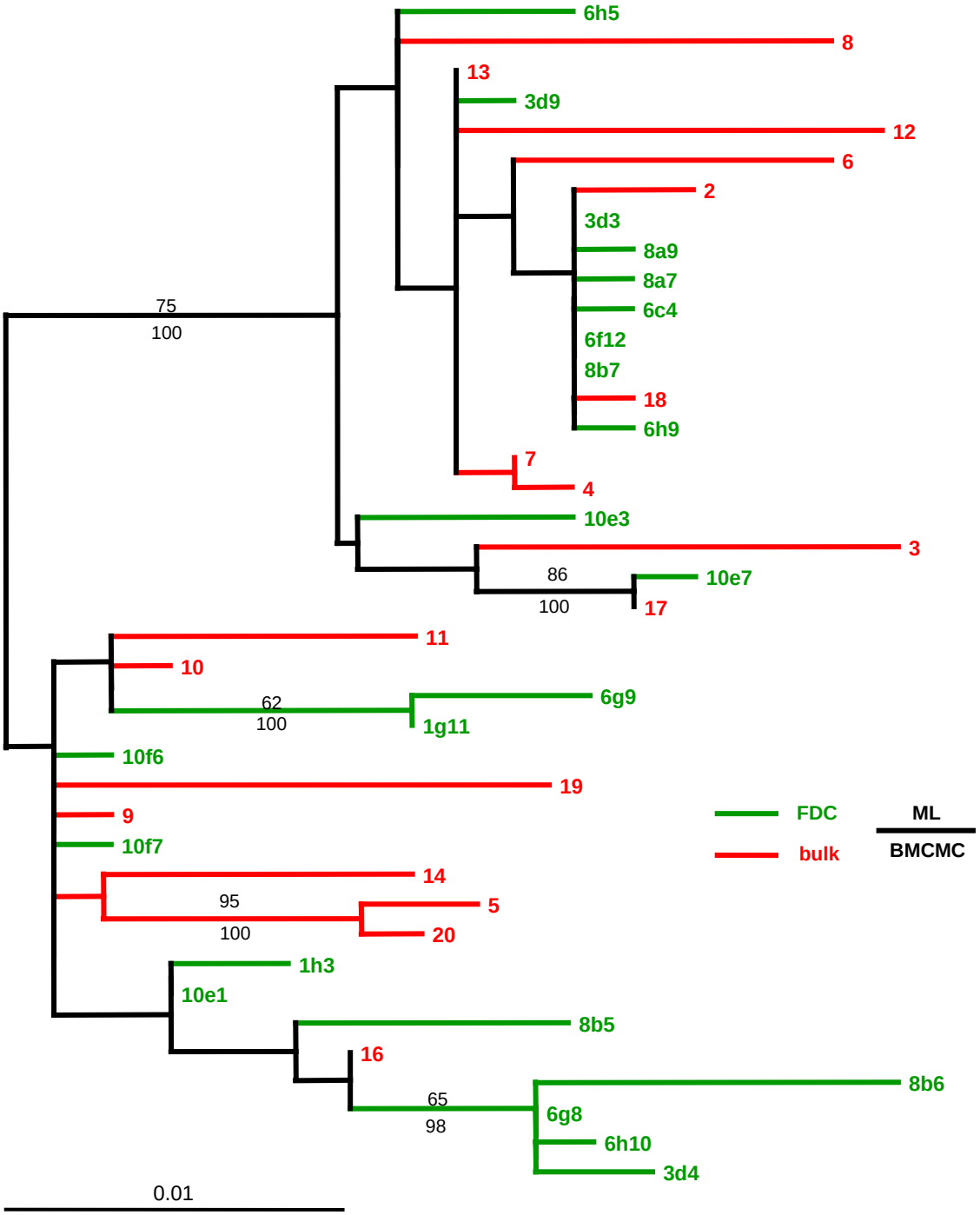

Figure 21. FDC-trapped HIV-1 gp120 is partially represented by bulk sequences from the same LN. C2-C3 sequences isolated from FDCs (**FDC**) from the pancreatic LN, and bulk sequences (**bulk**) from the pancreatic LN were subjected to both Maximum Likelihood and Bayesian phylogenetic analyses. Maximum Likelihood bootstrap values (**ML**) appear above the branches and Bayesian Markov Chain Monte Carlo (**BMCMC**) inference values below the branches.

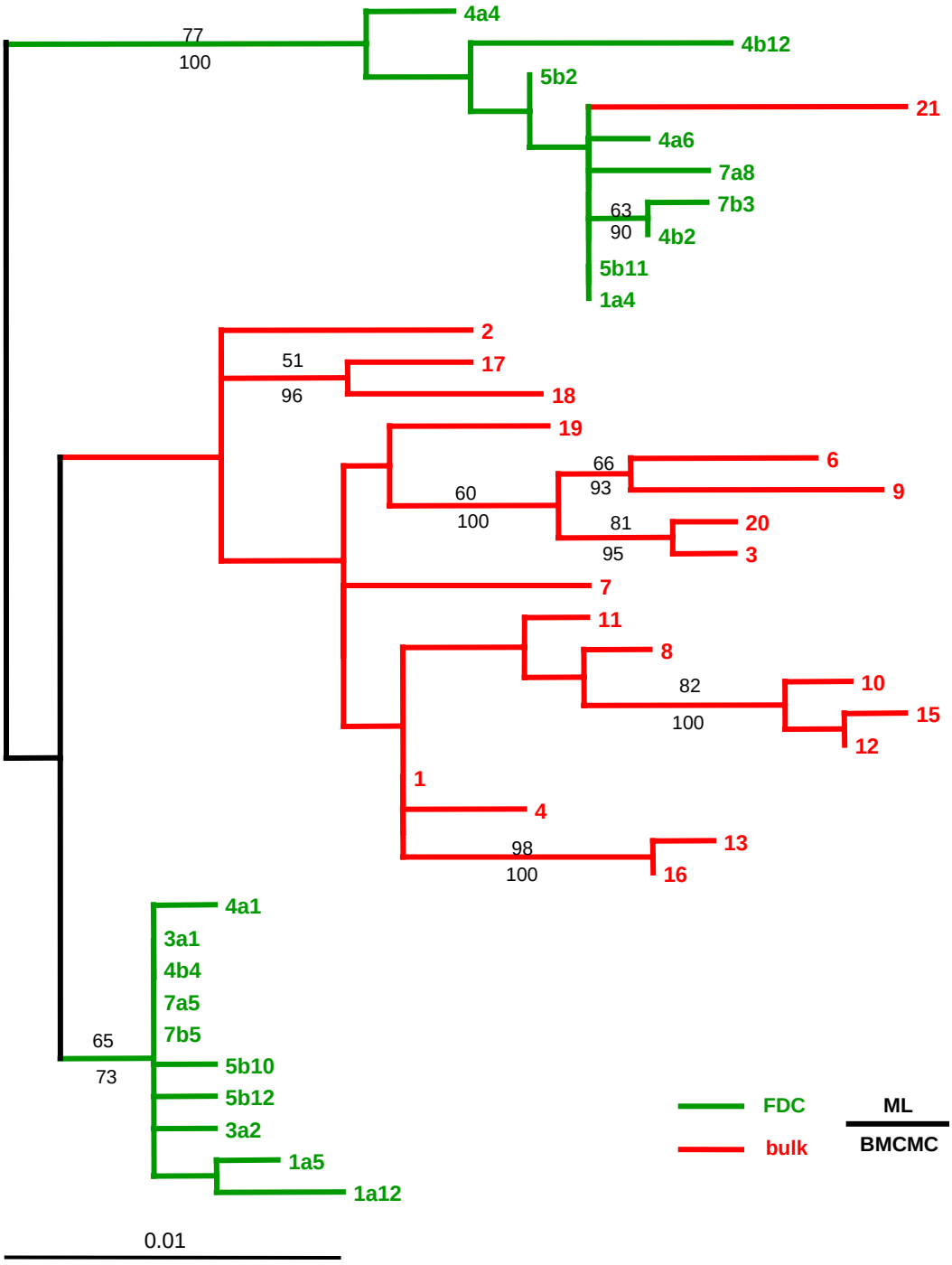

Figure 22. Splenic FDC-trapped HIV-1 gp120 is not represented by bulk sequences from the spleen. C2-C3 sequences isolated from FDCs (**FDC**) from the spleen, and bulk sequences (**bulk**) from the spleen were subjected to both Maximum Likelihood and Bayesian phylogenetic analyses. Maximum Likelihood bootstrap values (**ML**) appear above the branches and Bayesian Markov Chain Monte Carlo (**BMCMC**) inference values below the branches.

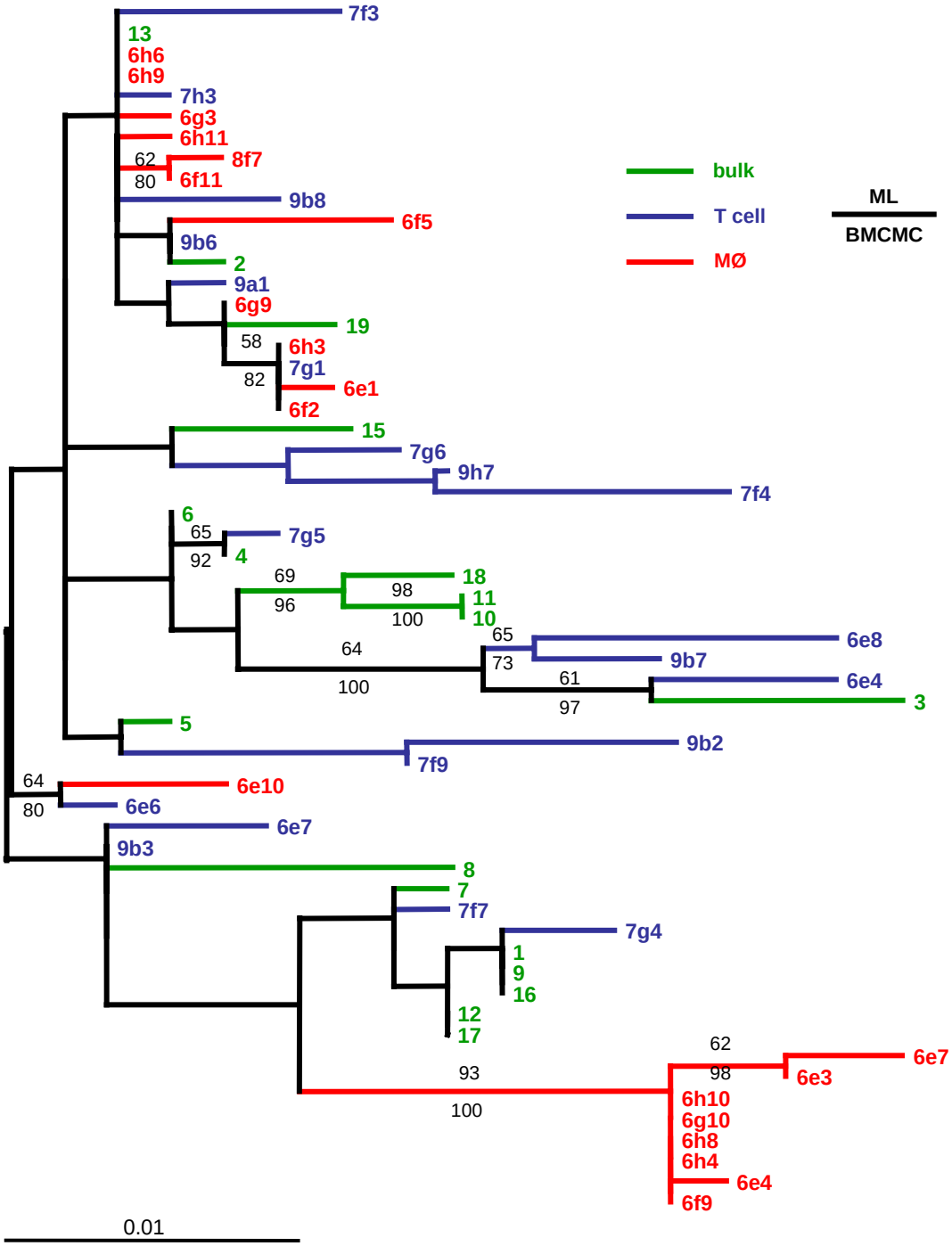

Figure 23. MØ HIV-1 gp120 provirus is under-represented by bulk sequences from the same LN. C2-C3 sequences isolated from **T cells**, **MØs**, and bulk sequences (**bulk**) from the pancreatic LN were subjected to both Maximum Likelihood and Bayesian phylogenetic analyses. Maximum Likelihood bootstrap values (**ML**) appear above the branches and Bayesian Markov Chain Monte Carlo (**BMCMC**) inference values below the branches.

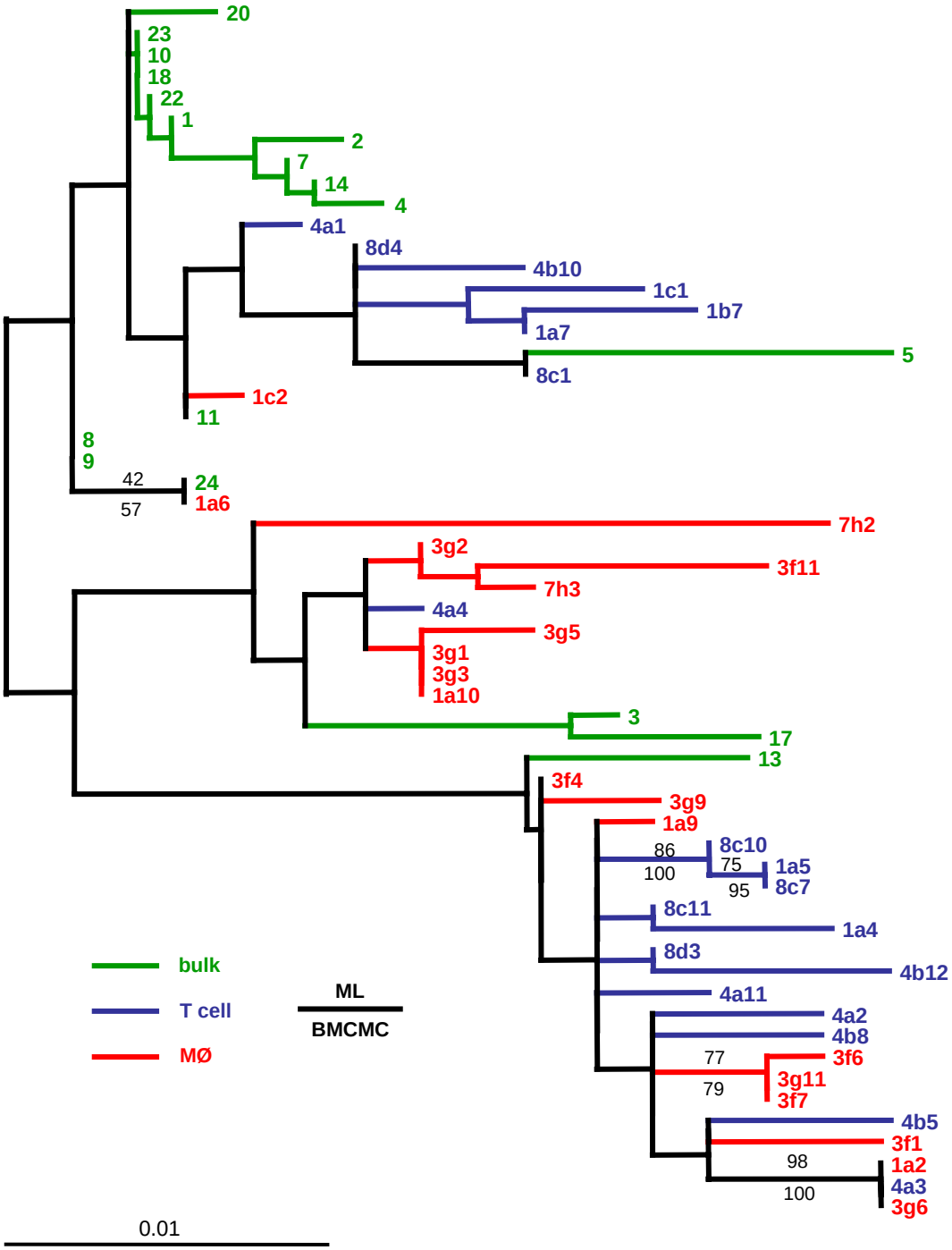

Figure 24. Splenic T cell and MØ HIV-1 gp120 provirus is under-represented by bulk sequences from the spleen. C2-C3 sequences isolated from **T cells**, **MØs**, and bulk sequences (**bulk**) from the spleen were subjected to both Maximum Likelihood and Bayesian phylogenetic analyses. Maximum Likelihood bootstrap values (**ML**) appear above the branches and Bayesian Markov Chain Monte Carlo (**BMCMC**) inference values below the branches.

APPENDIX

As described previously, when a host is challenged with foreign antigen, the antigen is rapidly opsonized with specific antibody and/or complement proteins to form immune complexes (ICs). These ICs are transported to the draining lymph nodes (39). Here, the vast majority of ICs are eliminated by phagocytes. However, a small portion are trapped and retained on the surface of FDCs (40-41). Work in this area demonstrates that the principle receptors that trap ICs are CD21 (or CR2), which binds complement 3b fragments, and CD32 (or FcγRII), which binds the Fc portion of IgG molecules (44-45). Early in acute infection, HIV-1 virions become coated with specific antibody and/or complement (51-54). FDCs trap these HIV ICs via CD21 and CD32 in enormous quantities, estimated at $\sim 1.5 \times 10^8$ copies of viral RNA per gram of lymphoid tissue (37, 58).

Treatment using a single HIV-1 reverse transcriptase inhibitor (RTI) in infected subjects fails to decrease the viral burden on FDCs (58). Moreover, even if three RTIs are used concomitantly, only a moderate impact on lymphoid tissue viral load is observed (119-120). However, analysis of FDCs during multi-drug therapy containing at least one HIV-1 protease inhibitor (PI), i.e. HAART, reveals an unexpected decrease of FDC-trapped virus as early as two days post HAART initiation (37). In fact, 6 months of HAART is enough to clear more than 99.9% of detectable FDC-trapped HIV-1 in some subjects (37). In the short term (i.e. two days), viral control of patients treated with HAART does not appear to differ significantly from that achieved by patients taking multiple RTIs (119-122).

Several studies demonstrate that PIs affect regular cellular processes. For example, the PI Ritonavir inhibits antiviral cytotoxic T lymphocyte activity, and impairs Major Histocompatibility Complex (MHC) class I-restricted epitope presentation in mice infected with lymphocytic choriomeningitis virus (123). It appears that Ritonavir affects these processes via inhibition of the chymotrypsin-like activity of the 20S proteasome (123). Other reports also demonstrate that PIs alter the normal function of the proteasome (124-126). Perhaps more relevant to my study, research also shows that PIs negatively affect the activation of Nuclear Factor Kappa B (NF-κB) (127-128). This is significant because NF-κB regulates the expression of CD21 (129). Finally, studies also show that PIs down-regulate the expression of Dendritic-cell Specific Intercellular adhesion molecule – 3 Grabbing Nonintegrin (DC-SIGN or CD209), a cell surface receptor on dendritic cells (130-131).

Since FDCs trap and retain ICs, including HIV-1, by virtue of CD21 and CD32, I postulated that HAART (expressly PIs) affects the expression of these receptors, negatively impacting the stability/half-life of FDC-trapped HIV-1. I isolated FDCs from fragments of LN biopsies from six HIV-1 infected subjects. In all six cases two biopsies were taken; the first biopsy was taken on the day HAART was to begin (i.e. before treatment started); the second biopsy was taken three days post initiation of HAART. These tissue samples were obtained via collaborations with Drs Ashley Haase and Tim Schacker at the University of Minnesota. I immuno-purified FDCs, isolated FDC RNA and reverse transcribed it into cDNA according to the procedures outlined in the Materials and Methods section.

Quantitative PCR reactions were performed using the 7500 Real-Time PCR System (Applied Biosytems) utilizing Taqman technology. I obtained the following validated primer/probes from Applied Biosystems (primer sequences are proprietary and therefore not included): CD21 primer/probe Hs00269610_m1 (probe sequence: 5'-FAM-AAGTTGGGGCTGAGAACACAATCAC-NFQ (non-fluorescent quencher that binds the minor groove)-3'; GAPDH primer/probe product #4326371 (all sequences are proprietary). The GAPDH probe is labeled 5'-VIC and 3'-NFQ and the primers are limiting and so reactions were run in a multiplex format. The primers for all the above reactions span exon splice junctions. I utilized the Taqman Universal PCR Master Mix (Applied Biosytems). It is supplied at a 2X concentration and contains AmpliTaq Gold DNA Polymerase, AmpErase UNG, dNTPs with dUTP, the passive reference dye ROX, and optimized buffer components. All reactions were performed in 25 µl volumes using the following conditions: initial incubation at 95°C for 10 min; 50 cycles of 95°C for 15 sec followed by 60°C for 1 min.

Using the paired samples of LN biopsies taken from HIV-1 infected patients I sought to test the hypothesis that HAART may be affecting FDC immune complex receptors. I used quantitative PCR to compare CD21 expression pre and three days post initiation of HAART and normalized this to GAPDH expression in the same samples (Appendix Figure 1). I observed a substantive decrease (ranging from 42% to >99%) in FDC CD21 mRNA in all six patients examined ($p=0.031$, Fisher sign test). Consistent with my observations, Cavert et al. found (using *in situ* hybridization) that two days post initiation of HAART, FDC viral loads were reduced by ~50% in several patients examined (37).

One of the most significant drawbacks to commencement of antiretroviral therapy is development of drug resistant virus within an individual. Therefore, alternative therapies designed to target host mechanisms rather than the viral life-cycle are becoming increasingly attractive. If the postulate that PIs are down-regulating CD21 and/or CD32 expression is proved correct, it provides a new therapeutic strategy which would seek to flush virus from this large and dangerous reservoir. That is, it opens the potential for designing drugs specifically to inhibit the expression of the receptors necessary for FDC viral trapping.

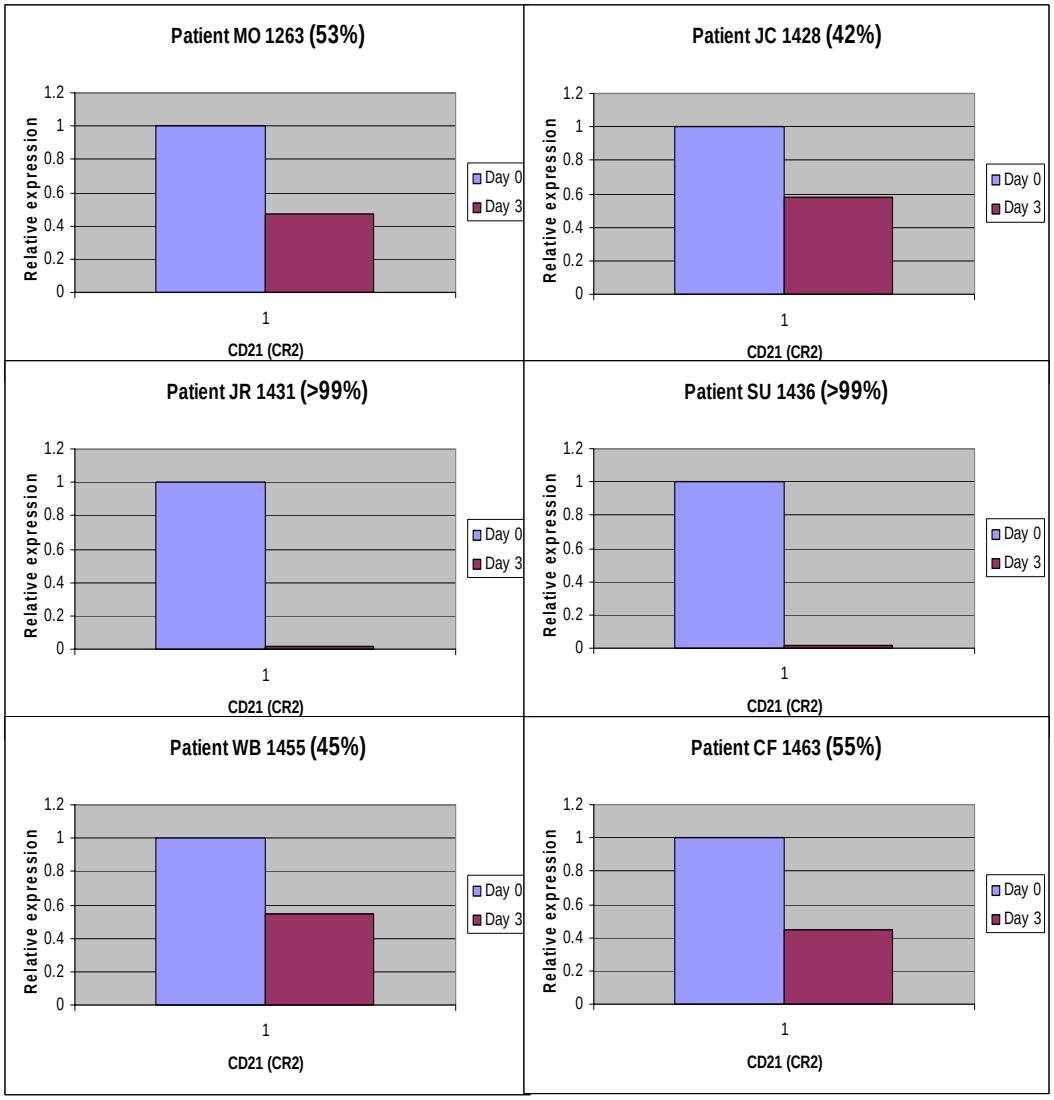

Appendix Figure 1. Decreased FDC expression of CD21 (CR2) ±HAART. FDCs were obtained from LN fragments of infected subjects pre and 3 days post HAART. RNA was isolated from FDCs, cDNA generated, and Q-PCR used to quantitate CD21 expression after normalizing to GAPDH expression in the same sample. Note that in 6 of 6 samples, CD21 expression was decreased between 42-99% by HAART**.**

REFERENCES

1. UNAIDS. 2006. 2006 Report on the global AIDS epidemic.

2. Chan, D. C., D. Fass, J. M. Berger, P. S. Kim. 1997. Core structure of gp41 from the HIV envelope glycoprotein. *Cell* 89:263-273.

3. Chan, D. C. and P. S. Kim. 1998. HIV entry and its inhibition. *Cell* 93:681-684.

4. Wyatt, R. and J. Sodroski. 1998. The HIV-1 envelope glycoproteins: fusogens, antigens, and immunogens. *Science* 280:1884-1888.

5. Coakley, E., C. J. Petropoulos, and J. M. Whitcomb. 2005. Assessing chemokine co-receptor usage in HIV. *Curr. Opin. Infect. Dis.* 18:9-15.

6. Milich, L., B. Margolin, and R. Swanstrom. 1993. V3 loop of the human immunodeficiency virus type 1 Env protein: interpreting sequence variability. *J. Virol.* 67:5623-5634.

7. Zhong, P., M. Peeters, W. Janssens, K. Fransen, L. Heyndrickx, G. Vanham, B. Willems, P. Piot, and G. van der Groen. 1995. Correlation between genetic and biological properties of biologically cloned HIV type 1 viruses representing subtypes A, B, and D. *AIDS Res. Hum. Retroviruses* 11:239-248.

8. Jensen, M. A. and A. B. van 't Wout. 2003. Predicting HIV-1 coreceptor usage with sequence analysis. *AIDS Rev.* 5:104-112.

9. Fouchier, R. A., M. Groenink, N. A. Kootstra, M. Tersmette, H. G. Huisman, F. Miedema, and H. Schuitemaker. 1992. Phenotype-associated sequence variation in the third variable domain of the human immunodeficiency virus type 1 gp120 molecule. *J. Virol.* 66:3183-3187.

10. De Jong, J. J., A. De Ronde, W. Keulen, M. Tersmette, and J. Goudsmit. 1992. Minimal requirements for the human immunodeficiency virus type 1 V3 domain to support the syncytium-inducing phenotype: analysis by single amino acid substitution. *J. Virol.* 66:6777-6780.

11. Resch, W., N. Hoffman, and R. Swanstrom. 2001. Improved Success of Phenotype Prediction of the Human Immunodeficiency Virus Type 1 from Envelope Variable Loop 3 Sequence Using Neural Networks. *Virology* 288:51-62.

12. Dong, X. N., X. Chen, Y. Chen, A. Ablimit, Z. Ye, Y. Wu, and Y. H. Chen. 2005. Short communication: HIV type 1 phenotype, tropism, and sequence patterns: association and preference. *AIDS Res. Hum. Retroviruses* 21:234-8.

13. Zhu, T., H. Mo, N. Wang, D. S. Nam, Y. Cao, R. A. Koup, and D. D. Ho. 1993. Genotypic and phenotypic characterization of HIV-1 patients with primary infection. *Science* 261:1179-1181.

14. van't Wout, A. B., N. A. Kootstra, G. A. Mulder-Kampinga, N. Albrecht-van Lent, H. J. Scherpbier, J. Veenstra, K. Boer, R. A. Coutinho, F. Miedema, and H. Schuitemaker. 1994. Macrophage-tropic variants initiate human immunodeficiency virus type 1 infection after sexual, parenteral, and vertical transmission. *J. Clin. Invest.* 94:2060-2067.

15. Zhu, T., N. Wang, A. Carr, D. S. Nam, R. Moor-Jankowski, D. A. Cooper, and D. D. Ho. 1996. Genetic characterization of human immunodeficiency virus type 1 in blood and genital secretions: evidence for viral compartmentalization and selection during sexual transmission. *J. Virol.* 70:3098-3107.

16. Wu, L., W. A. Paxton, N. Kassam, N. Ruffing, J. B. Rottman, N. Sullivan, H. Choe, J. Sodroski, W. Newman, R. A. Koup, and C. R. Mackay. 1997. CCR5 levels and expression pattern correlate with infectability by macrophage-tropic HIV-1, in vitro. *J. Exp. Med.* 185:1681-1691.

17. Koot, M., A. B. van't Wout, N. A. Kootstra, R. E. de Goede, M. Tersmette, and H. Schuitemaker. 1996. Relation between changes in cellular load, evolution of viral phenotype, and the clonal composition of virus populations in the course of human immunodeficiency virus type 1 infection. *J. Infect. Dis.* 173:349-354.

18. Moore, J. P. 1997. Coreceptors: implications for HIV pathogenesis and therapy. *Science* 276:51-52.

19. Coffin, J. M. 1995. HIV population dynamics in vivo: implications for genetic variation, pathogenesis, and therapy. *Science* 267:483-489.

20. Robertson, D. L., B. H. Hahn, and P. M. Sharp PM. 1995. Recombination in AIDS viruses. *J. Mol. Evol.* 40:249-259.

21. Brown, P. O. 1997. Integration. In (ed. J. M. Coffin et al.), *Retroviruses*, pp 161-203. Cold Spring Harbor Laboratory Press, Cold Spring Harbor.

22. Zheng, Y. H., N. Lovsin and B. M. Peterlin. 2005. Newly identified host factors modulate HIV replication. *Immunol. Lett.* 97:225-234.

23. Rabson, A. B. and B. J. Graves. 1997. Synthesis and processing of viral RNA. In (ed. J. M. Coffin et al.), *Retroviruses*, pp 205-261. Cold Spring Harbor Laboratory Press, Cold Spring Harbor.

24. Swanstrom, R. and J. W. Wills. 1997. Synthesis, assembly and processing of viral proteins. In (ed. J. M. Coffin et al.), *Retroviruses*, pp 263-334. Cold Spring Harbor Laboratory Press, Cold Spring Harbor.

25. Hammer, S. M., K. E. Squires, M. D. Hughes, J. M. Grimes, L. M. Demeter, J. S. Currier, J. J. Eron Jr, J. E. Feinberg, H. H. Balfour Jr, L. R. Deyton, J. A. Chodakewitz, and M. A. Fischl. 1997. A controlled trial of two nucleoside analogues plus indinavir in persons with human immunodeficiency virus infection and CD4 cell counts of 200 per cubic millimeter or less. AIDS Clinical Trials Group 320 Study Team. *N. Engl. J. Med.* 337:725-33.

26. Gulick, R. M., J. W. Mellors, D. Havlir, J. J. Eron, C. Gonzalez, D. McMahon, D. D. Richman, F. T. Valentine, L. Jonas, A. Meibohm, E. A. Emini, and J. A. Chodakewitz. 1997. Treatment with indinavir, zidovudine, and lamivudine in adults with human immunodeficiency virus infection and prior antiretroviral therapy. *N. Engl. J. Med.* 337:734-739.

27. Perelson, A. S., P. Essunger, Y. Cao, M. Vesanen, A. Hurley, K. Saksela, M. Markowitz, and D. D. Ho. 1997. Decay characteristics of HIV-1-infected compartments during combination therapy. *Nature* 387:188-191.

28. Blankson, J. N., D. Persaud, and R. F. Siliciano. 2002. The challenge of viral reservoirs in HIV-1 infection. *Annu. Rev. Med.* 53:557-593.

29. Ho, D. D., A. U. Neumann, A. S. Perelson, W. Chen, J. M. Leonard, and M. Markowitz. 1995. Rapid turnover of plasma virions and CD4 lymphocytes in HIV-1 infection. *Nature* 373:123-126.

30. Wei, X., S. K. Ghosh, M. E. Taylor, V. A. Johnson, E. A. Emini, P. Deutsch, J. D. Lifson, S. Bonhoeffer, M. A. Nowak, B. H. Hahn BH, M. S. Saag, and G. M. Shaw. 1995. Viral dynamics in human immunodeficiency virus type 1 infection. *Nature* 373:117-122.

31. Perelson, A. S., A. U. Neumann, M. Markowitz, J. M. Leonard, and D. D, Ho DD. 1996. HIV-1 dynamics in vivo: virion clearance rate, infected cell life-span, and viral generation time. *Science* 271:1582-1586.

32. Zhang, Z., T. Schuler, M. Zupancic, S. Wietgrefe, K. A. Staskus, K. A. Reimann, T. A. Reinhart, M. Rogan, W. Cavert, C. J. Miller, R. S. Veazey, D. Notermans, S. Little, S. A. Danner, D. D. Richman, D. Havlir, J. Wong, H. L. Jordan, T. W. Schacker, P. Racz, K. Tenner-Racz, N. L. Letvin, S. Wolinsky, and A. T. Haase. 1999. Sexual transmission and propagation of SIV and HIV in resting and activated CD4+ T cells. *Science* 286:1353-1357. Erratum. *Science* 286:2273.

33. Chun, T. W., L. Carruth, D. Finzi, X. Shen, J. A. DiGiuseppe, H. Taylor, M. Hermankova, K. Chadwick, J. Margolick, T. C. Quinn, Y. H. Kuo, R. Brookmeyer,

M. A. Zeiger, P. Barditch-Crovo, and R. F. Siliciano. 1997. Quantification of latent tissue reservoirs and total body viral load in HIV-1 infection. *Nature* 387:183-188.

34. Chun, T. W., D. Finzi, J. Margolick, K. Chadwick, D. Schwartz, and R. F. Siliciano. 1995. In vivo fate of HIV-1-infected T cells: quantitative analysis of the transition to stable latency. *Nat. Med.* 1:1284-1290.

35. Igarashi, T., C. R. Brown, Y. Endo, A. Buckler-White, R. Plishka, N. Bischofberger, V. Hirsch, and M. A. Martin. 2001. Macrophages are the principal reservoir and sustain high virus loads in rhesus macaques after the depletion of CD4+ T cells by a highly pathogenic simian immunodeficiency virus/HIV type 1 chimera (SHIV): Implications for HIV-1 infections of humans. *Proc. Natl. Acad. Sci. U S A.* 98:658-663.

36. van Furth R. 1989. Origin and turnover of monocytes and macrophages. *Curr. Top. Pathol.* 79:125-150.

37. Cavert, W., D. W. Notermans, K. Staskus, S. W. Wietgrefe, M. Zupancic, K. Gebhard, K. Henry, Z. Q. Zhang, R. Mills, H. McDade, C. M. Schuwirth, J. Goudsmit, S. A. Danner, and A. T. Haase. 1997. Kinetics of response in lymphoid tissues to antiretroviral therapy of HIV-1 infection. *Science* 276:960-964.

38. Hlavacek, W. S., N. I. Stilianakis, D. W. Notermans, S. A. Danner, and A. S. Perelson. 2000 Influence of follicular dendritic cells on decay of HIV during antiretroviral therapy. *Proc. Natl. Acad. Sci. U S A.* 97:10966-10971.

39. Szakal, A. K., K. L. Holmes, and J. G. Tew. 1983. Transport of immune complexes from the subcapsular sinus to lymph node follicles on the surface of nonphagocytic cells, including cells with dendritic morphology. *J. Immunol.* 131:1714-1727.

40. Tew, J. G., M. H. Kosco, and A. K. Szakal. 1989. The alternative antigen pathway. *Immunol. Today.* 10:229-232.

41. Szakal, A. K., M. H. Kosco, and J. G. Tew. 1989. Microanatomy of lymphoid tissue during the induction and maintenance of humoral immune responses: structure function relationships. *Ann. Rev. Immunol.* 7:91-109.

42. Tew, J. G., G. F. Burton, L. I. Kupp, and A. Szakal. 1993. Follicular dendritic cells in germinal center reactions. *Adv. Exp. Med. Biol.* 329:461-465.

43. Tew, J. G., M. H. Kosco, G. F. Burton, and A. K. Szakal. 1990. Follicular dendritic cells as accessory cells. *Immunol. Rev.* 117:185-211.

44. Banki, Z., L. Kacani, P. Rusert, M. Pruenster, D. Wilflingseder, B. Falkensammer, H. J. Stellbrink, J. van Lunzen, A. Trkola, M. P. Dierich, and H. Stoiber. 2005. Complement dependent trapping of infectious HIV in human lymphoid tissues. *AIDS.* 19:481-486.

45. Smith-Franklin, B. A., B. F. Keele, J. G. Tew, S. Gartner, A. K. Szakal, J. D. Estes, T. C. Thacker, and G. F. Burton. 2002. Follicular dendritic cells and the persistence of HIV infectivity: the role of antibodies and Fcgamma receptors. *J. Immunol.* 168:2408-2414.

46. Nie, X., S. Basu, and J. Cerny. 1997. Immunization with immune complex alters the repertoire of antigen-reactive B cells in the germinal centers. *Eur. J. Immunol.* 27:3517-3525.

47. Song, H., X. Nie, S. Basu, and J. Cerny. 1998. Antibody feedback and somatic mutation in B cells: regulation of mutation by immune complexes with IgG antibody. *Immunol. Rev.* 162:211-218.

48. Carroll, M. C. 1998. The role of complement and complement receptors in induction and regulation of immunity. *Ann. Rev. Immunol.* 16:545-568.

49. Mandel, T. E., R. P. Phipps, A. Abbot, and J. G. Tew. 1980. The follicular dendritic cell: long term antigen retention during immunity. *Immunol. Rev.* 53:29-59.

50. Kosco, M. H., A. K. Szakal, and J. G. Tew. 1988. In vivo obtained antigen presented by germinal center B cells to T cells in vitro. *J. Immunol.* 140:354-360.

51. Fox, C. H., and M. Cottler-Fox. 1992. The pathobiology of HIV infection. *Immunol. Today.* 13:353-356.

52. Fox, C. H., K. Tenner-Racz, P. Racz, A. Firpo, P. A. Rizzo, and A. S. Fauci. 1991. Lymphoid germinal centers are reservoirs of human immunodeficiency virus type 1 RNA. *J. Infect. Dis.* 164:1051-1057. Erratum. *J. Infect. Dis.* 165:1161.

53. Stoiber, H., A. Clivio, and M. P. Dierich. 1997. Role of complement in HIV infection. *Annu. Rev. Immunol.* 15:649-674.

54. Heath, S. L., J. G. Tew, A. K. Szakal, and G. F. Burton. 1995. Follicular dendritic cells and human immunodeficiency virus infectivity. *Nature* 377:740-744.

55. Racz, P. 1988. Molecular, biologic, immunohistochemical, and ultrastructural aspects of lymphatic spread of the human immunodeficiency virus. *Lymphology* 21:28-35.

56. Biberfeld, P., A. Porwit, G. Biberfield, M. Harper, A. Bodner, and R. Gallo. 1988. Lymphadenopathy in HIV (HTLV-III LAV) infected subjects: the role of virus and follicular dendritic cells. *Cancer. Detect. Prev.* 12:217-224.

57. Schacker, T., S. Little, E. Connick, K. Gebhard-Mitchell, Z. Q. Zhang, J. Krieger, J. Pryor, D. Havlir, J. K. Wong, D. Richman, L. Corey, and A. T. Haase. 2000. Rapid accumulation of human immunodeficiency virus (HIV) in lymphatic tissue reservoirs during acute and early HIV infection: implications for timing of antiretroviral therapy. *J. Infect. Dis.* 181:354-357.

58. Haase, A. T., K. Henry, M. Zupancic, G. Sedgewick, R. A. Faust, H. Melroe, W. Cavert, K. Gebhard, K. Staskus, Z.-Q. Zhang, P. Dailey, H. H. Balfour, Jr., A. Erice, and A. S. Perelson. 1996. Quantitative image analysis of HIV-1 infection in lymphoid tissue. *Science* 274:985-989.

59. Schmitz, J., J. van Lunzen, K. Tenner-Racz, G. Grossschupff, P. Racz, H. Schmitz, M. Dietrich, and F. T. Hufert. 1994. Follicular dendritic cells retain HIV-1 particles on their plasma membrane, but are not productively infected in asymptomatic patients with follicular hyperplasia. *J. Immunol.* 153:1352-1359.

60. Smith, B. A., S. Gartner, Y. Liu, A. S. Perelson, N. I. Stilianakis, B. F. Keele, T. M. Kerkering, A. Ferreira-Gonzalez, A. K. Szakal, J. G. Tew, and G. F. Burton. 2001. Persistence of infectious HIV on follicular dendritic cells. *J. Immunol.* 166:690-696.

61. Masuda, A., G. F. Burton, B. A. Fuchs, B. S. Bhogal, R. Rupper, A. K. Szakal, and J. G. Tew. 1994. Follicular dendritic cell function and murine AIDS. *Immunology* 81:41-46.

62. Masuda, A., G. F. Burton, B. A. Fuchs, A. K. Szakal, and J. G. Tew. 1993. Destruction of follicular dendritic cells in murine acquired immunodeficiency syndrome (MAIDS). *Adv. Exp. Med. Biol.* 329:411-416.

63. Burton, G. F., A. Masuda, S. L. Heath, B. A. Smith, J. G. Tew, and A. K. Szakal. 1997. Follicular dendritic cells (FDC) in retroviral infection: host/pathogen perspectives. *Immunol. Rev.* 156:185-197.

64. Nickle, D. C., M. A. Jensen, D. Shriner, S. J. Brodie, L. M. Frenkel, J. E. Mittler, and J. I. Mullins. 2003. Evolutionary indicators of human immunodeficiency virus type 1 reservoirs and compartments. *J. Virol.* 77:5540-5546.

65. Reinhart, T. A., M. J. Rogan, D. Huddleston, D. M. Rausch, L. E. Eiden, and A. T. Haase. 1997. Simian immunodeficiency virus burden in tissues and cellular compartments during clinical latency and AIDS. *J. Infect. Dis.* 176:1198-1208.

66. Pantaleo, G., C. Graziosi, L. Butini, P. A. Pizzo, S. M. Schnittman, D. P. Kotler, and A. S. Fauci. 1991. Lymphoid organs function as major reservoirs for human immunodeficiency virus. *Proc. Natl. Acad. Sci. USA*. 88:9838-9842.

67. Embretson, J., M. Zupancic, J. L. Ribas, A. Burke, P. Racz, K. Tenner-Racz, and A. T. Haase. 1993. Massive covert infection of helper T lymphocytes and macrophages by HIV during the incubation period of AIDS. *Nature* 362:359-362.

68. Pantaleo, G., C. Graziosi, J. F. Demarest, L. Butini, M. Montroni, C. H. Fox, J. M. Orenstein, D. P. Kotler, and A. S. Fauci. 1993. HIV infection is active and progressive in lymphoid tissue during the clinically latent stage of disease. *Nature* 362:355-358.

69. Delassus, S., R. Cheynier, and S. Wain-Hobson. 1992. Nonhomogeneous distribution of human immunodeficiency virus type 1 proviruses in the spleen. *J. Virol.* 66:5642-5645.

70. Delwart, E. L., J. I. Mullins, P. Gupta, G. H. Learn, Jr., M. Holodniy, D. Katzenstein, B. D. Walker, and M. K. Singh. 1998. Human immunodeficiency virus type 1 populations in blood and semen. *J. Virol.* 72:617-623.

71. Dittmar, M. T., G. Simmons, Y. Donaldson, P. Simmonds, P. R. Clapham, T. F. Schulz, and R. A. Weiss. 1997. Biological characterization of human immunodeficiency virus type 1 clones derived from different organs of an AIDS patient by long-range PCR. *J. Virol.* 71:5140-5147.

72. Epstein, L. G., C. Kuiken, B. M. Blumberg, S. Hartman, L. R. Sharer, M. Clement, and J. Goudsmit. 1991. HIV-1 V3 domain variation in brain and spleen of children with AIDS: tissue-specific evolution within host-determined quasispecies. *Virology* 180:583-590.

73. Gratton, S., R. Cheynier, M. J. Dumaurier, E. Oksenhendler, and S. Wain-Hobson. 2000. Highly restricted spread of HIV-1 and multiply infected cells within splenic germinal centers. *Proc. Natl. Acad. Sci. USA*. 97:14566-14571.

74. Itescu, S., P. F. Simonelli, R. J. Winchester, and H. S. Ginsberg. 1994. Human immunodeficiency virus type 1 strains in the lungs of infected individuals evolve independently from those in peripheral blood and are highly conserved in the C-terminal region of the envelope V3 loop. *Proc. Natl. Acad. Sci. USA***.** 91:11378-11382.

75. Keys, B., J. Karis, B. Fadeel, A. Valentin, G. Norkrans, L. Hagberg, and F. Chiodi. 1993. V3 sequences of paired HIV-1 isolates from blood and cerebrospinal fluid cluster according to host and show variation related to the clinical stage of disease. *Virology* 196:475-483.

76. Korber, B. T., K. J. Kunstman, B. K. Patterson, M. Furtado, M. M. McEvilly, R. Levy, and S. M. Wolinsky. 1994. Genetic differences between blood- and brain-derived viral sequences from human immunodeficiency virus type 1-infected patients: evidence of conserved elements in the V3 region of the envelope protein of brain-derived sequences. *J. Virol.* 68:7467-7481.

77. Panther, L. A., L. Tucker, C. Xu, R. E. Tuomala, J. I. Mullins, and D. J. Anderson. 2000. Genital tract human immunodeficiency virus type 1 (HIV-1) shedding and inflammation and HIV-1 env diversity in perinatal HIV-1 transmission. *J. Infect. Dis.* 181:555-563.

78. Poss, M., H. L. Martin, J. K. Kreiss, L. Granville, B. Chohan, P. Nyange, K. Mandaliya, and J. Overbaugh. 1995. Diversity in virus populations from genital secretions and peripheral blood from women recently infected with human immunodeficiency virus type 1. *J. Virol.* 69:8118-8122.

79. Shapshak, P., D. M. Segal, K. A. Crandall, R. K. Fujimura, B. T. Zhang, K. Q. Xin, K. Okuda, C. K. Petito, C. Eisdorfer, and K. Goodkin. 1999. Independent evolution of HIV type 1 in different brain regions. *AIDS Res. Hum. Retrovir.* 15:811-820.

80. van't Wout, A. B., L. J. Ran, C. L. Kuiken, N. A. Kootstra, S. T. Pals, and H. Schuitemaker. 1998. Analysis of the temporal relationship between human immunodeficiency virus type 1 quasispecies in sequential blood samples and various organs obtained at autopsy. *J. Virol.* 72:488-496.

81. Agopian, K., B. L. Wei, J. V. Garcia, and D. Gabuzada. 2007. CD4 and MHC-1 downregualtion are conserved in primary HIV-1 Nef alleles from brain and lymphoid tissues, but Pak2 activation is highly variable. *Virology* 358:119-135.

82. Burkala, E. J., J. He, J. T. West, C. Wood, and C. K. Petito. 2005. Compartmentalization of HIV-1 in the central nervous system: role of the choroid plexus. *AIDS.* 19:675-684.

83. Nokta, M. A., X. D. Li, L. Al-Harthi, J. Nichols, A. Pou, D. Asmuth, A. Landay, and R. B. Pollard. 2002. Entrapment of recent thymic emigrants in lymphoid tissues from HIV-infected patients: association with HIV cellular viral load. *AIDS.* 16:2119-2127.

84. Zhang L., L. Rowe, T. He, C. Chung, J. Yu, W. Yu, A. Talal, M. Markowitz, and D. D. Ho. 2002. Compartmentalization of surface envelope glycoprotein of human immunodeficiency virus type 1 during acute and chronic infection. *J. Virol.* 76:9465-9473.

85. Haddad D. N., C. Birch, T. Middleton, D. E. Dwyer, A. L. Cunningham, and N. K. Saksena. 2000. Evidence for late stage compartmentalization of HIV-1 resistance

mutations between lymph node and peripheral blood mononuclear cells. *AIDS.* 14:2273-2281.

86. Morris A., M. Marsden, K. Halcrow, E. S. Hughes, R. P. Brettle, J. E. Bell, and P. Simmonds. 1999. Mosaic structure of the human immunodeficiency virus type 1 genome infecting lymphoid cells and the brain: evidence for frequent in vivo recombination events in the evolution of regional populations. *J. Virol.* 73:8720-8731.

87. Wong J. K., C. C. Ignacio, F. Torriani, D. Havlir, N. J. Fitch, and D. D. Richman. 1997. In vivo compartmentalization of human immunodeficiency virus: evidence from the examination of pol sequences from autopsy tissues. *J. Virol.* 71:2059-71.

88. Haggerty S. and M. Stevenson. 1991. Predominance of distinct viral genotypes in brain and lymph node compartments of HIV-1-infected individuals. *Viral Immunol.* 4:123-131.

89. Hunt, P. W., P. R. Harrigan, W. Huang, M. Bates, D. W. Williamson, J. M. McCune, R. W. Price, S. S. Spudich, H. Lampiris, R. Hoh, T. Leigler, J. N. Martin, and S. G. Deeks. 2006. Prevalence of CXCR4 tropism among antiretroviral-treated HIV-1-infected patients with detectable viremia. *J. Infect. Dis.* 194:926-930.

90. Westby, M., M. Lewis, J. Whitcomb, M. Youle, A. L. Pozniak, I. T. James, T. M. Jenkins, M. Perros, and E. van der Ryst. 2006. Emergence of CXCR4-using human immunodeficiency virus type 1 (HIV-1) variants in a minority of HIV-1-infected patients following treatment with the CCR5 antagonist maraviroc is from a pretreatment CXCR4-using virus reservoir. *J. Virol.* 80:4909-4920.

91. Koot, M., I. P. Keet, A. H. Vos, R. E. de Goede, M. T. Roos, R. A. Coutinho, F. Miedema, P. T. Schellekens, and M. Tersmette. 1993. Prognostic value of HIV-1 syncytium-inducing phenotype for rate of CD4+ cell depletion and progression to AIDS. *Ann. Intern. Med.* 118:681-688.

92. Thompson, J. D., T. J. Gibson, F. Plewniak, F. Jeanmougin, and D. G. Higgins. 1997. The ClustalX windows interface: flexible strategies for multiple sequence alignment aided by quality analysis tools. *Nucl. Acids Res.* 24:4876-4882.

93. Maddison, D. R., and W. P. Maddison. 2000. MacClade 4: Analysis of Phylogeny and Character Evolution, version 4.0. Sinauer Associates.

94. Felsenstein, J. 1981. Evolutionary trees from DNA sequences: a maximum likelihood approach. *J. Mol. Evol.* 17:368-376.

95. Felsenstein, J. 1985. Confidence limits on phylogenies: an approach using the bootstrap. *Evolution* 39:783-791.

96. Guindon, S., and O. Gascuel. 2003. A simple, fast, and accurate algorithm to estimate large phylogenies by maximum likelihood. *Syst. Biol.* 52:696-704.

97. Huelsenbeck, J. P., B. Larget, R. E. Miller, and F. Ronquist. 2002. Potential applications and pitfalls of Bayesian inference of phylogeny. *Syst. Biol.* 51:673-688.

98. Ronquist, F., and J. P. Huelsenbeck. 2003. MrBayes 3: Bayesian phylogenetic inference under mixed models. *Bioinformatics* 19:1572-1574.

99. Posada, D., and T. R. Buckley. 2004. Model selection and model averaging in phylogenetics: Advantages of akaike information criterion and Bayesian approaches over likelihood ratio tests. *Syst. Biol.* 53:793-808.

100. Posada, D., and K. A. Crandall. 1998. MODELTEST: testing the model of DNA substitution. *Bioinformatics* 14:817-818.

101. Rambaut, A., and A. J. Drummond. 2003. Tracer v1.2.1, available from http:\\evolve.zoo.ox.ac.uk\.

102. Clement, M., D. Posada, and K. Crandall. 2000. TCS: a computer program to estimate gene genealogies. *Mol. Ecol.* 9:1657-1660.

103. Yang, Z. 1997. PAML: a program package for phylogenetic analysis by maximum likelihood. *Comput. Appl. Biosci.* 13:555-556 (http://abacus.gene.ucl.ac.uk/software/paml.html).

104. Goldman, N., and Z. Yang. 1994. A codon-based model of nucleotide substitution for protein-coding DNA sequences. *Mol. Biol. Evol.* 11:725-736.

105. Yang, Z., R. Nielsen, N. Goldman, and A. M. K. Pedersen. 2000. Codon-substitution models for heterogeneous selection pressure at amino acid sites. *Genetics* 155:431–449.

106. Nielsen, R., and Z. Yang. 1998. Likelihood models for detecting positively selected amino acid sites and applications to the HIV-1 envelope gene. *Genetics* 148:929-936.

107. Shioda, T., J. A. Levy, and C. Cheng-Mayer. 1991. Macrophage and T cell-line tropisms of HIV-1 are determined by specific regions of the envelope gp120 gene. *Nature* 349:167-169.

108. Cheng-Mayer C., T. Shioda, and J. A. Levy. 1991. Host range, replicative, and cytopathic properties of human immunodeficiency virus type 1 are determined by very few amino acid changes in tat and gp120. *J. Virol.* 65:6931-6941.

109. Hwang, S. S., T. J. Boyle, H. K. Lyerly, and B. R. Cullen. 1991. Identification of the envelope V3 loop as the primary determinant of cell tropism in HIV-1. *Science* 253:71-74.

110. Cann, A. J., M. J. Churcher, M. Boyd, W. O'Brien, J. Q. Zhao, J. Zack, and I. S. Chen. 1992. The region of the envelope gene of human immunodeficiency virus type 1 responsible for determination of cell tropism. *J. Virol.* 66:305-309.

111. Shioda, T., J. A. Levy, and C. Cheng-Mayer. 1992. Small amino acid changes in the V3 hypervariable region of gp120 can affect the T-cell-line and macrophage tropism of human immunodeficiency virus type 1. *Proc. Natl. Acad. Sci.* 89:9434-9438.

112. Mandel, T. E., R. P. Phipps, A. P. Abbot, and J. G. Tew. 1981. Long-term antigen retention by dendritic cells in the popliteal lymph node of immunized mice. *Immunology* 43:353-362.

113. Hosmalin, A., A. Samri, M. J. Dumaurier, Y. Dudoit, E. Oksenhendler, M. Karmochkine, B. Autran, S. Wain-Hobson, and R. Cheynier. 2001. HIV-specific effector cytotoxic T lymphocytes and HIV-producing cells colocalize in white pulps and germinal centers from infected patients. *Blood* 97:2695-2701.

114. Tew, J. G., T. E. Mandel, and G. A. Miller. 1979. Immune retention: immunological requirements for maintaining an easily degradable antigen *in vivo*. *Aust. J. Exp. Biol. Med. Sci.* 57:401-414.

115. Rosenberg, Y. J., G. Janossy. 1999. The importance of lymphocyte trafficking in regulating blood lymphocyte levels during HIV and SIV infections. *Semin. Immunol.* 11:139-154.

116. Dumaurier, M. J., S. Gratton, S. Wain-Hobson, R. Cheynier. 2005. The majority of human immunodeficiency virus type 1 particles present within splenic germinal centres are produced locally. *J. Gen. Virol.* 86:3369-3373.

117. Estes, J. D., B. F. Keele, K. Tenner-Racz, P. Racz, M. A. Redd, T. C. Thacker, Y. Jiang, M. J. Lloyd, S. Gartner, and G. F. Burton. 2002. Follicular dendritic cell-mediated up-regulation of CXCR4 expression on CD4 T cells and HIV pathogenesis. *J. Immunol.* 169:2313-2322.

118. Estes, J. D., T. C. Thacker, D. L. Hampton, S. A. Kell, B. F. Keele, E. A. Palenske, K. M. Druey, and G. F. Burton. 2004. Follicular dendritic cell regulation of CXCR4-mediated germinal center CD4 T cell migration. *J. Immunol.* 173:6169-6178.

119. Cohen, O. J., G. Pantaleo, M. Holodniy, S. Schnittman, M. Niu, C. Graziosi, G. N. Pavlakis, J. Lalezari, J. A. Bartlett, R. T. Steigberg, et al. 1995. Decreased human

immunodeficiency virus type 1 plasma viremia during antiretroviral therapy reflects downregulation of viral replication in lymphoid tissue. *Proc. Natl. Acad. Sci.* 92:6017-6021.

120. Lafeuillade, A., C. Poggi, N. Profizi, C. Tamalet, and O. Costes. 1996. Human immunodeficiency virus type 1 kinetics in lymph nodes compared with plasma. *J. Infect. Dis*. 174:404-407.

121. 2000. Highly active antiretroviral therapy including protease inhibitors does not confer a unique CD4 cell benefit. The AVANTI and INCAS Study Groups. *AIDS.* 14:1383-1388.

122. Rey, D., M. P. Schmitt, M. Partisani, G. Hess-Kempf, V. Krantz, E. de Mautort, C. Bernard-Henry, M. Priester, C. Cheneau, and J. M. Lang. 2001. Efavirenz as a substitute for protease inhibitors in HIV-1 infected patients with undetectable plasma viral load on HAART: a median follow-up of 64 weeks. *J. Acquir. Immune. Defic. Syndr.* 27:459-462.

123. Andre, P., M. Groettrup, P. Klenerman, et al. 1998. An inhibitor of HIV-1 protease modulates proteasome activity, antigen presentation, and T cell responses. *Proc. Natl. Acad. Sci.* 95:13120-13124.

124. Liang, J. S., O. Distler, D. A. Cooper, H. Jamil, R. J. Deckelbaum, H. N. Ginsberg, and S. L. Sturley. 2001. HIV protease inhibitors protect apolipoprotein B from degradation by the proteasome: a potential mechanism for protease inhibitor-induced hyperlipidemia. *Nat. Med.* 7:1327-1331.

125. Schmidtke, G., H. G. Holzhutter, M. Bogyo, et al. 1999. How an inhibitor of the HIV-I protease modulates proteasome activity. *J. Biol. Chem.* 274:35734-35740.

126. Gaedicke, S., E. Firat-Geier, O. Constantiniu, et al. 2002. Antitumor effect of the human immunodeficiency virus protease inhibitor ritonavir: induction of tumor-cell apoptosis associated with perturbation of proteasomal proteolysis. *Cancer. Res.* 62: 6901-6908.

127. Dewan, M. Z., J. N. Uchihara, K. Terashima, M. Honda, T. Sata, M. Ito, N. Fujii, K. Uozumi, K. Tsukasaki, M. Tomonaga, Y. Kubuki, A. Okayama, M. Toi, N. Mori, and N. Yamamoto. 2006. Efficient intervention of growth and infiltration of primary adult T-cell leukemia cells by an HIV protease inhibitor, ritonavir. *Blood* 107:716-724.

128. Pati, S., C. B. Pelser, J. Dufraine, J. L. Bryant, M. S. Reitz Jr, and F. F. Weichold. 2002. Antitumorigenic effects of HIV protease inhibitor ritonavir: inhibition of Kaposi sarcoma. *Blood* 99:3771-3779.

129. Tolnay, M., L. A. Vereshchagina, and G. C. Tsokos. 2002. NF-kappaB regulates the expression of the human complement receptor 2 gene. *J. Immunol.* 169:6236-6243.

130. Whelan, K. T., C. L. Lin, M. Cella, A. J. McMichael, J. M. Austyn, et al. 2003. The HIV protease inhibitor indinavir reduces immature dendritic cell trans-endothelial migration. *Eur. J. Immunol.* 33:2520-2530.

131. Rappocciolo, G., P. Piazza, C. L. Fuller, T. A. Reinhart, S. C. Watkins, D. T. Rowe, M. Jais, P. Gupta, and C. R. Rinaldo. 2006. DC-SIGN on B lymphocytes is required for transmission of HIV-1 to T lymphocytes. *PLoS. Pathog.* 2:e70.